PROCEEDINGS

of the

Fifteenth
International Tissue Elasticity Conference™

Lake Morey, Vermont, USA
October 16 – 19, 2016

PROCEEDINGS

of the

Fifteenth International Tissue Elasticity Conference™

Lake Morey, Vermont, USA
October 16-19, 2016

Table of Contents

Foreword 3
Conference–At–A–Glance 5
Program by Date and Time 6
Author Index 21
Abstracts 23
Session TUT- Tutorials. 23
Session SAS: Oral Presentations of Finalists for Student Awards Session 25
Session POS: Poster Session 32
Session CVE: Cardiovascular Elasticity 40
Session SIP: Signal and Image Processing 43
Session CAA–1: Clinical and Animal Applications – I 51
Session MIP–1: Methods for Imaging Elastic Tissue Properties – I 57
Session MMT: Mechanical Measurements Techniques for Tissues 63
Session MPT: Mechanical Properties of Tissues 67
Session INS: Instrumentation including Phantoms 71
Session FIP–1: Forward and Inverse Problems – I 75
Session MIP–2: Methods for Imaging Elastic Tissue Properties – II 83
Session MIP–3: Methods for Imaging Elastic Tissue Properties – III 86
Session CAA–2: Clinical and Animal Applications – II 92
Session FIP–2: Forward and Inverse Problems – II 98
Conference Evaluation and Questionnaire 103

Original Cover Photo by Dr JC Bamber

QUESTIONS OR COMMENTS ARE WELCOME AT ANY TIME AT <secretariat@elasticityconference.org>

Some abstracts may have been edited by the reviewers for clarity of presentation.

FOREWORD

Dear Conference Delegate:

Welcome to the Fifteenth annual International Tissue Elasticity Conference™ (ITEC™), and welcome to Lake Morey, Fairlee, Vermont, USA. We are delighted to be here for our first ITEC™ in New England. The venue should provide a peaceful and comfortable retreat, with excellent conference facilities and a relaxing atmosphere within which we can present and discuss our science, as well as renew and create friendships while looking upon a beautiful landscape.

You may wish to take the time to explore. With luck there may still be some spectacular carotenoid and anthocyanin color remaining on the trees, a particular feature of this area of the USA. Being on the border of Vermont and New Hampshire, there is spectacular scenery in all directions from Fairlee. The historic town of Hanover is only 20 minutes' drive south of Fairlee, with Ivy League university Dartmouth College. A little further south one reaches White River Junction, the confluence of the White River and the Connecticut River, from where it is not far to the beautiful Quechee Gorge and then to the charming and historic town of Woodstock. To the west, on the way to the city of Burlington on the shore of Lake Champlain, one finds the Mt Mansfield State Forest and Waterbury Reservoir, with skiing mountains such as in the area around Stowe. Hiking trails abound, including a section of the Appalachian Trail that crosses Hanover. Cycling is very popular. To the north one has the Big Deer State Park and Mountain Trail, and to the east the magnificent White Mountains. It is also worth looking at what's on in the local towns. At this time of year theatres, art exhibitions, museums, historic sites and various societies tend to put on their best shows.

I am sad to say that Jonathan and Karen Ophir will again not be able to join us. Jonathan and Karen are two of the Founding Organizers of ITEC, and they were the principle driving force behind the ITEC series of conferences from 2002-2012. They have kindly sent their good wishes for the conference. We wish them both well and we plan to involve them in the conference at various points, via Skype.

This year we continue the format of starting the conference with two tutorial speakers, one that is clinical applications and practical methods based, and another that is more related to the theory and basic science of elastography. I am delighted that Elisa Konofagou has agreed to open ITEC 2016 with a lecture that describes the exciting work going on in the area of myocardial elastography and electomechanical wave imaging. Elisa's team pioneered this advanced field of elasticity imaging and has been leading it for many years now. To complement this, our more basic science tutorial will be presented by Assad Oberai, who will educate us on the computational methods used for solving inverse problems to enable biomechanical imaging. Assad has been at the forefront of this field for well over a decade. It is a substantial task to prepare an ITEC tutorial, and I am grateful to both Elisa and Assad for agreeing to pass on their knowledge and experience in this way.

Many volunteers and colleagues have helped to bring about this conference, especially our conference secretary, Cheryl Taylor. Please join me in thanking Cheryl for, once again, working tirelessly to make the conference a timely success. It is a pleasure also to acknowledge contributions from the administration of the Institute of Cancer Research, especially Liam Blake and Alan Hill for assistance in financial and legal matters, and Neil Walford's team for assistance with audio-visual equipment. Finally, we are extremely grateful to all those who have participated as helpers, sponsors, reviewers, session chairs, award judges and contributors, without whom the conference could not happen.

When Jonathan Ophir and Kevin Parker first conceived this conference series they expressed the purpose as "to advance the field of measurement and imaging of the elastic attributes of soft tissues through tutorials and scientific presentations of the state of the art in the field, within a unique and unified forum that would bring together researchers from several countries and ultimately contribute to the rapid development and clinical introduction of this new medical imaging technology". Our presence here suggests that we all strongly agree that we continue to value such a conference. However, ITEC must evolve if it is to continue to serve the needs of researchers and practitioners in the field of tissue elasticity measurement and imaging. Please complete the feedback forms in this Proceedings Book or, if you prefer, speak directly to me or Cheryl to discuss your suggestions. Feedback is of immense value to us in planning future ITECs.

May your research be inspired by the presentations and discussions during the Fifteenth ITEC, and may you make new friends, establish productive collaborations and renew old acquaintances.

Next year, for the Sixteenth annual ITEC, we will be returning to Europe in late September and aim again to have a successful "Elastography Week" by joining forces with the clinical Sonoelastography meeting.

Jeffrey Bamber
General Conference Organizer
Lake Morey, Fairlee, Vermont, USA, October 16-19, 2016

CONFERENCE-AT-A-GLANCE

Fifteenth International Tissue Elasticity Conference™

Lake Morey, Vermont, USA October 16-19, 2016

Sunday, October 16 9:00A - 8:30P

9.00A-12.00P		Oral Presenters load presentations (CD or USB drive)	Morey Room
		Poster Presenters set up presentations	Morey Room
9:00A - 5:30P		Registration Desk Open	Foyer
11:00A -5:30P	**Session EEX**:	Equipment Exhibit (*during breaks & Reception*)	Morey Room
12:00P- 2:00P	**Session TUT:**	**Tutorials**	Morey Room
2:00P – 2:30P		*Coffee Break*	Morey Room
2:30P – 4:15P	**Session SAS:**	**Oral Presentations of Finalists for Student Awards Session**	Morey Room
4:15P – 5:00P		*Recess*	
5:00P – 6:00P	**Session POS:**	**Poster Session - Live Oral Summaries**	Morey Room
6:00P – 8:30P		Opening Dinner Reception	Lake Dining Room

Monday, October 17 8:45A - 10:30P

8:45A - 5:30P		Registration Desk Open	Foyer
8:45A – 5:30P	**Session POS:**	Posters	Morey Room
8:45A – 5:30P	**Session EEX:**	Equipment Exhibit	Morey Room
8:45A - 9:00A		Opening Remarks	Morey Room
9:00A - 9:45A	**Session CVE:**	**Cardiovascular Elasticity**	Morey Room
9:45A - 10:30A		*Coffee Break*	Morey Room
10:30A - 12:30P	**Session SIP:**	**Signal and Image Processing**	Morey Room
12:30P - 2:00P		*Group Lunch*	Lakeside Dining Room
2:00P - 3:30P	**Session CAA-1:**	**Clinical and Animal Applications I**	Morey Room
3:30P - 4:00P		*Coffee Break*	Morey Room
4:00P - 5:30P	**Session MIP-1:**	**Method for Imaging Elastic Tissue Properties – I**	Morey Room
7:30P - 10:30P		*Conference Dinner*	Lakeside Dining Room

Tuesday, October 18 8:45A – 5:30P

8:45A - 5:30P		Registration Desk Open	Foyer
8:45A - 5:30P	**Session POS:**	Posters	Morey Room
8:45A - 5:30P	**Session EEX:**	Equipment Exhibit	Morey Room
9:00A - 9:52A	**Session MMT:**	**Mechanical Measurements Techniques for Tissues**	Morey Room
10:00A - 10:30A		*Coffee Break*	Morey Room
10:30A - 11:30A	**Session MPT:**	**Mechanical Properties of Tissues**	Morey Room
11:30A – 12:20P	**Session INS:**	**Instrumentation including Phantoms**	Morey Room
12:30P - 2:00P		*Group Lunch*	Lakeside Dining Room
2:00P - 4:00P	**Session FIP-1:**	**Forward & Inverse Problems- I**	Morey Room
4:00P - 4:30P		*Coffee Break*	Morey Room
4:30P - 5:07P	**Session MIP-2:**	**Method for Imaging Elastic Tissue Properties – II**	Morey Room
5:10P – 5:30P		*Group Photo*	TBA
5.30P		*No Conference Activities*	

Wednesday, October 19 9:15A -7:00P

9:00A - 3:30P	**Session POS:**	Posters	Morey Room
9:00A - 3:30P	**Session EEX:**	Equipment Exhibit	Morey Room
9:15A - 10:35A	**Session MIP-3:**	**Method for Imaging Elastic Tissue Properties – III**	Morey Room
10:35A - 11:05A		*Coffee Break*	Morey Room
11:05A – 12:35P	**Session CAA2:**	**Clinical and Animal Applications II**	Morey Room
12:35A - 2:05P		*Group Lunch*	Lakeside Dining Room
2:05P – 3:10P	**Session FIP-2:**	**Forward & Inverse Problems – II**	Morey Room
3:10P – 5:00P		*Recess & coffee*	
5:00P – 7:00P		*Closing PIZZA reception*	Lakeside Dining Room

PROGRAM

Fifteenth International Tissue Elasticity Conference™

Lake Morey, Vermont, USA

October 16-19, 2016

Sunday, October 16 9:00A - 8:30P

9:00A – 12:00P Presentation Set Up

All Oral Presenters load presentations onto Conference computers — Morey Room
Poster Presenters set up presentation — Morey Room
Exhibitors set up exhibits — Morey Room

9:00A – 5:30P Registration Desk Open — Foyer

12:00P – 5:30P Session EEX: Equipment Exhibit — Morey Room

Sunday 12:00P – 2:00P
Session TUT: Tutorials:
Chair: JC Bamber, UK *Co–Chair: PE Barbone, USA* — Morey Room

Page No.

12:00P – 12:45P

084 MYOCARDIAL ELASTOGRAPHY AND ELECTOMECHANICAL WAVE IMAGING. 23
EE Konofagou[1,]*
[1]Columbia University, New York, NY, USA.

12:45P – 1:00P Discussion

1:00P – 1:45P

083 COMPUTATIONAL METHODS FOR INVERSE PROBLEM SOLUTIONS FOR ELASTOGRAPHIC AND BIOMECHANICAL IMAGING PROBLEMS. 24
AA Oberai[1,]*
[1] Scientific Computation Research Center, Rensselaer Polytechnic Institute, Troy, NY 12180, USA.

1:45P – 2:00P Discussion

2:00P – 2:30P COFFEE BREAK — Morey Room

Sunday **2:30P – 4:15P**
Session SAS: **Oral Presentations of Finalists for Student Awards Session**
Chair: BS Garra, USA *Co–Chair: CL De Korte, The Netherlands* Morey Room
Page No.

2:30P – 2:45P

011 COMPARISON OF THE VISCOELASTIC POWER LAW PARAMETERS ESTIMATED BY MR ELASTOGPRHY AND MULTI-FREQUENCY MR ELASTOGRAPHY. 25
J Testu[1], MDJ McGarry[2], F Dittman[3], JB Weaver[4], KD Paulsen[4], I Sack[3], EEW Van Houten[1].*
[1]University of Sherbrooke, Sherbrooke, Qc, CANADA; [2]Columbia University, New York, NY, USA; [3]Charité-Universitätsmedizin, Berlin, GERMANY; [4]Darmouth College, Hanover, NH, USA.

2:45P – 3:00P

026 OPTIMIZATION OF TRANSMIT PARAMETERS FOR TWO-DIMENSIONAL CARDIAC STRAIN ESTIMATION WITH COHERENT COMPOUNDING *IN SILICO, IN VITRO,* AND *IN VIVO.* 26
V Sayseng[1], J Grondin[1], C Papadacci[1], EE Konofagou[1].*
[1]Columbia University, New York, NY, UNITED STATES.

3:00P – 3:15P

031 SHEAR WAVE SPEED ESTIMATION COMPARISON OF EARLY AND LATE PREGNANCY IN THE *IN VIVO* HUMAN UTERINE CERVIX. 27
LC Drehfal[1], H Feltovich[1,2], I Rosado-Mendez[1], ML Palmeri[3], TJ Hall[1]*
[1]University of Wisconsin, Madison, WI, USA; [2]Intermountain Healthcare, Provo, UT, USA; [3]Duke University, Durham, NC, USA.

3:15P – 3:30P

035 REPRODUCIBILITY AND ANGLE INDEPENDENCE OF ELECTROMECHANICAL WAVE IMAGING FOR THE MEASUREMENT OF ELECTROMECHANICAL ACTIVATION DURING SINUS RHYTHM IN HEALTHY HUMANS. 28
L Melki[1], EE Konofagou[2].*
[1]Columbia University, New York, NY, USA.

3:30P – 3:45P

046 A COMPARISON OF ULTRASONIC SHEAR WAVE ATTENUATION ESTIMATES USING 2-D TRANSFORM AND AMPLITUDE-BASE METHODS. 29
SL Lipman[1], NC Rouze[1], ML Palmeri[1], KR Nightingale[1].*
[1]Duke University, Durham, NC, USA.

3:15P – 4:00P

061 COMPLIANCE ESTIMATION AND MAPPING USING PULSE WAVE IMAGING (PWI): *IN VITRO* VALIDATION AND *IN VIVO* FEASIBILITY. 30
IZ Apostolakis[1], P Nauleau[1], M D J McGarry[1], EE Konofagou[1].*
[1]Columbia University, New York, NY, USA; [2]Dartmouth College, Hanover, NH, USA.

4:00P – 4:15P

062 TOWARD VALIDATION FOR SHEAR WAVE ELASTOGRAPHY USING TORSIONAL VIBRATION RHEOMETRY IN SOFT GELS. 31
SS Yengul[1], PE Barbone[1], B Madore[2].*
[1]Boston University, Boston, MA, 02215, USA; [2]Harvard University and Brigham and Women's Hospital, Boston, MA, 02115, USA.

Sunday 5:00P – 6:00P

Session POS: Poster Session – Live Oral Summaries

Chair: J Jiang, USA *Co–Chair: AK Thittai, India* Morey Room

Page No.

5:00P – 5:02P

050 POROELASTIC MECHANICAL PROPERTIES OF BRAIN TUMORS USING INTRINSIC ACTUATION MR ELASTOGRAPHY. 32

L Solamen[1], MDJ McGarry[2], EEW Van Houten[3], J Hong[4], L Ronan[4], JB Weaver[5], KD Paulsen[1,5].*

[1]Thayer School of Engineering, Dartmouth College, Hanover, NH, USA; [2]Columbia University, New York, NY, USA; [3]University de Sherbrooke, Sherbrooke Quebec, CANADA; [4]Dartmouth Hitchcock Medical Center, Lebanon, NH, USA; [5]Geisel School of Medicine, Dartmouth College, Hanover, NH USA.

5:03P – 5:05P

059 ELASTIC WAVES IN A STRONG MAGNETIC FIELD. 33

DI Gendin[1], PE Barbone[1].*

[1]Boston University, Boston, Massachusetts, USA.

5:06P – 5:08P

072 ASSESSING THE VISCOELASTIC PROPERTIES OF ABDOMINAL TUMOR MODELS *IN VIVO* USING MRE. 34

J Li[1], L Asher[1], F Lopes[1], C Cummings[1], A Koers[1], LS Danielson[1], L Chesler[1], CJ Springer[1], JC Bamber[1], R Sinkus[2], Y Jamin[1], SP Robinson[1].*

The Institute of Cancer Research, London, UK; [2]King's College London, King's Health Partners, St. Thomas' Hospital, London, UK.

5:09P – 5:11P

015 THE AUDIBLE HUMAN PROJECT: STUDY OF ACOUSTIC TRANSMISSION WITH A FRACTAL BASED MODEL OF THE HUMAN AIRWAYS 35

B Henry[1], TJ Royston[1].*

[1]University of Illinois at Chicago, Chicago, IL, USA.

5:12P – 5:14P

073 SHEAR WAVE ELASTOGRAPHY IN THE PROSTATE INTEROBSERVER REPRODUCIBILITY & COMPARISON WITH FUNCTIONAL MR BIOMARKERS. 36

H Harvey[1], V Morgan[2], J Fromageau[1,2], T O'Shea[1,2], R Eeles[1,2], JC Bamber[1,2], N DeSouza[1,2]*

[1]The Institute of Cancer Research, London, UK; [2]The Royal Marsden Hospital, London, UK.

5:15P – 5:17P

074 HISTOPATHOLOGICAL CORRELATES OF YOUNG'S MODULUS ESTIMATED BY SHEAR WAVE ELASTOGRAPHY IN HUMAN BRAIN TUMOURS. 37

*H W Chan[1], T Jacques[2], C Uff[3], A Chakraborty[4], N Dorward[1], J Bamber[5]**

[1]The National Hospital for Neurology and Neurosurgery, London, UK; [2]Great Ormond Street Hospital, London, UK; [3]Royal London Hospital, London, UK; [4]Southampton General Hospital, Southampton, UK; [5]Institute of Cancer Research and the Royal Marsden Hospital, London, UK.

5:18P – 5:20P

075 CLINICAL APPLICATION OF SHEAR WAVE ELASTOGRAPHY FOR ASSISTING BRAIN TUMOUR RESECTION. 38

*H W Chan[1], C Uff[2], A Chakraborty[3], N Dorward[1], J Bamber[4]**

[1]The National Hospital for Neurology and Neurosurgery, London, UK; [2]Royal London Hospital, London, UK; [3]Southampton General Hospital, Southampton, UK; [4]Institute of Cancer Research and the Royal Marsden Hospital, London, UK.

(Session POS continued on next page)

(Session POS continued from previous page)

5:21P – 5:23P

076. TEMPORAL REGULARISATION OF LONG ULTRASOUND SEQUENCE TRACKING AND USE FOR MOTION COMPENSATION IN RADIOTHERAPY. 39
T O'Shea[1], M Fast[1], S Nill[1], U Oelfke[1], JC Bamber[1], EJ Harris[1].*
[1]Joint Department of Physics, The Royal Marsden NHS Foundation Trust and The Institute of Cancer Research, Sutton and London, UK.

5:30P – 6:00P **Discussion**

Sunday 6:00P – 8:30P
Opening Dinner Reception

Lakeside Dining Room

Monday, October 17 8:45A - 10:30P

8:45A - 5:30P
Registration Desk Open — Foyer
8:45A - 5:30P **Session EEX:** **Equipment Exhibit** — Morey Room
8:45A - 5:30P **Session POS:** **Posters** — Morey Room

Monday 8:45A - 9:00A
OPENING REMARKS

JC Bamber — Morey Room

Monday 9:00A – 9:45A
Session CVE: CARDIOVASCULAR ELASTICITY

Chair: EE Konofagou, USA *Co–Chair: PE Barbone, USA* — Morey Room

Page No.

9:00A - 9:15A

034 EXPERIMENTAL AND NUMERICAL STUDY OF CIRCUMFERENTIAL AND AXIAL CYLINDRICAL WAVES IN PVA PHANTOMS SURROUNDED BY WATER OR EMBEDDED INTO SOFTER PVA MATERIAL. 40
DA Shcherbakova[1], N Debusschere[1], M Kersemans[1], A Caenen[1], M Pernot[2], P Segers[1], A Swillens[1].*
[1]Ghent University, Ghent, BELGIUM; [2]Institute Langevin, Paris, FRANCE.

9:15A - 9:30A

017 HIGH FRAME RATE ACCURATE TRACKING OF TISSUE MOTION AFTER VALVE CLOSURE. 41
HJ Vos [1,2], M Strachinaru [1], BM van Dalen [1], I Heinonen [1], J Bercoff [3], JG Bosch[1], AFW van der Steen [1,2], N de Jong [1,2].*
[1]Erasmus MC, Rotterdam, THE NETHERLANDS; [2]Delft University of Technology, Delft, THE NETHERLANDS; [3]Supersonic Imagine, Aix en Provence, FRANCE.

9:30A - 9:45A

010 EVALUATE CAROTID ARTERY ANISOTROPY USING PRINCIPAL STRAIN ELASTOGRAPHY. 42
R Nayak[1], G Schifitto[2], MM Doyley[1].*
[1]University of Rochester, Rochester, New York, USA; [2]University of Rochester Medical Center, Rochester, New York, USA.

9:45A - 10:30A
COFFEE BREAK — Morey Room

Monday 10:30A - 12:30P
Session SIP: SIGNAL and IMAGE PROCESSING

Chair: MS Richards, USA *Co–Chair: R Daigle, USA* *Morey Room*

Page No.

10:30A - 10:45A

001 HOW DOES ULTRAFAST IMAGING AFFECT SHEAR WAVE VISUALIZATION? 43
A Caenen[1], M Pernot[2], D Shcherbakova[1], IK Ekroll[3], P Segers[1], A Swillens[1].*
[1]Ghent University, Ghent, BELGIUM; [2]Institute Langevin, Paris, FRANCE; [3]Nowegian University of Science and Technology, Trondheim, NORWAY.

10:45A - 11:00A

028 SHEAR WAVE SPEED ESTIMATES WITH VELOCITY AND DISPLACEMENT DATA: THEORY, SIMULATIONS, AND EX VIVO APPLICATIONS IN THE CERVIX OF THE RHESUS MACAQUE. 44
IM Rosado-Mendez[1], LC Drehfal[1], ML Palmeri[2], H Feltovich[1,3], TJ Hall[1].*
[1]University of Wisconsin-Madison, Madison, Wisconsin, USA; [2]Duke University, Durham, North Carolina, USA; [3]Intermountain Healthcare, Provo, Utah, USA.

11:00A - 11:15A

052 STRATEGIES FOR QUALITY ASSESSMENT OF SHEAR WAVE SPEED ESTIMATES: *EX VIVO* APPLICATION IN THE RHESUS MACAQUE CERVIX. 45
IM Rosado-Mendez[1], LC Drehfal[1], ML Palmeri[2], H Feltovich[1,3], TJ Hall[1].*
[1]University of Wisconsin-Madison, Madison, Wisconsin, USA; [2]Duke University, Durham, North Carolina, USA; [3]Intermountain Healthcare, Provo, Utah, USA.

11:15A - 11:30A

013 ESTIMATION OF PULSE WAVE VELOCITY IN ARTERIES: A NEW METHOD BASED ON CROSS-CORRELATION. 46
P Nauleau[1], IZ Apostolakis[1], M McGarry[1], EE Konofagou[1,2].*
[1]Columbia University, New York, NY, USA; [2]Columbia University, New York, NY, USA.

11:30A - 11:45A

005 A NOVEL METHOD TO ENHANCE THE CONTRAST TO NOISE RATIO OF ACOUSTIC RADIATION FORCE IMPULSE (ARFI) IMAGING. 47
M Vejdani-Jahromi[1], J Freedman[1], PD Wolf[1].*
[1]Duke University, Durham, NC, USA.

11:45A - 12:00P

051 ACCURACY ASSESSMENT OF TIME DELAY ESTIMATION IN ULTRASOUND ELASTOGRAPHY. 48
M Ghasemi Amidabadi[1], O Ahmad[1], H Rivaz[1,2]*.*
[1]Department of Electrical and Computer Engineering, Concordia University, De Maisonneuve Blvd. W, Montreal, Quebec, CANADA; [2]PERFORM center , Concordia University, 7141 Sherbrooke St. W, Montreal, Quebec, CANADA.

12:00P - 12:15P

012 LINEAR ACTUATOR-ASSISTED TRANSDUCER TO OBTAIN SUB-PITCH RESOLUTION FOR ELASTOGRAPHY. 49
Selladurai S[1], AK Thittai[1].*
[1]Indian Institute Of Technology Madras, Chennai, Tamil Nadu, INDIA.

Session SIP continued on next page)

(Session SIP continued from previous page)

12:15P - 12:30P

044 PLURAL SPECTRAL FREQUENCY DIVISIONS FOR HIGH FRAME RATE ULTRASONIC TISSUE DISPLACEMENT VECTOR MEASUREMENT. 50
*C Sumi**.
Sophia University, 4 Yonban-cho, Chiyoda-ku, Tokyo, 102-0081, JAPAN.

12:30P – 2:00P

GROUP LUNCH Lakeside Dining Room

Monday 2:00P – 3:30P

Session CAA -1: Clinical and Animal Applications - 1

Chair: KJ Parker USA *Co-Chair: M Dhyani, USA* Morey Room

Page No.

2:00P – 2:15P

006 THE EFFECTS OF TENDINOPATHY AND EXERCISE INTERVENTIONS ON MULTIAXIAL STRAINS IN THE ACHILLES TENDON INSERTION. 51
RL Chimenti[1,2], M Kelly[1], M Bucklin[1], JP Ketz[1], AS Flemister[1], MS Richards[1], MR Buckley[1].*
[1]University of Rochester, Rochester, NY, USA; [2]University of Iowa, Iowa City, IA, USA.

2:15P – 2:30P

054 FUNCTIONAL CHANGES IN CORTICAL STIFFNESS OBSERVED WITH MAGNETIC RESONANCE ELASTOGRAPHY. 52
S Patz[1], N Nazari[2], PE Barbone[2], R Sinkus[3].*
[1]Harvard Medical School and Brigham and Women's Hospital, Boston, MA, USA; [2]Boston University, Boston, MA, USA; [3]Kings College London, London, UK.

2:30P – 2:45P

040 REAL-TIME HARMONIC MOTION IMAGING FOR FOCUSED ULTRASOUND FOR ABLATION MONITORING OF HIGH-INTENSITY FOCUSED ULTRASOUND TREATMENT *IN VITRO* AND *IN VIVO.* 53
Y Han[1], S Wang[1], T Payen[1], EE Konofagou[1].*
[1]Columbia University, New York, NY, USA.

2:45P – 3:00P

029 SHEAR WAVE ASSESSMENT OF CERVIAL SOFTENING IN PREGNANT RHESUS MACAQUES: *IN VIVO* COMPARISON OF EARLY VS LATE PREGNANCY. 54
IM Rosado-Mendez[1], QW Guerrero[1], LC Drehfal[1], AP Santoso[1], S Kohn[1], M Shotzko[2], ML Palmeri[3], H Feltovich[1,4], TJ Hall[1].*
[1]University of Wisconsin-Madison, Madison, Wisconsin, USA; [2]Wisconsin National Primate Research Center, Madison, Wisconsin, USA; [3]Duke University, Durham, North Carolina, USA; [4]Intermountain Healthcare, Provo, Utah, USA.

3:00P – 3:15P

060 MONITORING GLIOMA PROGRESSION IN MOUSE BRAIN WITH MRE 55
N Nazari[1], M Nowicki[2,4], S Lawler[2,4], R Sinkus[3], PE Barbone[1], S Patz[2,4].*
[1]Boston University, Boston, MA, USA; [2]Harvard Medical School, Boston, MA, USA; [3]Kings College London, London, UK; [4]Brigham and Women's Hospital, Boston, MA, USA.

3:15P – 3:30P

078 INVESTIGATING SKIN MECHANICAL ANISOTROPY USING SHEAR WAVE ELASTOGRAPHY UNDER MULTI-DIRECTIONAL TENSILE STRAIN. 56
E Simon[1,2], JC Bamber[1]*
[1]Joint Department of Physics and Cancer Imaging Centre, the Institute of Cancer Research and Royal Marsden Hospital, Sutton, London, UK; [2]François Rabelais University, Inserm UMR U930 and University Hospital Center of Tours, Tours, FRANCE

3:30P – 4:00P
COFFEE BREAK Morey Room

Monday 4:00P – 5:30P
Session MIP–1: Methods for Imaging Elastic Tissue Properties – I

Chair: TJ Hall, USA *Co-Chair: TJ Royston, USA* Morey Room

Page No.

4:00P – 4:15P

065 MAXIMAL SHEAR STRAIN ESTIMATION FOR IMPROVED BREAST CANCER DETECTION IN AUTOMATED BREAST VOLUME SCANNING. 57

GAGM Hendriks[1], C Chen[1], HHG Hansen[1], CL De Korte[1].*

[1]Medical UltraSound Imaging Center, Radboud University Medical Center, Nijmegen, THE NETHERLANDS.

4:15P – 4:30P

022 MINIMUM VARIANCE BEAMFORMING WITH SPATIAL COMPOUNDING FOR IMPROVED PERFORMANCE OF PLANE WAVE VASCULAR ELASTOGRAPHY. 58

P Verma[1], MM Doyley[1].*

[1]University of Rochester, Rochester, NY, USA.

4:30P – 4:45P

008 IMPROVING ROTATION ELASTOGRAM QUALITY USING SYNTHETIC TRANSMIT APERTURE TECHNIQUE: EXPERIMENTAL RESULTS. 59

Lokesh B[1], AK Thittai[1].*

[1]Indian Institute of technology, Madras, Chennai, Tamil Nadu, India.

4:45P – 5:00P

064 VASCULAR SHEAR WAVE ELASTOGRAPHY: COMPARING SHEAR WAVE VELOCITY IN THE LONGITUDINAL AND TRANSVERSE IMAGING PLANE. 60

HHG Hansen[1], M Pernot[2], S Chatelin[2], M Tanter[2].*

[1]Radboud University Medical Center, Nijmegen, THE NETHERLANDS; [2]Institut Langevin, Paris, FRANCE.

5:00P – 5:15P

033 QUANTITATIVE OPTICAL COHERENCE ELASTOGRAPHY. 61

L Dong[1], P Wijesinghe[2], JT Dantuono[1], DD Sampson[2], PRT Munro[3], BF. Kennedy[2], AA Oberai[1].*

[1]Rensselaer Polytechnic Institute, Troy, NY, USA; [2]The University of Western Australia, Crawley, WA, AUSTRALIA; [3]University College London, UK.

5:15P – 5:30P

066 ELASTOGRAPHY OF PORCINE CORNEA BY TRACKING THE PROPAGATION OF SURFACE ACOUSTIC WAVES USING OPTICAL COHERENCE ELASTOGRAPHY. 62

F Zvietcovich[1], J Yao[1], M Ramirez[1], MR Buckley[1], JP. Rolland[1], KJ Parker[1].*

[1]University of Rochester, Rochester, NY, USA.

Monday 7:30P – 10:30P
Conference Dinner,

Lakeside Dining Room

Proceedings Book Signing

Tuesday, October 18 9:00A – 5:30P*

8:45A – 5:30P
Registration Desk Open — Lobby

8:45A – 5:30P **Session EEX: Equipment Exhibit**
Morey Room

Tuesday 9:00A – 9:52A
Session MMT: Mechanical Measurement Techniques for Tissues

Chair: HHG Hansen, The Netherlands *Co-Chair: S Patz. USA* Morey Room

Page No.

9:00A – 9:15A
071 SIMULTANEOUS ACQUISITION OF MRE AND SLDV FOR COMPARISON OF MAGNETIC RESONANCE AND OPTICAL ELASTOGRAPHY. 63
S Brinker [1], SP. Kearney [1,2], TJ Royston [1,3]. D Klatt[1,3].*
[1]Department of Mechanical & Industrial Engineering, University of Illinois at Chicago, Chicago, IL, USA; [2]Advanced Photon Source, Argonne National Laboratory, Argonne, IL, USA;[3]Richard and Loan Hill Department of Bioengineering, University of Illinois at Chicago, Chicago, IL, USA.

9:15A – 9:30A
045 STUDY OF NONLINEAR INVERSION PARAMETERS FOR MR ELASTOGRAPHY ON PHANTOMS AND HUMAN BRAIN. 64
AT Anderson[1], CL Johnson[2], LM Solamen[3], MDJ McGarry[3], KD Paulsen[3], BP Sutton[1], EEW Van Houten[3,4], JG Georgiadis[1,5].*
[1]University of Illinois at Urbana-Champaign, Urbana, IL, USA; [2]University of Delaware, Newark, DE, USA; [3]Dartmouth College, Hanover, NH, USA; [4]Université de Sherbrooke, Sherbrooke, QC, CANADA; [5]Illinois Institute of Technology, Chicago, IL, USA.

9:30A – 9:37A
036 LOW COST ALTERNATIVE FOR ULTRASOUND HARMONIC ELASTOGRAPHY. 65
CF Otesteanu, SJ Sanabria, O Goksel.*
[1]ETH Zurich, Zurich, SWIZERLAND.

9:37A – 9:52A
027 SINGLE TRANSDUCER LOVIT–ENABLED PHOTOACOUSTIC IMAGING: A FEASIBILITY STUDY. 66
M Theodorou[1], M Jaeger[2], J Fromageau[1], T Petrosyan[2], MX Tang[3], M Frenz[2], JC Bamber[1].*
[1]Joint Department of Physics and CRUK Cancer Imaging Centre, The Institute of Cancer Research and The Royal Marsden NHS Foundation Trust, Sutton, London, UK; [2]Division of Biomedical Photonics, University of Bern, Bern, SWITZERLAND; [3]Department of Bioengineering, Imperial College London, London, UK.

10:00A – 10:30A
COFFEE BREAK — Morey Room

Tuesday 10:30A – 11:30A
Session MPT: MPT: Mechanical Properties of Tissues

Chair: JB Weaver, USA *Co-Chair: T O'Shea, UK* Morey Room

Page No.

10:30A – 10:45A

003 SOFT TISSUE VASCULARITY AND SHEAR WAVE SPEED. 67
KJ Parker[1], J Ormachea[1].*
[1]University of Rochester, Rochester, NY, USA.

10:45A – 11:00A

024 ELASTIC PROPERTIES OF THE ANIMAL LENS AT DIFFERENT INTRAOCULAR PRESSURES. 68
S Park[1], H Yoon[2], C Wu[3], KV Larin[3,4], SY Emelianov[2,5], SR Aglyamov[1].*
[1]University of Texas at Austin, Austin, TX, USA; [2]Georgia Institute of Technology, Atlanta, GA, USA [3]University of Houston, Houston, TX, USA; [4]Baylor College of Medicine, USA; [5]Emory University School of Medicine, Atlanta, GA, USA.

11:00A – 11:15A

025 ULTRASOUND SHEARWAVE ELASTOGRAPHY WITH FORCE SENSING – INTEGRATION DESIGN AND PRELIMINARY *EX-VIVO* RESULTS. 69
MM Nguyen[1], MA Graule[2], AY Huang[2], V Shamdasani[3], BW Anthony[2], H Xie[1]*
[1]Philips Research North America, Cambridge, MA, USA; [2]Massachusetts Institute of Technology, Cambridge, MA, USA; [3]Philips Healthcare, Bothell, WA, USA.

11:15A – 11:30A

082 PERMELASTOGRAPHY: QUANTITATIVE POROELASTIC PROPERTY IMAGING BY COMBINING SHEAR WAVE AND STRAIN ELASTOGRAPHY WITH A FORCE SENSOR. 70
M Theodorou[1,2], J Fromageau[1,2], NM deSouza[2,3], JC Bamber[1,2]*
[1]Joint Department of Physics, Sutton, London, UK; [2]Cancer Research UK Cancer Imaging Centre, Sutton, London, UK; [3]Royal Marsden NHS Foundation Trust, Sutton, London, UK.

Tuesday 11:30A – 12:20P
Session INS: Instrumentation including Phantoms

Chair: AK Thittai, India *Co-Chair: J Benson, USA* Morey Room

Page No.

11:30A – 11:45A

002 CONTROLLING THE SHEAR WAVE FIELD IN SOFT TISSUE USING VIBRATOR ARRAY. 71
C Zemzemi[12], A Zorgani[12], S Catheline[1,2].*
[1]LabTAU INSERM U1032, Lyon, FRANCE; [2]Universtité de Lyon, FRANCE.

11:45A – 12:00P

019 INTRAVASCULAR VS. INTRACARDIAC ARFI: A FINITE-ELEMENT SIMULATION OF CORONARY PLAQUE RESPONSE. 72
CD Herickhoff[1], KT Looby[1], JR Doherty[2], JJ Dahl[1].*
[1]Stanford University, Palo Alto, CA, USA; [2]Kona Medical, Inc., Bellevue, WA, USA.

12:00P – 12:05P

058 ACTUATION SYSTEM FOR LOW FREQUENCY ELASTICITY IMAGING. 73
SW Gordon-Wylie[1], :L Solamen[1], L Tan[1], MDJ McGarry[3], EEW Van Houten[4], JB Weaver[2], KD Paulsen[1,2].*
[1]Thayer School of Engineering, Dartmouth College, Hanover, NH, USA; [2]Geisel School of Medicine, Dartmouth College, Hanover, NH USA; [3]Columbia University, New York, NY, USA; [4]University de Sherbrooke, Sherbrooke Quebec, CANADA.

(Session INS continued on next page)

(Session INS continued from previous page)

12:05A – 12:20P

079 A TOOL FOR SHEAR WAVE GENERATION AND VISUALIZATION WITH THE VERASONICS RESEARCH ULTRASOUND SYSTEM. 74

R Daigle[1], Y Sheng Tung[1].*
[1]Verasonics, Inc, 12016 115th Avenue, NE Kirkland, WA 98034, USA.

12:30P – 2:00P

GROUP LUNCH Lakeside Dining Room

Tuesday 2:00P – 4:00P

Session FIP–1: Forward & Inverse Problems – I

Chair: KD Paulsen, USA *Co-Chair: TJ Hall, USA* Morey Room

Page No.

2:00P – 2:15P

004 REVERBERANT SHEAR WAVE FIELDS IN TISSUES. 75

KJ Parker[1]*, J Ormachea[1], F Zvietcovich[1], B Castaneda[2].*
[1]University of Rochester, Rochester, NY, USA; Pontificia Universidad Católica del Perú, Lima, Perú.

2:15P – 2:30P

038 GENERALIZED ADJOINT METHOD FOR POROELASTIC IMAGE RECONSTRUCTION. 76

L Tan[1]*, MDJ McGarry[3], EEW Van Houten[4], L Solamen[1], JB Weaver[2], KD Paulsen[1,2]*
[1]Thayer School of Engineering, Dartmouth College, Hanover, NH, USA; [2]Geisel School of Medicine, Dartmouth College, Hanover, NH USA; [3]Columbia University, New York, NY, USA; [4]University de Sherbrooke, Sherbrooke Quebec, CANADA.

2:30P – 2:45P

041 COMPLIANCE BOUNDARY CONDITIONS FOR ELASTICITY RECONSTRUCTION USING FEM INVERSE PROBLEM. 77

E Ozkan[1]*, O Goksel[1].*
[1]ETH Zurich, Zurich, SWITZERLAND.

2:45P – 3:00P

047 AN ANALYSIS OF INTRINSIC VARIATIONS OF LOW-FREQUENCY SHEAR WAVE SPEED IN A STOCHASTIC TISSUE MODEL: THE FIRST APPLICATION ON LIVER FIBROSIS. 78

Y Wang[1], M Wang[1], J Jiang[1].*
Michigan Technological University, Houghton, MI, USA.

3:00P – 3:15P

048 BUILDING AN OPEN-SOURCE SIMULATION PLATFORM OF ACOUSTIC RADIATION FORCE-BASED BREAST ELASTOGRAPHY. 79

Y Wang[1], M Wang[1], J Jiang[1].*
Michigan Technological University, Houghton, MI, USA.

3:15P – 3:30P

055 FULL WAVE INVERSION APPROACH FOR ULTRASOUND ELASTOGRAPHY. 80

OA Babaniyi[1]*, M Bayat[2], M Fatemi[2], W Aquino[1].*
[1]Duke University, Durham, NC, USA; [2]Mayo Clinic College of Medicine, Rochester, MN, USA.

3:30P – 3:45P

053 THE COUPLED ADJOINT-STATE EQUATION IN FORWARD AND INVERSE ELASTICITY. 81

DT Seidl[1]*, PE Barbone[2], AA Oberai[3].*
[1]Sandia National Laboratories, Albuquerque, NM USA; [2]Boston University, Boston, MA USA; [3]Rensselaer Polytechnic Institute, Troy, NY USA.

(Session FIP continued on next page)

(Session FIP continued from previous page)

3:45P – 4:00P

030 SPATIALLY VARYING COMPLIANCE ESTIMATED THROUGH THE PULSE WAVE INVERSE PROBLEM: REPEATABILITY IN HEALTHY CAROTID ARTERIES. 82

MDJ McGarry[1,2], IZ Apostolakis[1], P Nauleau[1], EE Konofagou[1].*
[1]Columbia University, New York, NY, USA; [2]Dartmouth College, Hanover, NH, USA.

4:00P – 4:30P

COFFEE BREAK Morey Room

Tuesday 4:30P – 5:07P

Session MIP–2: Methods for Imaging Elastic Tissue Properties – II

Chair: AA Oberai, USA *Co-Chair: C Sumi, Japan* Morey Room

Page No.

4:30P – 4:45P

009 EXPERIMENTAL RESULTS ON THE IMPROVEMENTS IN ROTATION ELASTOGRAM QUALITY USING SPATIAL COMPOUNDING APPROACH. 83

A Arshad Kothawala[1], AK Thittai[1].*
[1]Indian Institute of Technology Madras, Chennai, India.

4:45P – 5:00P

021 GENERATION OF SHEAR WAVES BY LASER IN SOFT MEDIA IN THE ABLATIVE AND THERMOELASTIC REGIMES. 84

P. Grasland-Mongrain[1], Y Lu[1,2], F Lesage[2,3], S Catheline[4], G Cloutier[1,2,5]*
[1]Laboratory of Biorheology and Medical Ultrasonics, University of Montreal Hospital Research Center (CRCHUM), Montreal (QC), CANADA; [2]Institute of Biomedical Engineering, École Polytechnique and University of Montreal, Montreal (QC), CANADA; [3]Department of Electrical Engineering, École Polytechnique of Montreal, Montreal (QC), CANADA; [4]Laboratory of Therapeutic Applications of Ultrasound, Inserm u1032, Inserm, Lyon, FRANCE; [5]Department of Radiology, Radio-Oncology and Nuclear Medicine, University of Montreal, Montreal (QC), CANADA

5:00P – 5:07P

023 BI-PLANE ARTERIAL WALL STIFFNESS ESTIMATION USING SHEAR WAVE IMAGING: A SIMULATION AND PHANTOM STUDY. 85

Y Guo[1], HY Lo[1,2], WN Lee[1,2].*
[1]Department of Electrical and Electronic Engineering, The University of Hong Kong, HONG KONG; [2]Medical Engineering, The University of Hong Kong, HONG KONG.

5.10P – 5.30P ***Group Photograph***

After 5:30P *No Conference Activities*

Wednesday, October 19 9:15A -7:00P

9:00A – 3:00P
Registration Desk Open — Lobby

9:00A – 3:00P **Session EEX: Equipment Exhibit** — Morey Room

Wednesday 9:15A – 10:35A
Session MIP–3: Methods for Imaging Elastic Tissue Properties – III

Chair: EEW Van Houten, USA *Co-Chair: H Xie, USA* — Morey Room

Page No.

9:15A – 9:30A

043 THREE-DIMENSIONAL *IN-VIVO* ELASTICITY IMAGING OF BREAST TISSUE. 86
M Tyagi[1], Y Wang[2], T Hall[2], PE Barbone[3], AA Oberai[1].*
[1]Rensselaer Polytechnic Institute, Troy, NY, 12180, USA; [2]University of Wisconsin-Madison, WI, 53705, USA; [3]Boston University, Boston, MA, 02215, USA.

9:30A – 9:45A

032 NON-LINEAR CHARACTERIZATION OF THE LIVER BY COMBINING SHEAR AND LONGITUDINAL WAVE SPEED WITH STRAIN OBSERVATIONS. 87
SJ Sanabria[1], M Rominger[2], CF Otesteanu[1], E Mazza[3], O Goksel[1].*
[1] Computer-assisted Applications in Medicine (CAiM), ETH Zurich, SWITZERLAND;
[2] Diagnostic and Interventional Radiology, University Hospital of Zurich (USZ DIR), SWITZERLAND;[3]Dept. of Mechanical and Process Engineering, ETH Zurich, SWITZERLAND.

9:45A – 9:50A

063 APPARATUS FOR IMAGING AND MODEL FITTING OF *EX-VIVO* PORCINE KIDNEY. 88
C Schneider[1], M Honarvar[1], R Rohling[1], SE Salcudean[1], C Nguan[2].*
[1] The University of British Columbia, Vancouver, British Columbia, CANADA.
[2] Department of Urology, Vancouver General Hospital, British Columbia, CANADA.

9:50A – 10:05A

007 APPLICATION OF CARDIAC MRI TAGGING SEQUENCES FOR LIVER FIBROSIS STAGING. 89
L Petitclerc[1], G Gilbert[2], G Cloutier[1,3], A Tang[1].*
[1]University of Montreal Hospital Research Center, Montreal, Quebec, CANADA; [2]Philips Healthcare Canada, Montreal, QC, CANADA; [3] Laboratory of Biorheology and Medical Ultrasonics, Montreal, Quebec, CANADA.

10:05A – 10:20A

020 PANCREATIC CANCER DETECTION IN HUMAN RESECTED SPECIMEN USING HARMONIC MOTION IMAGING (HMI). 90
T Payen[1], KP Olive[2], EE Konofagou[1,3] .*
[1]Columbia University, New York, NY, USA; [2]Herbert Irving Comprehensive Cancer Center, Columbia University Medical Center, New York, NY, USA; [3]Columbia University Medical Center, New York, NY, USA.

10:20A – 10:35A

018 GLOBAL TIME DELAY ESTIMATION IN ULTRASOUND ELASTOGRAPHY. 91
HS Hashemi[1,2], H Rivaz[1,2].*
[1]Concordia University, Montreal, Quebec, CANADA; [2]PERFORM Center, Montreal, Quebec, CANADA.

10:35A – 11:05A
COFFEE BREAK — Morey Room

Wednesday 11:05A – 12:35P

Session CAA -2: Clinical and Animal Applications: Breast. – II

Chair: CL De Korte, The Netherlands *Co-Chair: SR Aglyamov, USA* Morey Room

Page No.

11:05A – 11:20A

067 ULTRASOUND ACTIVITY IN THE RSNA-QUANTITATIVE IMAGING BIOMARKER ALLIANCE. 92

TJ Hall[1], BS Garra[2], PL Carson[3], A Milkowski[4], JB Fowlkes[3], O Kripfgans[3], RG Barr[5], M Averkiou[6]*

[1]University of Wisconsin, Madison, WI, USA; [2]VA Medical Center, Washington DC, USA; [3]University of Michigan, Ann Arbor, MI, USA. [4]Siemens Ultrasound, Issaquah, WA, USA; [5]Southwoods Imaging, Boardman, OH, USA; [6]University of Washington, Seattle, Washington, USA.

11:20A – 11:35A

069 THE RSNA-QIBA SHEAR WAVE SPEED PROFILE: CURRENT STATUS, METHODS IN GENERATING THE PROFILE AND A DISCUSSION OF CURRENTLY OPEN AND CLOSED ISSUES. 93

M Dhyani[1], AE Samir[1], ML Palmeri[2], A Milkowski[3], RG Barr[4], D Cosgrove[5], TJ Hall[6], PL Carson[7], BS Garra[8].*

[1]Massachusetts General Hospital, Boston, MA; [2]Duke University, Durham, NC; [3]Siemens Ultrasound, Issaquah, WA, USA; [4]Southwoods Imaging, Boardman, OH, USA; [5]Imperial College School of Medicine, London, UK; [6]University of Wisconsin, Madison, WI, USA; [7]University of Michigan, Ann Arbor, MI, USA; [8]VA Medical Center, Washington DC.

11:35A – 11:50A

068 THE QIBA SHEAR WAVE SPEED PROFILE: IMPLICATIONS FOR QUALITY ASSURANCE, QUALITY MONITORING, REGULATORY EVALUATION AND CLINICAL ACCEPTANCE OF QUANTITATIVE ELASTOGRAPHY. 94

BS Garra[8], M Dhyani[1], AE Samir[1], RG Barr[4], TJ Hall[6], A Milkowski[3], PL Carson[7], D Cosgrove[5].*

[1]Massachusetts General Hospital, Boston, MA; [2]Duke University, Durham, NC; [3]Siemens Ultrasound, Issaquah, WA, USA; [4]Southwoods Imaging, Boardman, OH, USA; [5]Imperial College School of Medicine, London, UK; [6]University of Wisconsin, Madison, WI, USA; [7]University of Michigan, Ann Arbor, MI, USA; [8]VA Medical Center, Washington DC.

11:50A – 12:05P

070 RSNA-QIBA SHEAR WAVE SPEED PROFILE – WHAT THE CLINICAL WORKFLOW WOULD LOOK LIKE AND A REVIEW OF BIOLOGICAL CONFOUNDERS. 95

AE Samir[1], M Dhyani[1], ML Palmeri[2], A Milkowski[3], RG Barr[4], D Cosgrove[5], TJ Hall[6], PL Carson[7], BS Garra[8].*

[1]Massachusetts General Hospital, Boston, MA; [2]Duke University, Durham, NC; [3]Siemens Ultrasound, Issaquah, WA, USA; [4]Southwoods Imaging, Boardman, OH, USA; [5]Imperial College School of Medicine, London, UK; [6]University of Wisconsin, Madison, WI, USA; [7]University of Michigan, Ann Arbor, MI, USA; [8]VA Medical Center, Washington DC.

12:05P – 12:20P

037 RSNA-QIBA COMPARISON OF SHEAR WAVE SPEED ESTIMATION IN VISCOELASTIC PHANTOMS. 96

ML Palmeri[1], TJ Hall[2], BS Garra[3], A Milkowski[4], T Lynch[5], S Chen[6], NC Rouze[1], RG Barr[7], V Shamdasani[8], M Macdonald[9], G Guenette[10], M Dhyani[11], Z Hah[12], A Gee[13], M Couade[14], R Managuli[15], J Chen[7], NA Obuchowski[16], PL Carson[17].*

[1]Duke Univ, Durham, NC, USA; [2]Univ Wisconsin, Madison, WI, USA; [3]VA Med Center, Wash DC, USA; [4]Siemens Ultrasound, Issaquah, WA, USA; [5]CIRS, Inc., Norfolk, VA, USA; [6]Mayo Clinic, Rochester, MN, USA; [7]Southwoods Imaging, Boardman, OH, USA; [8]Philips Ultrasound, Bothell, WA, USA; [9]GE, Milwaukee, WI, USA; [10]Toshiba Medical Research Institute, Redmond, WA, USA; [11]MA Gen Hos, Boston, MA, USA; [12]Samsung Medison, Seoul, SOUTH KOREA; [13]Zonare Medical Systems, Mountain View, CA, USA; [14]Supersonic Imagine, Aix-en-Provence, FRANCE; [15]Hitachi Aloka Medical America, Inc., Wallingford, CT, USA; [16]The Cleveland Clinic, Cleveland, OH, USA; [17]Univ Michigan, Ann Arbor, MI, USA.

(Session CAA continued on next page)

(Session CAA continued from previous page)

12:20P – 12:35P

080 A CROSS-MACHINE COMPARISON OF SHEAR WAVE SPEED ESTIMATIONS IN A PHANTOM AND THE NORMAL FEMALE BREAST. 97

S Sharma[1], R Sinnatamby [2], EO' Flynn[1], A Kirby[1], JC Bamber[1], EJ Harris [1]*

[1]The Institute of Cancer Research and Royal Marsden NHS Foundation Trust, London, UK; [2] Cambridge University Hospitals NHS Foundation Trust, Cambridge, UK.

12:35P – 2:05P

GROUP LUNCH Lakeside Dining Room

Wednesday 2:05P – 3:10P

Session FIP–2: Forward & Inverse Problems – II

Chair: H Rivaz, USA *Co-Chair: J Bamber, UK* Morey Room

Page No.

2:05P – 2:20P

039 PRESSURE BOUNDARY CONDITION ESTIMATION FROM DISPLACEMENT DATA FOR POROELASTIC IMAGE RECONSTRUCTION. 98

*L Tan[1], MDJ McGarry[3], EEW Van Houten[4], L Solamen[1], JB Weaver[2], KD Paulsen[1,2]**

[1]Thayer School of Engineering, Dartmouth College, Hanover, NH, USA; [2]Geisel School of Medicine, Dartmouth College, Hanover, NH USA; [3]Columbia University, New York, NY, USA; [4]University de Sherbrooke, Sherbrooke Quebec, CANADA.

2:20P – 2:35P

049 CONTRAST DETAIL ANALYSIS AND EVALUATION OF MR ELASTOGRAPHY INVERSION ALGORITHMS. 99

L Solamen[1], M McGarry[2], E Van Houten[3], JB Weaver[4], KD Paulsen[1,4]*

[1]Thayer School of Engineering, Dartmouth College, Hanover, NH, USA; [2]Columbia University, New York, NY, USA; [3]University de Sherbrooke, Sherbrooke Quebec, CAN; [4]Geisel School of Medicine, Dartmouth College, Hanover, NH USA.

2:35P – 2:50P

056 CALIBRATED AND DIRECT ELASTIC MODULUS RECONSTRUCTION FROM ULTRASOUND COMPRESSION ELASTOGRAPHY. 100

OA Babaniyi[1], AA Oberai[2], PE Barbone[3].*

[1]Duke University, Durham, NC, USA; [2]Rensselaer Polytechnic Institute, Troy, NY, USA; [3]Boston University, Boston, MA, USA.

2:50P – 2:55P

014 MECHANICAL PROPERTY RECONSTRUCTION OF A BREAST PHANTOM USING 3D DIGITAL IMAGE CORRELATION ABD THE DIET METHOD. 101

A Brazy [1], E Van Houtten[1]*

[1]Université de Sherbrooke, Sherbrooke, Quebec, CANADA.

2:55P – 3:10P

057 COMPARISON OF DIRECT AND NON-LINEAR INVERSION FOR MEASUREMENT OF MECHANICAL PROPERTIES OF THE HIPPOCAMPUS USING MAGNETIC RESONACE ELASTOGRAPHY. 102

LV Hiscox[1], CL Johnson[2], S Hirsch[3], E Barnhill[3], I Sack[3], MDJ McGarry[4], J Huston,[5] E van Beek[1], JM Starr[1], N Roberts[1].*

[1]Univ Edinburgh, UK; [2]Univ Delaware, Newark, DE, USA; [3]Charité Universitätsmedizin, Berlin, GERMANY; [4]Columbia Univ, New York, NY, USA; [5]Mayo Clinic, Rochester, MN, USA.

3:10P – 5:00P

Recess

Wednesday 5:00P – 7:00P

Closing Dinner Reception

Proceeding Book Signing Bar Area

Thank you to Verasonics for their continued support.

Verasonics, Inc.
Redmond, Washington, USA.

Verasonics®

AUTHOR INDEX

AUTHOR	PAGE	AUTHOR	PAGE
Aglyamov, SR	68	Guenette, G	54, 96
Ahmed, O	48	Guo, Y	85
Anderson, AT	64	Hah, Z	96
Anthony, BW	69	Hall, TJ	27, 44, 45, 54, 86, 92, 93, 94, 95, 96
Apostolakis, IZ	30, 46, 82	Han, Y	53
Aquino, W	80	Hansen, HHG	57, 60
Asher, L	34	Harvey, H	36
Averkiou, M	92	Hashemi, HS	91
Babaniyi, OA	80, 100	Heninonen, I	41
Bamber, JC	34, 36, 37, 38, 39, 56, 66, 70, 97	Henry, B	35
Barbone, PE	31, 33, 52, 55, 81, 86, 100	Hendriks, GAGM	57
Barnhill, E	102	Herickhoff, CD	72
Barr, RG	92, 95, 96, 97, 98	Harris, EJ	39, 97
Bayat, M	80	Hirsch, S	102
Bercoff, J	41	Hiscox, LV	102
Bosch, JG	41	Honarvar, M	88
Brazy, A	101	Hong, J	32
Brinker, S	63	Huang, AY	69
Buckley, MR	51, 62	Huston, J	102
Bucklin, M	51	Jaeger, M	66
Caenen, A	40, 43	Jamin, Y	34
Carson, PL	92, 93, 94, 95, 96	Jiang, J	78, 79
Castañeda, B	75	Johnson, CL	102, 64
Catheline, S	71, 84	Kearney, SP	63
Chan, HW	37, 38	Kelly, M	51
Chatelin, S	60	Kennedy, BF	61
Chen, C	55	Kersemans, M	40
Chen, J	96	Ketz, JP	51
Chen, S	96	Kirby, A	97
Chesler, L	34	Klatt, D	63
Chimenti, RL	51	Koers, A	34
Cloutier, G	84, 89	Kohn, S	54
Cosgrove, D	93, 94, 95	Konofagou, EE	23, 26, 28, 30, 46, 53, 82, 90
Costet, A	26	Kothawala, A	83
Couade, M	96	Kripfgans, O	92
Cummings, C	34	Larin, KV	68
Dahl, JJ	72	Lawler, S	57
Daigle, R	74	Lee, W-N	87
Danielson, L	34	Lesage, F	84
Dantuono, JT	61	Li, J	34
Debusschere, N	40	Lipman, SL	29
De Jong, N	41	Lokesh, B	59
De Korte, CL	57	Looby, KT	72
De Souza, N	36, 70	Lopes, F	34
Dhyani, M	93, 94, 95, 96	Lu, Y	84
Dittman, F	25	Lynch, T	96
Doherty, JR	72	Macdonald, M	96
Dong, L	61	Madore, B	31
Doyley, MM	42, 58	Managuli, R	96
Drehfal, LC	27, 44, 45, 54	Mazza, E	87
Eeles, R	36	McGarry, MDJ	25, 102, 33, 32, 46, 64, 73, 76, 82, 98, 99
Ekroll, IK	43	Melki, L	28
Emelianov, SY	68	Milkowski, A	92, 93, 94, 95, 96
Fast, M	39	Morgan, V	36
Fatemi, M	80	Munro, PRT	61
Feltovich, H	27, 44, 45, 54	Nauleau, P	30, 46, 82
Flemister, AS	51	Nayak, R	40
Fowlkes, JB	92	Nazari, N	52, 55
Freedman, J	47	Nguyen, MM	69
Frenz, M	66	Nightingale,KR	29
Fromageau, J	36, 66, 70	Nill, S	39
Garra, BS	92, 93, 94, 95, 96	Nowicki, M	55
Gee, A	96	Oberai, AA	24, 61, 81, 86, 100
Gendin, DI	33	Obuchowski, NA	96
Georgiadis, JG	64	Oelfke, U	39
Ghasemi Amidabadi, M	48	Olive, KP	90
Gilbert, G	89	Ormachea, J	67, 75
Göksel, O	65, 75, 85	O'Flynn, E	97
Gordon -Wylie, SW	73	O'Shea, T	36, 39
Grasland-Mongrain, P	84	Otesteanu, CF	65, 87
Graule, MA	69	Ozkan, E	77
Grondin, J	26	Palmeri, ML	27, 29, 44, 47, 54, 93, 95, 96

AUTHOR	PAGE	AUTHOR	PAGE
Papadacci, C	26	Yao, J	62
Park, S	68	Yengul, SS	31
Parker, KJ	62, 67, 75	Yoon, H	68
Patz, S	52, 55	Yuen Lo, H	85
Paulsen, KD	32, 64, 73, 76, 98, 99	Zemzemi, C	71
Payen, T	53, 90	Zorgani, A	71
Peng, B	79	Zvietcovich, F	62, 75
Pernot, M	40, 43, 60		
Petitclerc, L	89		
Petrosyan, P	66		
Ramirez, M	62		
Richards, MS	51		
Rivaz, H	48, 91		
Roberts, N	102		
Robinson, SP	34		
Rohling, R	88		
Rolland, JP	62		
Rominger, M	87		
Ronan, L	32		
Rosado - Mendez, IM	27, 44, 45, 54		
Rouze, NC	29, 96		
Royston, TJ	35, 63		
Sack, I	25, 102		
Salcudean, SE	88		
Samir, AE	93, 94, 95		
Sampson, DD	61		
Sanabria, SJ	65, 87		
Santoso, AP	54		
Sayseng, V	26		
Schifitto, G	42		
Schneider, C	88		
Segers, P	40, 43		
Seidl, DT	81		
Selladurai, S	49		
Shamdasani, V	69, 96		
Sharma, S	97		
Shcherbakova, DA	40, 43		
Shotzko, M	54		
Simon, E	56		
Sinkus, R	34, 52		
Sinnatamby, R	97		
Solamen, L	32, 64, 73, 76, 98, 99		
Springer, CJ	34		
Starr, JM	102		
Strachinaru, M	41		
Sumi, C	50		
Sutton, BP	64		
Swillens, A	40, 43		
Tan, L	73, 76, 98		
Tang, A	89		
Tang, M-X	66		
Tanter, M	60		
Testu, J	25		
Theodorou, M	66, 70		
Thittai, AK	49, 59, 83		
Tung, YS	74		
Tyagi, M	86		
van Beek, E	102		
Van Dalen, BM	41		
van der Steen, AFW	41		
van Houten, EEW	25, 32, 64, 73, 76, 98, 99, 101		
Vejdani – Jahromi, M	47		
Verma, P	58		
Vos, HJ,	41		
Wang, M	78		
Wang, S	53		
Wang, Y	78, 79, 86		
Weaver, JB	25, 32, 73, 76, 98, 99		
Wijesinghe, P	61		
Wolf, PD	47		
Wu, C	68		
Xie, H	69		

Session TUT: Tutorials
Sunday , October 16 12.00P – 2.00P

084 **MYOCARDIAL ELASTOGRAPHY AND ELECTOMECHANICAL WAVE IMAGING.**

Elisa Konofagou[1].*

[1]Columbia University, 630 West 168th St, P&S 19-418, New York, NY, 10032, USA.

According to the latest report on Heart Disease and Stroke Statistics by the American Heart Association, more than 2150 Americans die of cardiovascular disease each day, an average of 1 death every 40 seconds. Cardiovascular disease currently claims more lives each year in both men and women than the next two most deadly diseases combined, i.e., cancer and chronic lower respiratory disease. Among the cardiovascular diseases, coronary artery disease (CAD) is by far the most deadly causing approximately 1 of every 6 deaths in the United States in 2010. Approximately every 34 seconds, 1 American has a coronary event, and approximately every 1 minute 23 seconds, an American will die of one. It is estimated that an additional 150,000 silent first myocardial infarctions occur each year. Cardiac arrhythmias also lead to a significant number of cardiovascular morbidity and mortality. This irregular heart rhythm causes the heart to suddenly stop pumping blood.

This tutorial will describe the techniques of myocardial elastography and electromechanical wave imaging which have been developed as early detection and diagnosis tools for the aforementioned diseases. These techniques encompass imaging of mechanical (cumulative) or electromechanical (incremental or transient) strain or activation times to respectively highlight the mechanical or electrical function of the myocardium. Myocardial elastography benefits from the development of techniques that have been used for high precision 2D time-shift based strain estimation and high frame rates available to obtain a detailed map of the transmural strain in normal, ischemic and infarcted cases in vivo. These strain imaging techniques aim at achieving high precision estimates through recorrelation techniques and customized cross-correlation methods and are thus successful in mapping the full 2D and 3D strain tensors. Electromechanical wave imaging has been shown to be capable of noninvasively mapping the conduction wave during propagation. High frame rate (>500 frames/s (fps)) and precise 2D imaging of the cardiac deformation is feasible, which allows the transient cardiac motion resulting from the fast electromechanical wave to be mapped in murine, canine and human hearts in vivo.

083 **COMPUTATIONAL METHODS FOR INVERSE PROBLEM SOLUTIONS FOR ELASTOGRAPHIC AND BIOMECHANICAL IMAGING PROBLEMS.**

Assad Oberai[1]*.

[1]Scientific Computation Research Center, Rensselaer Polytechnic Institute, Troy, NY 12180, USA.

Certain types of diseases lead to changes in the microstructural organization of tissue. Altered microstructure in turn leads to altered macroscopic tissue properties, which are often easier to image than the microstructure itself. Thus the measurement of macroscopic properties offers a window into tissue microstructure and health. In Elastography, or more generally Biomechanical Imaging (BMI), we aim to utilize this association between the macroscopic mechanical properties of tissue and its health by generating images of the mechanical properties and using these to infer tissue microstructure and health.

At the heart of BMI lies the solution of an inverse problem in continuum mechanics: given the deformation of the medium (tissue) and a constitutive model, determine the spatial distribution of the material properties. In this talk, I will discuss the well-posedness of this inverse problem and describe efficient and robust algorithms for solving it. I will also describe the development of new constitutive models that are motivated by tissue microstructure, applications of Biomechanical Imaging that include improved non-invasive diagnosis of breast cancer, and quantification of elastic properties from the sub-cellular level to the level of an organ.

Acknowledgements: The support of NIH (NCI-R01CA100373 & NCI-R01CA140271) and the NSF (Grant Nos. 1148124, and 1148111) is acknowledged.

011 **COMPARISON OF THE VISCOELASTIC POWER LAW PARAMETERS ESTIMATED BY MR ELASTOGPRHY AND MULTI-FREQUENCY MR ELASTOGRAPHY.**

J Testu[1], MDJ. McGarry[2], F Dittmann[3], JB. Weaver[4], KD. Paulsen[4], I Sack[3], EEW. Van Houten[1].*
[1]University of Sherbrooke, 2500, boulevard de l'Université, Sherbrooke, Québec, CANADA; [2]Columbia University, 351 Engineering Terrace, MB 8904, 1210 Amsterdam Ave., New York, NY 10027, USA; [3]Charité-Universitätsmedizin Berlin, Departments of Radiology, Charitéplatz 1, Berlin, GERMANY; [4]Dartmouth College, Thayer School of Engineering, 14 Engineering Drive, Hanover, NH 03755, USA.

Background: The use of a reconstruction algorithm able to perform accurate multifrequency magnetic resonance elastography (MMRE) requires some knowledge on the mechanical behavior over frequency of the tissue of interest. Regardless of the use of a rheological model or not, numerous studies agree that the evolution of the complex shear modulus in biological tissue, which has been linked to a wide range of pathologies, takes the form of a power law (PL) [1]. Without the use of any specific viscoelastic model, it is possible to relate the mechanical stimuli with its response in frequency with a two parameter PL to describe independently the storage modulus and the loss modulus. In this case, the PL exponents for both parts of the complex modulus are not constrained to have the same value [2].

Aims: The aim of this study was to compare the PL parameters describing the evolution of the two parts of the complex shear modulus for a multifrequency reconstruction and a combination of reconstructions of the data for the same frequency range (10-20 Hz).

Methods: With data collected from a single volunteer at three frequencies in the range between 10 Hz and 20 Hz two variations of the nonlinear inversion technique (NLI) [3] have been used to reconstruct the frequency dependent viscoelastic properties. The first method is three distinct reconstructions for each frequency while the second is a single multifrequency reconstruction based on the combination of the three sets of data. The multifrequency reconstruction algorithm calculates the two parameters of the PL which best describe the evolution of the storage and loss modulus independently. Alternatively, based on reconstructions from the first method, the average values of both parts of the complex modulus calculated independently at each frequency can be used in a linear regression to find the two PL parameters for these properties.

Results: The averages of the PL exponent, found with a linear regression applied in each voxel of the region of interest for the independent reconstruction at each frequency, are 1.25 for the storage modulus (μ_R) and 0.57 for the loss modulus (μ_I). The PL exponent values calculated with the multifrequency reconstruction algorithm for NLI-MRE are 0.42 and 0.78 for μ_R and μ_I respectively.

Conclusions: Preliminary results show that the PL exponents obtained with the linear regression of the independent reconstruction and with the multifrequency reconstruction are within a similar range of values. These results also suggest that the use of a PL to express the evolution of the both parts of the complex shear modulus with independent exponents is appropriate.

Acknowledgements: EEWH acknowledges financial support from NSERC for this work and is a member of the FRQ-S-funded Centre de recherché du Centre hospitalier universitaire de Sherbrooke (CR-CHUS).

References: [1] Sack I et al.: Soft Matter, 9: pp. 5672-5690, 2013. [2] Clayton EH et al.: Phys. Med. Bio., 56: pp. 2391-2406, 2011. [3] Van Houten E et al.: Magn Reson Med, 45: pp. 827-837, 2001.

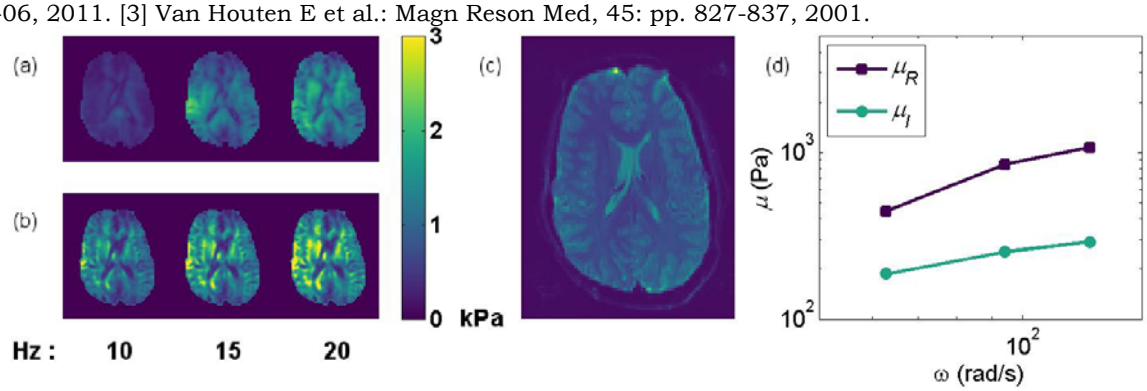

Figure 1 : (a) μ_R independently reconstruct at the three actuation frequency. (b) μ_R calculated with a MMRE reconstruction algorithm providing the two PL parameters. (c) T2 weighted image of the slice of interest. (d) Averages of the storage and loss modulus for the frequencies between 10 and 20 Hz.

026 **OPTIMIZATION OF TRANSMIT PARAMETERS FOR TWO-DIMENSIONAL CARDIAC STRAIN ESTIMATION WITH COHERENT COMPOUNDING *IN SILICO, IN VITRO,* AND *IN VIVO.***

V Sayseng[1], J Grondin[1], C Papadacci[1], A Costet[1], EE Konofagou[1].*
[1]Columbia University, 630 West 168th St, P&S 19-418, New York, NY, 10032, UNITED STATES.

Background: Myocardial elastography identifies ischemia and infarction by imaging the geometric cardiac strains. Diverging waves (DW) allow acquisitions at high frame rates, trading off spatial resolution. Our group has shown that coherent compounding of diverging waves improves the stain estimation quality while maintaining a high frame rate, but the optimal transmit parameters remain unknown.
Aims: Determine how three transmit parameters—number of DW transmitted, number of elements in subaperture (SA), and angular aperture (AA)—affect strain estimation accuracy in silico, in vitro, and in vivo.
Methods: *In silico:* Short-axis cross-sectional views of the systolic left ventricle were simulated in Field II as a 2D annulus undergoing symmetric radial thickening over 100 frames. Decorrelation was simulated by adding uncorrelated noise with the same power spectrum as the RF; the amplitude ratio of RF to noise was defined as SNR_{decorr}. The numerical phantom (SNR_{decorr}=[2-5]) was imaged with following parameter ranges: DW=[1-15], SA=[11-51], and AA=[60°-120°] using a simulated 64-element and 2.5 MHz phased array. Interframe axial and lateral strains were derived from 2D interframe displacements obtained via 1D normalized cross-correlation. The mean strain difference was calculated as the mean of the point-by-point differences between the estimated and theoretical values. *In vitro:* A hemiellipsoid polyvinyl alcohol (PVA) phantom was attached to a water pump that created roughly 30% strain radially in order to mimic the systolic left ventricle. A Vantage system (Verasonics, Redmond, WA) was programmed with the same sequences used in the simulation and cross-sectional views were acquired. 2-D cumulative strains were derived from cumulative displacements. Strain areas with the highest estimator ambiguity, where strains fluctuated around 0%, are the most challenging to estimate. The axial strain error was thus defined as the mean strain value in a lateral ROI, and the lateral strain error was defined as the mean strain value in an anterior ROI. *In vivo*: A canine's LAD was ligated. After 4 days, open chest echocardiography was performed with the Vantage using a single diverging wave (DW=1/SA=64/AA=90°) sequence and an optimized compounding one (DW=11/SA=21/AA=90°). The heart was harvested and stained with tetrazolium chloride (TTC) to localize the infarct.
Results: *In silico:* At SNR_{decorr}=2, parameters DW=15, SA=11, and AA=60° reduced interframe axial/lateral strain error by 47%/44%, 13%/18%, and 13%/8%, compared to DW=3, SA=15, and AA=120°, respectively. Similar error reductions were found with SNR_{decorr}>2 (Fig. 1A-B). *In vitro:* Comparing DW number, DW=3/SA=11/AA=90° reduced cumulative axial/lateral strain error by 10%/32% relative DW=1/SA=64/AA=90°. Comparing SA, DW=3/SA=11/AA=90° reduced axial/lateral strain error by 22%/21% relative DW=3/SA=51/AA=90°. Comparing AA, DW=3/SA=31/AA=120° and DW=3/SA=31/AA=90° yielded <1% difference in either axial or lateral strain error. *In vivo*: The LAD ligation generated an infarct in the anterior-septal region. Both single-wave and compounding ME localized the infarct via radial strain estimation, but the former erroneously identified the anterior-lateral region as infarcted as well (Fig. 1C-D).

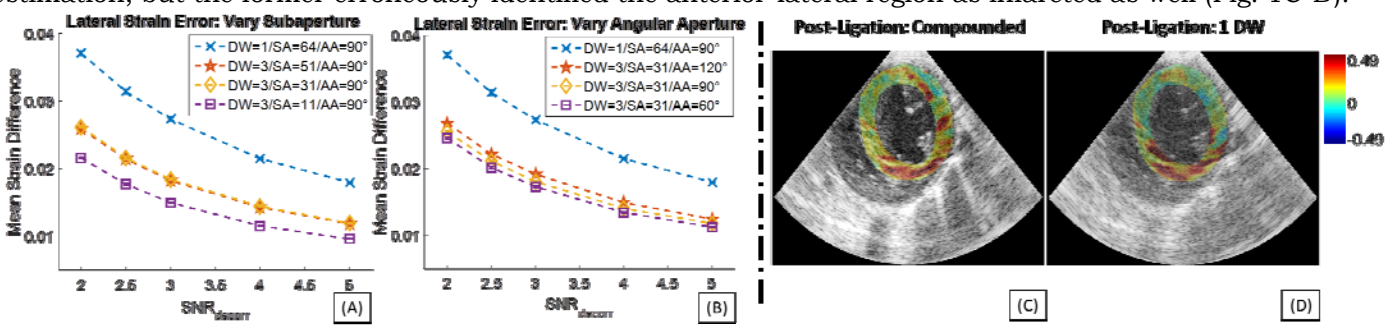

Fig 2. *(A,B): In silico* results showing that SA=11 and AA=60° estimated interframe lateral strain with the least error over SNR_{decorr}=[2,5]. *(C,D):* Short-axis views of canine heart 4 days after LAD ligation, imaged with DW=1/SA=64/AA=90° (D) and DW=11/SA=21/AA=90° (C). Both sequences localize the infarct, but the single wave sequence (D) incorrectly identifies the anterior-lateral region as infarcted.

Conclusions: *In silico* results indicated that DW=15, SA=11, and AA=60° gave the most accurate strain estimates. *In vitro* strain estimates corroborated those simulation results: DW=5, SA=11, and AA=90° yielded the lowest strain errors (DW=5 was the highest value tested, and AA=60° generated a field-of-view too narrow for the phantom). *In vivo* results indicate that DW=11/SA=21/AA=90° produces considerably more accurate strains compared to the single diverging wave sequence.

Acknowledgements: Supported in part by NIH funding (EB006042 and HL094410)

.

031 **SHEAR WAVE SPEED ESTIMATION COMPARISON OF EARLY AND LATE PREGNANCY IN THE *IN VIVO* HUMAN UTERINE CERVIX.**

LC. Drehfal[1], H Feltovich[1,2], IM Rosado-Mendez[1], ML. Palmeri[3], TJ. Hall[1].*
[1]University of Wisconsin, Madison, WI, USA; [2]Intermountain Healthcare, Provo, UT, USA. [3]Duke University, Durham, NC, USA.

Background: The cervix plays a critical role during pregnancy. It must remain firm throughout most of the gestational period, but then soften, shorten, and dilate to allow for vaginal delivery of the fetus at term. This process is referred to as cervical remodeling and premature changes during this process may lead to preterm birth.[1] Currently, there is a need for a non-invasive objective method to assess changes in cervical softness. Shear Wave Elasticity Imaging (SWEI) is a promising technique for quantifying elastic properties of soft tissues. As pregnancy progresses, and the cervix softens, shear wave speed (SWS) should decrease in the cervix.

Aims: The aim of this study is to determine if there is a significant difference between shear wave speed in early (1st trimester) and late (3rd trimester) pregnancy to assess sensitivity of SWEI at detecting changes in cervical remodeling.

Methods: For a previous 3rd trimester study [2], female patients (n = 18) scheduled for induction of labor at term with cervical ripening were recruited. Patients (n=10) in the 1st trimester (<14 weeks) were recruited. Scanning was performed using a Siemens Acuson S-series Ultrasound system. A prototype catheter transducer (128 elements, 14mm aperture, 3mm diameter) operated in linear array mode was used to scan from the outside of the cervix. The probe was secured to the clinician's hand, with the active aperture on her fingertip, and then placed into a sterile glove filled with gel for acoustic coupling. The clinician's finger was placed on top of the anterior (3rd trimester) or posterior (1st trimester) cervix and aligned parallel to the endocervical canal midway between the external os and the internal os. 10 replicate SWS measurements were made at this location. Displacements were estimated using Loupas' algorithm [3] and SWS was estimated using a RANdom SAmple Consensus method (RANSAC).[4]

Results: For 1st trimester, the SWS estimates at the posterior position were 4.09+/-1.18 m/s (n = 10) and in 3rd trimester SWS estimates were 2.13+/-0.66 m/s (n = 18) at the anterior position. Using a Wilcoxon signed rank test a p-value < 0.001 was obtained, indicating a significant difference between 1st and 3rd trimester SWS estimates.

Conclusions: Previous studies have shown there is large spatial variability in SWS estimates in the non-pregnant cervix and determined an appropriate sampling location.[5] That study did find a slight difference between anterior and posterior mid-positions in the *ex vivo* non-pregnant cervix but differences were small and likely due to inadequate sample numbers. The significant difference in SWS estimates in 1st and 3rd trimester shows that SWEI is able to detect changes in the cervix in early vs. late pregnancy and may be a potential tool for applications in preterm birth.

Acknowledgements: This work was supported by National Institutes of Health grants T32CA009206 from the National Cancer Institute and F31HD082911 from the Eunice Kennedy Shriver National Institute of Child Health and Human Development and Intermountain Medical and Research Foundation. We are also grateful to Siemens Healthcare Ultrasound division for equipment loan and support.

References:

[1] Vink, J, Feltovich H. Cervical etiology of spontaneous preterm birth. *Semin Fetal Neonatoal Med* 2016; **21:** 106-112. [PMID: 16846143].
[2] Carlson, LC, Romero, ST, Palmeri, ML, del Rio, AM, Esplin, SM, Rotemberg, VM, Hall, TJ, Feltovich, H. Changes in shear wave speed pre- and post-induction of labor: a feasibility study. *Ultrasound Obstet Gynecol* 2015; **46:** 93-98. [PMID: 25200374].
[3] Pinton, GF, Dahl, JJ, Trahey, GE. Rapid tracking of small displacements with ultrasound. *IEEE Trans Ultrason Ferrorelectr Freq Control* 2006; **53:** 1103-1117. [PMID: 26776146].
[4] Wang, MH, Palmeri, ML, Rotemberg, VM, Rouze, NC, Nightingale, KR. Improving the robustness of time-of-flight based shear wave speed reconstruction methods using RANSAC in human liver in vivo. *Ultrasound Med Biol* 2010; **36:** 802-813. [PMID: 20381950].
[5] Carlson, LC, Feltovich, H, Palmeri, ML, del Rio, AM, Hall, TJ. Statistical analysis of shear wave speed in the uterine cervix. *IEEE Trans Ultrason Ferrorelectr Freq Control* 2014; **61:** 1651-1660. [PMID: 25392863].

035 **REPRODUCIBILITY AND ANGLE INDEPENDENCE OF ELECTROMECHANICAL WAVE IMAGING FOR THE MEASUREMENT OF ELECTROMECHANICAL ACTIVATION DURING SINUS RHYTHM IN HEALTHY HUMANS.**

L Melki[1], EE Konofagou[1].*
[1]Columbia University, PS 19-405, 6330 West 168th Street, New York, NY, 10032, USA.

Background: Electromechanical Wave Imaging (EWI) is an ultrasound-based technique that has been shown to directly and non-invasively map the transmural electromechanical activation in all four cardiac chambers in vivo [1]. In previous studies, EWI has been shown reproducible in simulations and canine experiments [2], as well as within same acquisitions across consecutive cardiac cycles in open-chest dogs [3]. However, reproducibility in closed-chest humans has not been investigated. Furthermore, it is critical for clinical applications to reliably measure the activation sequence independently of the imaging view.
Aims: In this study, we demonstrate the reproducibility and angle independence of EWI for the assessment of electromechanical activation during sinus rhythm in healthy humans.
Methods: A 2.5 MHz phased array was used with a Verasonics system (Verasonics, Redmond, WA) to perform EWI on a healthy human heart in three standard echocardiographic views: parasternal long-axis, and apical 4- and 2-chamber. We acquired RF frames successively twice for each view during sinus rhythm for 2 seconds at 2000 frames/s with an unfocused flash sequence at a depth of 20 cm. We estimated the axial incremental displacement and strains using 1D RF cross correlation with a window size of 9.2 mm and a window shift of 0.385 mm, and a least-squares kernel of 5 mm respectively. We defined the wavefront of electromechanical activation as the first time-point at which the incremental strain value changes from relaxation to contraction after the onset of the QRS complex. Activation maps of the zero-crossing timings were generated and compared *1)* within the same acquisition across consecutive cardiac cycles by computing the absolute activation time difference between the two isochrones (Fig.1); *2)* within the same view across successive acquisitions by averaging the activation times through similar myocardium wall regions; and *3)* within equivalent LV regions across different imaging angles by comparing the posterior wall between the parasternal and apical 2-chamber views, respectively the septal wall between the parasternal and apical 4-chamber views.

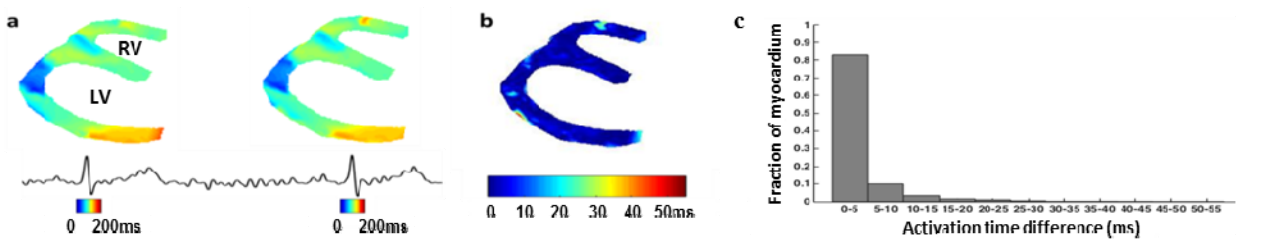

Fig.1: EWI repeatability during SR for healthy subject within same parasternal long-axis acquisition. The origin of the isochrones corresponds to the onset of the QRS complex. (a) Parasternal long-axis view isochrones for two consecutive cardiac cycles. (b) Difference map and (c) histogram of the absolute activation time difference between the two parasternal long-axis isochrones. LV = left ventricle, RV = right ventricle.

Results: *1)* In the 2-chamber view, 90% of the myocardium exhibits activation time differences between the two consecutive isochrones of less than 5 ms (ie. 3% of the maximum activation time), compared to 80% in the parasternal long-axis view (Fig.1). In the 4-chamber view, 50% of the activation time differences fall under 5 ms and 80% are under 10 ms. *2)* Comparison across acquisitions in the same view yielded very similar results. Average activation times in parasternal long-axis and 2-chamber view walls varied by 1.9%, respectively 2.6%. However in the 4-chamber view, we get the highest activation time average fluctuation of 12.4% in the lateral wall, with a small variation of 2.0% for the septal and RV walls. *3)* Finally at different imaging angles, we observed similar isochrone patterns ranging from 25 to 175 ms, even though activation times in specific regions could show discrepancies of up to 35 ms.
Conclusions: EWI was capable of characterizing the SR electromechanical activation and of reliably obtaining the same pattern across different acquisitions and views. These findings indicate that EWI is a reproducible and angle independent technique that can map the electromechanical activation in sinus rhythm in human hearts *in vivo*.
Acknowledgements: Supported in part by NIH EB006042 and HL094410.
References: [1] Provost J, Lee W-N, et al., Imaging the Electromechanical Activity of the Heart *In* Vivo, Proc. Natl. Acad. Sci. U.S.A., Vol. 108, No. 21, pp. 8565–8570, 2011. **[2]** Provost J, Gurev V, et al., Mapping of Cardiac Electrical Activation with Electromechanical Wave Imaging: An In Silico–*In Vivo* Reciprocity Study, Heart Rhythm, Vol. 8, No. 5, pp. 752-759, 2011. **[3]** Costet A, Provost J, et al., Electromechanical Wave Imaging of Biologically and Electrically Paced Canine Hearts *In Vivo*, Ultrasound in Med. & Biol., Vol. 40, No. 1, pp.177-187, 2014.

046 **A COMPARISON OF ULTRASONIC SHEAR WAVE ATTENUATION ESTIMATES USING 2-D FOURIER TRANSFORM AND AMPLITUD-BASED METHODS.**

SL Lipman[1], NC Rouze[1], ML Palmeri[1], KR Nightingale[1].*

[1]Duke University, Room 1427, FCIEMAS, 101 Science Drive, Box 90281, Durham, NC, USA

Background: Commercially available ultrasound shear wave (SW) reconstruction methods often assume that human tissues are elastic; however, tissues are known to be viscoelastic (VE) materials that are characterized by dispersion and attenuation. Several methods have been developed to measure SW dispersion, but quantifying SW attenuation has been less successful, particularly using amplitude based methods. Measured SW displacement amplitudes are dependent on geometric spreading [1], shear attenuation, jitter, and bias in ultrasonic displacement amplitude estimation. Recent developments using 3D single track location (STL) SW imaging have significantly reduced the error in effective tracking location arising from speckle bias, better preserving the relative amplitudes of the SW.

Aims: A SW can be modeled as a cylindrical wave, whose geometric decay is $1/\sqrt{(r)}$ when using a cylindrically symmetric source. We have developed an amplitude-based method that employs 3D STL SW imaging and geometric correction to quantify shear attenuation.

Methods: 3D finite element models simulated the dynamic response of an acoustic radiation force impulse (ARFI) excitation from a circular piston (beamwidth = 1.4 mm) in clinically-realistic three parameter VE material models. Gaussian white noise was added to the temporal SW velocity profiles to mimic jitter (25 dB SNR). Ten realizations of noise were combined to model 10 radial trajectories from the excitation in the lateral-elevation plane. The time-domain Fourier Transform (FT) of these profiles was computed and attenuation as a function of frequency was estimated using the ratio of the magnitude of the spectra at two radial positions (1.8 mm and 3.8 mm) accounting for geometric decay. The results are compared with shear attenuation estimation obtained using the spectral spreading 2D-FT attenuation method [2]. RMSE compared to the analytic solution was calculated for both methods over the frequency range of 150 Hz to 400 Hz.

Results: Figure 1 shows the frequency dependent SW attenuation from the analytic solution for an example VE material (μ_1 = 4 kPa, μ_2 = 16 kPa and η = 4 Pa-s), along with the estimated attenuation values from the amplitude-based method (RMSE= 0.26 Np/cm) and the 2D-FT method (RMSE= 0.50 Np/cm). The 2D-FT attenuation measurements show a consistent bias with frequency, whereas the amplitude-based methods have a smaller, but increasing bias with increasing frequency. Amplitude based methods may be challenged by low SNR of individual frequency components, but these methods can be used over a smaller spatial extent, whereas the 2D-FT methods use a larger field-of-view, and assume tissue homogeneity over that larger region.

Conclusions: These methods provide the foundation for using 3D SW imaging to experimentally quantify shear attenuation.

Acknowledgements: The authors would like to thank Ned Danieley for computer system administration and NIH funding source R01-EB002132.

References:

[1] N. C. Rouze, M. L. Palmeri, and K. R. Nightingale, “An analytic, fourier domain description of shear wave propagation in a viscoelastic medium using asymmetric gaussian sources,” The Journal of the Acoustical Society of America, vol. 138, no. 2, 2015.

[2] I.Z. Nenadic, M.W. Urban, Heng Zhao, W. Sanchez, P.E. Morgan, J.F. Greenleaf, and Shigao Chen. Application of attenuation measuring ultrasound shearwave elastography in 8 posttransplant liver patients. In Ultrasonics Symposium (IUS), 2014 IEEE International, pages 987{990, Sept 2014.

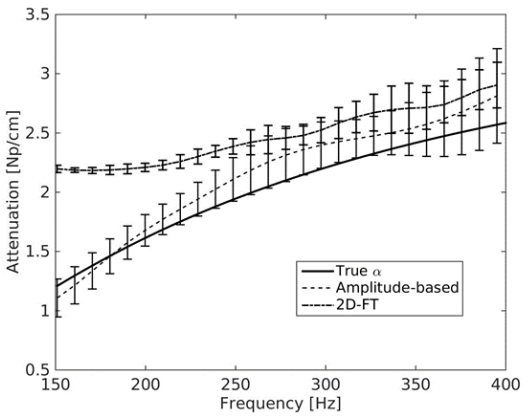

061 **COMPLIANCE ESTIMATION AND MAPPING USING PULSE WAVE IMAGING (PWI): *IN VITRO* VALIDATION AND *IN VIVO* FEASIBILITY**.

IZ Apostolakis[1]*, P Nauleau[1], MDJ. McGarry[1,2], EE. Konofagou[1].
[1]Columbia University, New York, NY, USA; [2]Dartmouth College, Hanover, NH, USA.

Background: Pulse Wave Velocity (PWV), a surrogate marker of arterial stiffness, has been associated to cardiovascular mortality, local vascular pathology and organ damage. Arterial compliance is the ability of a vessel to distend and increase volume with increasing intraluminal pressure and is used as an indication of arterial stiffness. The Bramwell-Hill equation links PWV with arterial compliance. Compared to the Moens-Korteweg model, the Bramwell-Hill model is considered to be more general since it does not assume thinned-walled and homogeneous arteries. Pulse wave imaging (PWI) is a noninvasive technique developed by our group for tracking the propagation of pulse waves along the arterial wall at high spatial and temporal resolution. It has been previously enhanced in order to track the piecewise PWVs (pPWVs) over smaller segments of the imaged arterial wall and produce PWI stiffness maps [1]. However, the Moens-Korteweg model used by that method suffers from a number of idealistic assumptions.

Aims: In the present study PWI was extended with the Bramwell-Hill model to produce PWI compliance measurements (CPWI) and also generate CPWI maps. Subsequently, these values were validated in vitro against independent compliance measurements. Finally, the feasibility of CPWI estimation and mapping was tested in vivo.

Methods: Silicone gel was used to construct a phantom with stiff and soft segments along the longitudinal axis. Subsequently, it was connected to a peristaltic pump generating pulse waves. The setup was scanned using a 5 MHz linear array connected to a research scanner (Verasonics Inc., Redmond, WA). A coherent compounding sequence was used with 5 plane waves at 1667 Hz to image the pulse wave propagation. Synchronized intraluminal pressure measurements were made with a pressure catheter inside the phantom's lumen. Consequently, using synchronized vessel diameter and intraluminal pressure measurements compliance was estimated independently by investigating the pressure-area relationship. Furthermore, the right common carotid arteries of 4 healthy volunteers and the carotids of 2 atherosclerotic patients were scanned with the same sequence. Axial wall velocities (v-PWI) were estimated and depicted over time to generate spatiotemporal maps of the pulse propagation. The regional and piecewise (40-point kernels, 50% overlap) PWVs and associated r2 values were calculated by performing linear regression on the 50% upstroke markers of the vPWI. Subsequently, the corresponding CPWI values were estimated via the Bramwell-Hill equation.

Results: Figs. 1(a), (b) show the CPWI maps generated for the soft and stiff sections of the phantom. In the soft section, mean regional CPWI was found to be 8.1±0.45·10-9 m2/Pa and in the case of the stiff section, 4.4±0.19·10-9 m2/Pa (3 pump cycles). These were in agreement with the dynamic testing compliance values in the case of the soft (8·10-9 m2/Pa) and the stiff phantom (4.23·10-9 m2/Pa) respectively. A CPWI map for a healthy subject is shown in Fig. 1(c). Among the 4 healthy subjects, mean regional CPWI was 1.05±0.4·10-9 m2/Pa. This is in agreement with values found in literature [2]. Finally, Figs. 1(d), (e) depict the compliance maps generated in the case of two atherosclerotic patients. These CPWI maps are characterized by increased variability as well as by some low values indicating calcifications. Especially in the case of Fig. 1(d) calcification in the center plaque is implied by the prominent acoustic shadowing of the posterior wall.

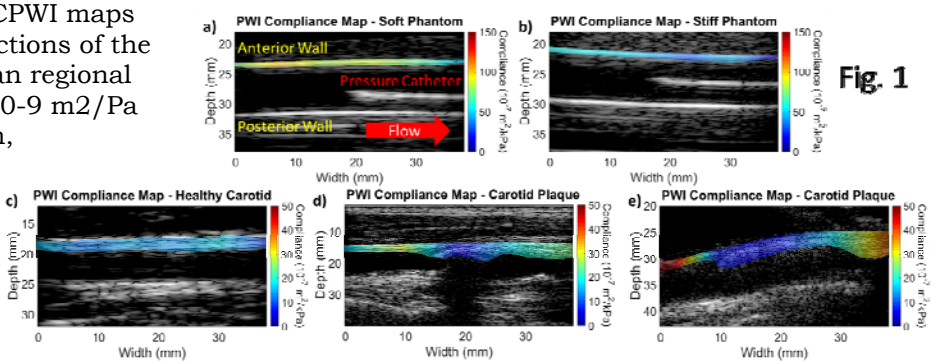

Fig. 1

Conclusions: This study validated CPWI measurements in vitro against independent compliance estimation. Furthermore, the feasibility of in vivo CPWI measurements and mapping was demonstrated in vivo in both healthy and atherosclerotic subjects. These measurements allow for detailed inspection of focal vascular pathology and may provide critical patient care information.

Acknowledgements: Funding from NIH R01HL098830

References: [1] Apostolakis et al., 2016, [2] Gamble et al., 1994.

062 **TOWARD VALIDATION FOR SHEAR WAVE ELASTOGRAPHY USING TORSIONAL VIBRATION RHEOMETRY IN SOFT GELS.**

SS. Yengul[1], PE. Barbone[1], B Madore[2].*
[1]Boston University, Boston, MA, 02215, USA;
[2]Harvard University and Brigham and Women's Hospital, Boston, MA, 02115, USA.

Background: Validating shear wave elastography (SWE) measurements between modalities or between an elastography modality and a mechanical measurement is hindered by one or both of two confounding factors: (a) the measurements being compared are not entirely independent [1],[2] and (b) the mechanical measurement is performed on a similar but not the same physical sample [2],[3].

Aims: Validate ultrasound acoustic radiation force impulse (ARFI) based SWE measurements in homogeneous soft gel samples by comparison to independent mechanical testing.

Methods: A custom phantom was designed using a recipe from [4]. A novel torsional vibration rheometry (TVR) technique was developed to allow both dynamic mechanical testing and SWE on the same sample. Viscoelastic solid material parameters are extracted from the raw torque and displacement rheometer measurements using a model-based technique that accounts for the torsional modes of vibration in the cylindrical sample. SWE code [5] was implemented on a Verasonics research ultrasound system and the data was analyzed using a shear wave spectroscopy technique [6] that enabled estimation of a frequency dependent complex shear modulus. Three samples each of two different bloom strength gelatin were measured five times each (2 TVR and 3 SWE measurements) in an interleaved fashion.

Results: Both TVR and SWE permit repeatable frequency dependent measurement of the complex shear modulus, i.e. of both the storage (G') and loss moduli (G''). The dispersion observed in G' shows good agreement between the two methods; G'' estimates are much higher in the TVR measurement than in the SWE measurement. The linear frequency extrapolation of the SWE-measured G' to zero frequency gives an erroneous prediction of quasi-static behavior.

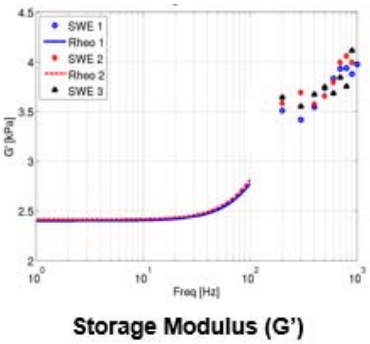

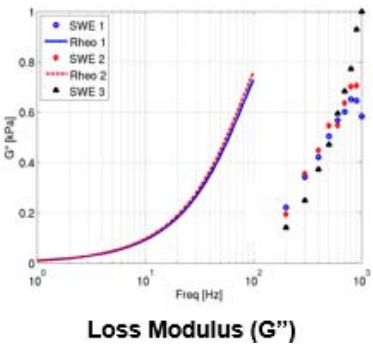

(a) (b) (c) (d)

Figures: (a) TVR setup (b) SWE setup & parameters (c), (d) plots showing comparison of two rheometry and three SWE measurements of G' and G'' on one of the six gelatin samples used in the study.

Conclusions: Frequency dependence of the shear modulus is an important consideration in comparing SWE measurements with mechanical testing, as found in earlier studies [7]. Torsional vibration rheometry appears to be overestimating the loss modulus (G'').

Acknowledgements: Financial support from the BU-BWH Partnership; Lab-space, equipment and helpful discussions from the BWH Focused Ultrasound Lab are gratefully acknowledged.

References:

[1] Catheline et al. JASA (2004) 116(6)
[2] Oudry et al. PMB 59 (2014)
[3] Okamoto et al. PMB 56 (2011)
[4] Hall T.J, et al. IEEE-UFFC 1997, 44(6), 1355-65
[5] Nordenfur, T., MS Thesis, KTH, 2013
[6] Deffieux, T. et al., IEEE-TMI 2009, 28(3)
[7] Nightingale, et al, IEEE-UFFC 2015, 62(1)

050 **POROELASTIC MECHANICAL PROPERTIES OF BRAIN TUMORS USING INTRINSIC ACTUATION MR ELASTOGRAPHY.**

L Solamen[1], MDJ McGarry[2], EEW Van Houten[3], J. Hong[4], L. Ronan[4], JB Weaver[5], KD Paulsen[1,5].*
[1]Thayer School of Engineering, Dartmouth College, Hanover, NH, USA; [2]Columbia University, New York, NY, USA; [3]University de Sherbrooke, Sherbrooke Quebec, CAN; [4] Dartmouth Hitchcock Medical Center, Lebanon, NH, USA; [5]Geisel School of Medicine, Dartmouth College, Hanover, NH USA.

Background: Intrinsically actuated poroelastic MR elastography (IA-pMRE) is a technique which estimates tissue mechanical and hydrodynamic properties using measurements of displacement during the cardiac cycle, and does not require external vibration as in traditional MRE. Compared to conventional MRE, which obtains displacements in the range of 25-100Hz, IA-pMRE uses intrinsically generated low frequency (1-2Hz) displacements for elastography reconstruction.

Aims: Non-invasive differentiation of brain tumors is not always definitive, and more accurate imaging assessments could inform patient management decisions. Externally actuated MRE has shown promise in biomechanical characterization of intracranial tumors. [1] Here, we present initial data on mechanical and hydrodynamical signatures of 7 patients (2 metastatic tumors, 1 meningioma, 4 glioblastoma) using low frequency IA-pMRE.

Methods: Intrinsic actuation MRE generates brain tissue displacement maps from the natural cerebrovascular pulsations arising from pressure variations during the cardiac cycle. [2] A retrospectively gated phase contrast angiography sequence is used to acquire 8 displacement images across one cardiac cycle followed by a Fourier transform to extract motion at the cardiac frequency. Harmonic equations of motion and a nonlinear inversion algorithm, which assumes a poroelastic mechanical model, is used to recover the shear modulus (stiffness) and hydraulic conductivity (ease of fluid flow) of brain tissue.[3] Seven patients diagnosed with various types of brain tumors were enrolled and compared to healthy controls with no known neurological conditions. Tumor regions were segmented and compared to the background brain tissue.

Results: Regions identified as tumor consistently had higher shear modulus values than the surrounding healthy tissue. Contrast between tumor and healthy brain tissue exists, however, stiffness does not appear to differentiate tumor types (similarly to findings from externally actuated MRE studies). [1]

Conclusions: IA-pMRE is a promising technique that enables study of neurological diseases without requiring externally applied vibration traditionally used during MRE exams and can be introduced as part of standard MRI protocols. Future work will increase the number of patients enrolled in the study and analyze other properties, for example, the hydraulic conductivity, to provide more information on the mechanical environment. [4]

Acknowledgements: This work was supported in part by NIH grant R01 EB018230 awarded by NIBIB

References: [1] Simon M., Guo, J., et al. "Non-invasive characterization of intracranial tumors by magnetic resonance elastography" New Journal of Physics, 2013, 15(8):085024. [2] Weaver, John B., Pattison, A.J., et al. "Brain mechanical property measurement using MRE with intrinsic activation." Physics in Medicine and Biology, 2012 57(22): 7275. [3] Perriñez, P., Pattison, A.J., et al. "Contrast detection in fluid-saturated media with magnetic resonance poroelastography." Medical Physics, 2010, 37(7): 3518-3526. [4] Pattison, A., McGarry, M., et al. "Spatially-Resolved Hydraulic Conductivity Estimation Via Poroelastic Magnetic Resonance Elastography" IEEE Transactions on Medical Imaging, 2014, 33(6): 1373-1380.

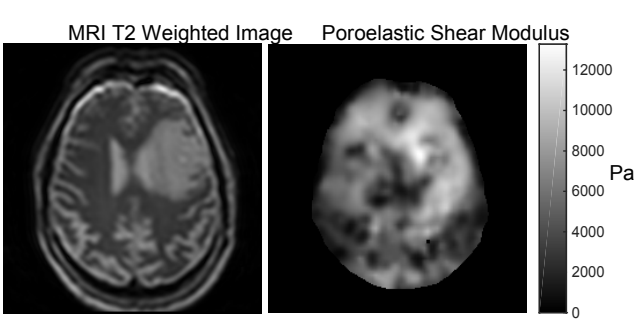

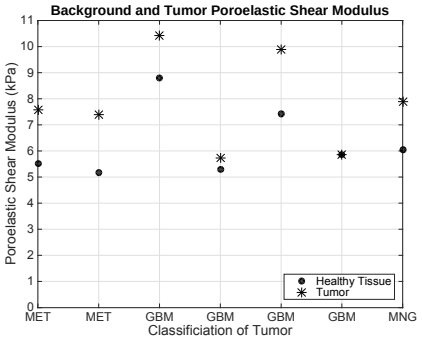

Figure 1:Cross sectional slices of patient with metastatic cancer. Clinical MRI T2 weighted image (left and poroelastic shear modulus map (right). Figure 2:Stiffness of segmented tumor (.) compared to the rest of the healthy tissue (*) for various tumor types.

059 **ELASTIC WAVES IN STRONG MAGNETIC FIELDS.**

DI Gendin[1], PE Barbone[1].*
[1]Boston University, Boston, Massachusetts, USA.

Background: Moving a conductor through a magnetic field can generate current and thus create a Lorentz force acting on the conductor. Recently, P. Grasland-Mongrain et al. [1] showed that a Lorentz force can induce elastic waves in a tissue mimicking phantom. Soft tissue is slightly conductive of electricity. Since MRE involves vibrating conducting tissue in a strong magnetic field, the question of how the magnetic field may effect elastic wave propagation naturally arises.

Aims: The purpose of this work is to evaluate the effect that the presence of a strong magnetic field has on wave propagation in an electrically conducting soft elastic medium.

Methods: We specialized the results described in [2]. We began by introducing a Lorentz force into the momentum equation, combined with Maxwell's equations, Ohm's Law, and Hooke's law. We thus derive a modified elasticity tensor $\tilde{C} = C + \alpha G \overline{C}$ that represents the effect of the magnetic field on elastic waves in the medium. Here C is the original elasticity tensor, G is shear modulus, and $\overline{C}$ is a non-dimensional rank four tensor. The non-dimensional parameter α measures the strength of the magneto-elastic effect on elastic wave propagation. It depends on frequency and a combination of electromagnetic and elastic parameters.

Results: For a 1 Tesla magnetic field and vibrations at a frequency of 100Hz, we estimate the range of the magnitude of α to be about 0.4-1.5; at a frequency of 1kHz the range of the magnitude of α is roughly 0.04-0.15. Therefore magneto-elastic effects are small in soft tissues at higher frequencies, such as 1kHz, but may produce measurable, even significant, effects at lower frequencies, such as 100Hz. To the extent they are present, magneto-elastic effects induce anisotropy and enhance damping in elastic wave fields. Magneto-elastic effects are completely absent in non-conducting phantoms.

Conclusions: Magneto-elastic effects can enhance damping and induce anisotropic wave propagation phenomena. The magnitude of the effect is inversely proportional to frequency and may be clinically observable at low frequencies, such as those used in [1].

References: [1]: Grasland-Mongrain, P., Souchon, R., Cartellier, F., Zorgani, A., Chapelon, J. Y., Lafon, C., & Catheline, S. (2014). Imaging of shear waves induced by Lorentz force in soft tissues. *Physical review letters*, *113*(3), 038101.
[2]: Eringen, A. C. (1980). Mechanics of continua. *Huntington, NY, Robert E. Krieger Publishing Co., 1980. 606 p., 1*.
[3]: Griffiths, D. J., & Reed College. (1999). *Introduction to electrodynamics* (Vol. 3). Upper Saddle River, NJ: prentice Hall.

072 **ASSESSING THE VISCOELASTIC PROPERTIES OF ABDOMINAL TUMOR MODELS *IN VIVO* USING MRE.**

J Li[1], L Asher[1], F Lopes[1], C Cummings[1], A Koers[1], L Danielson[1], L Chesler[1], CJ Springer[1], JC Bamber[1], R Sinkus[2], Y Jamin[1], SP Robinson[1].*

The Institute of Cancer Research, London, UK; [2]King's College London, King's Health Partners, St. Thomas' Hospital, London, UK.

Background:

Magnetic resonance elastography (MRE) is being increasingly exploited to directly visualise and quantify tumor mechanical properties *in vivo*. Our initial pre-clinical MRE investigations have demonstrated that MRE can provide acute imaging biomarkers of treatment-induced tumor necrosis [1], and that intracranially-implanted tumors are significantly softer and less viscous than surrounding brain parenchyma [2]. Orthotopic and transgenic mouse models of cancer, which more faithfully emulate human tumor growth patterns and tumor-host stromal interactions, are being increasingly exploited for pre-clinical cancer research. Their effective use must be underpinned by case-specific evidence, establishing that tumor development, progression, radiology and chemoresponsiveness recapitulates the human disease.

Aims: To evaluate the feasibility of using MRE to assess the viscoelastic properties of orthotopic pancreatic ductal adenocarcinoma (PDAC) xenografts, and tumors arising in a transgenic mouse model of *MYCN*-amplified neuroblastoma [3], within the mouse abdomen.

Methods: All experiments were performed in accordance with the UK Animals (Scientific Procedures) Act 1986. Anaesthetised CD1 *nu/nu* mice bearing orthotopic PDAC tumors derived from PANC-1 cells (n=2), and Th-*MYCN* transgenic mice bearing spontaneous neuroblastomas (n=5), were imaged using a 3cm birdcage coil on a 7T Bruker MicroImaging horizontal MRI system (Bruker Instruments, Ettlingen, Germany). MRE data was acquired in the axial plane using a purpose built platform as previously described [1]. Maps of the total amplitude of the mechanical wave (A_{tot}, μm), and absolute value of elasticity G_d and viscosity G_l (both kPa), were reconstructed with an isotropic pixel size of 300 μm, and G_d and G_l determined from a region of interest covering the whole tumor (mean ± 1 s.e.m.).

Results: A_{tot} was larger than 0.3 μm through both tumor types, with wave attenuation along the propagation depth (Figure 1). Homogeneously appearing PDAC xenografts in T_2-weighted images were associated with elevated and discretely distributed regions of elasticity and viscosity, and which enabled clear tumor delineation from surrounding (normal) tissue (Figure 1A). Neuroblastomas appeared more heterogeneous in both T_2-weighted images and maps of G_d and G_l (Figure 1B). Comparison of the quantitative viscoelastic properties between the two tumor types revealed the PDAC tumors to be markedly stiffer (G_d: PDAC 5.9 ± 1.0, neuroblastoma 4.1 ± 0.5 kPa) and viscous (G_l: PDAC 4.5 ± 1.1, neuroblastoma 2.3 ± 0.3 kPa).

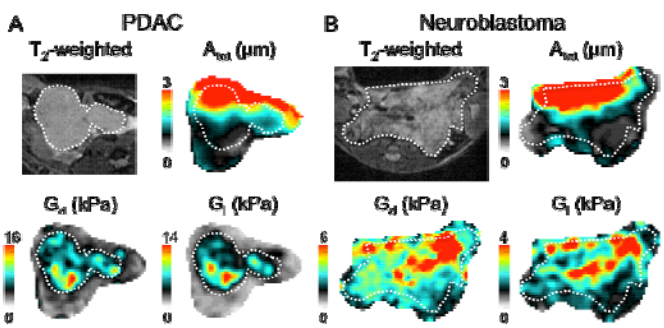

Figure1

Discussion: The feasibility of applying MRE to abdominal tumours using our preclinical platform was clearly demonstrated. The markedly elevated viscosity and elasticity quantified in the PDAC tumors is wholly in agreement with the well-described stromal-rich environment associated with solid pancreatic tumors [4]. Neuroblastoma is a pathologically diverse disease, with extensive vascularisation. Mechanical cues from the extracellular matrix have been shown to modulate the proliferation, differentiation and expression of *MYCN* in neuroblastoma *in vitro* [5], providing a strong motivation to exploit MRE-derived measurements of viscoelasticity *in vivo* in the Th-*MYCN* model shown here.

Conclusions: MRE can non-invasively assess the viscoelastic properties of deep-seated tumors arising within the abdomen of mice *in vivo*. Pancreatic tumours are markedly stiff, whilst neuroblastomas exhibit more heterogeneity in their biomechanical properties and are relatively soft.

Acknowledgements: Support from: European Union's Horizon 2020 research and innovative programme No 668039, CRUK and EPSRC to the Cancer Imaging Centre at ICR, MRC and DoH C1060/A16464, NIHR Biomedicine Research Centre, EPSRC, and Children with Cancer UK.

References: [1] Li *et al.*, ITEC; Deauxville, 2012. [2] Jamin *et al.*, Cancer Res; 75(7):1216-1224, 2015. [3] Weiss *et al.*, EMBO Journal; 1611:2985-2995, 1997. [4] Neesse *et al.*, Gut; 9(1):35, 2011. [5] Lam *et al.*, Molecular Cancer; 9(1):35, 2010.

015 **THE AUDIBLE HUMAN PROJECT: STUDY OF ACOUSTIC TRANSMISSION WITH A FRACTAL BASED MODEL OF THE HUMAN AIRWAYS.**

B Henry[1], TJ Royston[1].*

[1]Richard and Loan Hill Department of Bioengineering, University of Illinois at Chicago, Chicago, IL, USA.

Background: Creating an acoustic map of the airways may advance diagnostic possibilities for multiple pathologies, allowing for a robust detection scheme that can not only determine the severity of the disease but also the location. This can also be used in conjunction with Magnetic Resonance Elastography (MRE), which is a novel imaging methodology that can measure mechanical properties, such as stiffness and viscosity, through image processing of acoustic wave motion. This can also lead to a quantitative map of variation in mechanical properties that may correlate with injury, the progression of disease and/or the response to therapy.

Aims: To simulate the acoustic profile of a detailed airway structure analytically, in order to determine if the viscoelastic properties are different between healthy and diseased state models of a healthy adult pig.

Methods: Airway models were created in MATLAB using a quasi-volume halving method depicted by Tawhai 2001 [1]. Models were created inside of a healthy adult male pig excised lung via segmentation of the lung volume inside of ITK-SNAP. Once the airway models were created, an analytical solution of the 1D waveguide was solved in MATLAB via Royston 2008 [2] with some modifications. The acoustic pressure and wall radial motion was solved for at an acoustic range of 2 Hz to 2 kHz. In this study, a healthy case is compared against an identical lung fibrosis case with a change in the material stiffness (5 times the normal value) to model lung fibrosis.

Results: Models generated consisted of 15 generations of segments, 20478 segments total. Depicted in Figure 1a,b are the real part of the acoustic pressures and magnitude of the wall radial velocity. The acoustic pressure ranged from -0.1230 to 1.0541 Pa, while the magnitude of the wall velocity ranged from -228.0843 to -129.2443 dB. Figure 1c,d depict the fibrosis case acoustic pressure and magnitude of wall velocity. In the fibrosis case, the pressure ranged from 1.427e-3 to 1.4058 Pa, while the magnitude of the wall velocity ranged from -244.5561 to -148.8472 dB.

Conclusions: A numerical basis for differentiation between healthy and fibrosis test cases for airway insonfication is established through means of a 1D waveguide applied to a computer generated airway tree. The fibrosis case model exhibited a larger pressure along with a lower wall radial velocity. This leads to a further possible quantitative means of diagnosis through acoustic excitation, and can feed into MRE imaging and measurements. One major application of this study is the backward calculation of mechanical properties, which can be fed into MRE in order to noninvasively image and quantify tissue mechanical stiffness.

Acknowledgements: NIH Grant EB012142

References: [1] Tawhai, M., et al: 2001. Annals of Biomedical Engineering 28, pp. 793-802. [2] Royston, T.J., et a: 2008. The American Society of Mechanical Engineers 10.1115/1.802755.ch9, pp. 217-248

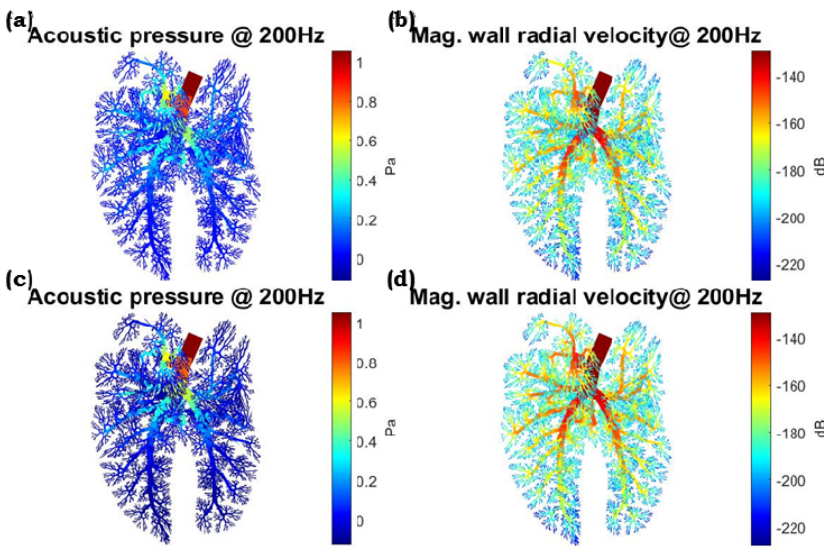

Figure 1. Depicted to the right are graphical representations of the airway model colored by the real part of the acoustic pressure (a and c) and magnitude of the wall radial velocity (b and d). (a) Depiction of the real part of the acoustic pressure for a healthy model. (b). Depiction of the real part of the magnitude of the wall radial velocity for a healthy model. (c) Depiction of the real part of the acoustic pressure for a fibrosis subject. (d) Depiction of the real part of the magnitude of the wall radial velocity for a fibrosis subject.

073 **SHEAR WAVE ELASTOGRAPHY IN THE PROSTATE: INTEROBSERVER REPRODUCIBILITY & COMPARISON WITH FUNCTIONAL MR BIOMARKERS.**

H Harvey[1], V Morgan[2], J Fromageau[1,2], T O'Shea[1,2], Prof R Eeles[1,2], JC Bamber[1,2], Prof N DeSouza[1,2]*
[1]The Institute of Cancer Research, London, UK; [2]The Royal Marsden Hospital, London, UK

Background:
No studies have yet looked at how Young's modulus (YM, measured in kPa) measured by shear wave elastography (SWE) correlates with standard magnetic resonance imaging (MRI) functional biomarkers. We hypothesised that as YM increases this corresponds to dense stroma that restricts water diffusion and hence results in a measurable reduction in apparent diffusion coefficient (ADC) on diffusion weighted (DW) MRI. Similarly an increase in tissue stiffness may be associated with changes in tissue perfusion, as measured using the dynamic contrast enhanced MRI (DCE-MRI) features capillary-to-interstitial transfer rate constant (Ktrans), fractional extravascular space volume (Ve), ratio of Ktrans/Ve (Kep) and initial area under the gadolinium curve (IAUGC). In addition, we investigated interobserver reproducibility of the SWE technique. Currently, there is only one published study of prostate SWE *intra*observer reproducibility, which found good reproducibility in a cohort of 80 patients (ICC =0.876, 95% CI=0.864–0.887). The study was, however, performed by only one radiologist [1]. No *inter*observer studies have yet been performed comparing quantitation in SWE of the prostate between two or more observers.

Aims: 1) To compare SWE Young's modulus with DW- and DCE-MRI quantified parameters. 2) To assess the interobserver variability of SWE Young's modulus quantitation between two trained observers.

Methods: 20 men from a large genetic screening trial (PROFILE, ICR) had same-day SWE (Aixplorer, Supersonic Imagine, France) and MRI of the prostate (3T Achieva, Philips), and a subset had subsequent prostate biopsy (n=18). 10 of these had SWE performed by 2 observers to assess reproducibility.
SWE was performed in a sextant fashion at the base, midgland and apex bilaterally, with ROIs placed centrally over the transitional zone (TZ) and peripheral zone (PZ) in each sextant by each blinded observer in turn, and mean YM was calculated for each 5mm circular ROI.
DW-MRI and DCE-MRI sequences were analyzed on a pixel-by-pixel basis using ROIs placed on matched slices, and quantitative parameters ADC, Ktrans, Ve, Kep and IAUGC were recorded. Intraclass correlation coefficients were used to assess interobserver reproducibility. Pearson's correlation and 2-tailed paired t-tests were used to assess relationship between YM and functional MRI values.

Results: Biomarker Relationships: YM measurements within the PZ had a weak but significant negative correlation with ADC (r=-0.15, p=0.0075) and Ve (r=-0.24, p=0.0072), and a weak positive correlation with Kep (r=0.27, p=0.0025). Ktrans and IAUGC did not correlate significantly with YM.
Interobserver Reproducibility: Mean YM interobserver reproducibility was fair to good (whole gland ICC=0.672, 95% CI=0.545 – 0.768). SWE measurements in the basal PZ (ICC=0.814) were more reproducible than those measured in the apex (ICC=0.360) and midgland (ICC=0.557). In the TZ, the midgland measurements were most reproducible (ICC = 0.727).

Conclusions: Biomarker Relationships: In the PZ, the weak inverse relationship between mean ADC and Young's modulus values supports the expected microstructural differences. Biomarkers of perfusion Ve and Kep also had weak correlations with YM. As cellularity and density increase, contrast flow into the extracellular space decreases (↓Ve), and so does stiffness (YM), with an accompanying reduction in water diffusivity (ADC). However, these tissue parameters are not equivalent in their assessment of the microenvironment, as shown by their overall weak correlations.
Interobserver Reproducibility: In 10 men reproducibility was fair to good for all locations, with best agreement in the PZ base, a common site for prostate cancer. The reproducibility reported here is the first true interobserver assessment of SWE in the prostate.

Acknowledgements: CRUK and EPSRC support to the Cancer Imaging Centre at ICR and RMH in association with MRC and Department of Health C1060/A10334, C1060/A16464 and NHS funding to the NIHR Biomedical Research Centre and the Clinical Research Facility in Imaging.

References: 1. Woo, S. et al, Shear Wave Elastography Assessment in the Prostate: an Intraobserver Reproducibility Study. Clinical imaging, 2014.

074 **HISTOPATHOLOGICAL CORRELATES OF YOUNG'S MODULUS ESTIMATED BY SHEAR WAVE ELASTOGRAPHY IN HUMAN BRAIN TUMOURS.**

H W Chan[1], T Jacques[2], C Uff[3], A Chakraborty[4], N Dorward[1], JC Bamber[5].*

[1]The National Hospital for Neurology and Neurosurgery, London, UK; [2]Great Ormond Street Hospital, London, UK; [3]Royal London Hospital, London, UK; [4]Southampton General Hospital, Southampton, UK; [5]Institute of Cancer Research and the Royal Marsden Hospital, London, UK.

Background: Neurosurgeons have always relied on visual inspection and tactile feedback when resecting brain tumours as they have different appearance and stiffness compared to normal brain. Human glioblastoma models implanted in mouse showed positive correlation between cellular density and microvessel density with elasticity and viscosity [1].

Aims: To determine whether Young's modulus (YM) of brain tumours estimated by shear wave elastography (SWE) are correlated with either tumour type, or histological characteristics.

Methods: Thirty five patients (aged 1-62 years; M:F=15:20) who underwent brain tumour resection were recruited. The intraoperative SWE scans were performed using Aixplorer® (SuperSonic Imagine, France) using a sector transducer (SE12-3) and a linear transducer (SL15-4) with a bandwidth of 3-12 MHz and 4-15 MHz, respectively, using the SWE mode. The histological diagnosis and features including gliosis, cellularity, proliferation and calcification were compared with YM measurements.

Results: Overall, the YM for all brain tumours were significantly higher than normal brain (median 33.4kPa vs 14.9kPa, p=0.003, Fig. 1). The YM of low grade tumours (median 39.5kPa) and metastases (median 169.6kPa) were significantly different from normal brain (median 14.9kPa) (p=0.036 and p=0.007, respectively, Fig. 2). There were no significant differences between the different tumour types. There was a non-significant negative correlation between cellularity and gliosis with YM measurements. Proliferation and calcifications had a non-significant positive correlation with YM measurements.

Conclusions: The YM for low and high grade gliomas had large standard deviations, implying heterogeneity in their histological structures within these tumour types. This preliminary study has provided some insight into the possible biological process that determines brain tumour stiffness. Future study with quantitative grading of histological features could improve our understanding into what actually makes a tumour stiff or soft.

Acknowledgements: This work was supported by the Royal Free Charity Fund (G90). Ethical approval was obtained from the National Research Ethics Service (NRES) Committee London – Queen Square Research Ethics Committee (Ref: 08/H0716/92). We also acknowledge CRUK support to the Cancer Imaging Centre at ICR.

References: [1] Jamin et al.: Cancer Res 2015: 75(7); pp1216-24.

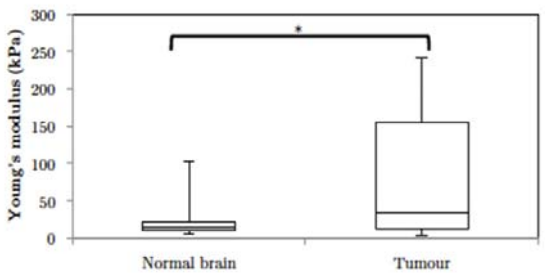

Fig. 1: Box and whisker plot for YM of brain tumours and normal brain. *There was a significant difference between YM for brain tumours and normal brain (p=0.003).

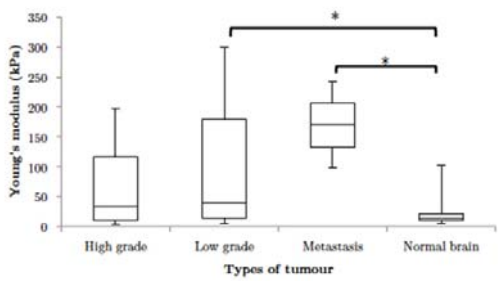

Fig. 2: Box and whisker plot for YM for various types of tumour and normal brain. *There were significant differences between low grade tumour and metastasis compared with normal brain (p=0.036 and p=0.007, respectively).

075 **CLINICAL APPLICATION OF SHEAR WAVE ELASTOGRAPHY FOR ASSISTING BRAIN TUMOUR RESECTION.**

H W Chan[1], C Uff[2], A Chakraborty[3], N Dorward[1], JC Bamber[4].*

[1]The National Hospital for Neurology and Neurosurgery, London, UK; [2]Royal London Hospital, London, UK; [3]Southampton General Hospital, Southampton, UK; [4]Institute of Cancer Research and the Royal Marsden Hospital, London, UK.

Background: The clinical outcomes for brain tumour resection have been shown to be significantly improved with increased extent of resection[1]. To achieve this, neurosurgeons employ various intra-operative tools to improve the extent of resection of brain tumours, including ultrasound, CT and MRI. Young's modulus (YM) of brain tumours has been shown to be different to that from normal brain [2] but the accuracy of SWE in assisting brain tumour resection has not been reported.

Aims: To determine the accuracy of SWE in detecting brain tumour residual using post-operative MRI scan as 'gold standard'.

Methods: Thirty five patients (aged 1-62 years, M:F = 15:20) with brain tumours were recruited into the study. The intraoperative SWE scans were performed using Aixplorer® (SuperSonic Imagine, France) using a sector transducer (SE12-3) and a linear transducer (SL15-4) with a bandwidth of 3-12 MHz and 4-15 MHz, respectively, using the SWE mode. The scans were performed before, during and after brain tumour resection. The presence of residual tumour was determined by the surgeon, ultrasound (US) B-mode and SWE. This was compared with the presence of residual tumour on a post-operative MRI scan.

Results: The YM of the brain tumours correlated significantly with surgeons' findings (ρ=0.845, $p<0.001$). The sensitivities of residual tumour detection by the surgeon, US B-mode and SWE were 36%, 73% and 94%, respectively, while their specificities were 100%, 63% and 77%, respectively. There was no significant difference between detection of residual tumour by SWE, US B-mode and MRI. SWE and MRI were significantly better than the surgeon's detection of residual tumour ($p=0.001$ and $p<0.001$, respectively).

Conclusions: SWE had a higher sensitivity in detecting residual tumour than the surgeons (94% vs 36%). However, the surgeons had a higher specificity than SWE (100% vs 77%). Therefore, using SWE in combination with surgeon's opinion may optimise the detection of residual tumour with current ultrasound technology, and hence improve the extent of brain tumour resection.

Acknowledgements: This work was supported by the Royal Free Charity Fund (G90). Ethical approval was obtained from the National Research Ethics Service (NRES) Committee London – Queen Square Research Ethics Committee (Ref: 08/H0716/92).). We also acknowledge CRUK support to the Cancer Imaging Centre at ICR.

References:

[1] Hervey-Jumper & Berger: Curr Treat Options in Neurol 2014:16(4):284.
[2] Imbault et al.: IEEE IUS Proceedings 2014: pp201-204.

076 **TEMPORAL REGULARISATION OF LONG ULTRASOUND SEQUENCE TRACKING AND USE FOR MOTION COMPENSATION IN RADIOTHERAPY**

T O'Shea[1], M Fast[1], S Nill[1], U Oelfke[1], JC Bamber[1], EJ Harris[1].*

[1]Joint Department of Physics, The Royal Marsden NHS Foundation Trust and The Institute of Cancer Research, Sutton and London, UK.

Background: Tumours influenced by patient respiration are known to displace by several centimeters reducing the intended accuracy of external beam radiation (EBRT) delivery. The use of ultrasound (US) for image-guidance in radiation delivery requires that the tumour position is estimated by a system that exhibits both high accuracy and low latency.

Aims: This study reports on efforts to (i) improve the accuracy of *in vivo* 2D ultrasound-based liver motion estimation and (ii) evaluate the system latency and resultant accuracy of a clinical 2/3D ultrasound-guided radiation therapy (USGRT) device (Clarity™, Elekta AB, Stockholm, Sweden) in US phantoms.

Methods: Long liver ultrasound sequence from ten healthy volunteers (up to 5.5 minutes in length and 15-23 Hz frame rate) were used to develop an off-line normalised cross-correlation (NCC) blood vessel matching algorithm which incorporated a specific similarity metric-based template update threshold and a prediction-based state observer. Five ultrasound sequences were used to train the algorithm with the remaining five sequence used for validation. To evaluate the performance (latency and accuracy) of the clinical USGRT device a tissue-mimicking US phantom was positioned on 3d motion platform and translated with 1d sinusoidal motion while imaging a 30mm hypo-echogenic spherical inclusion with the (mechanically-swept) 2/(3)d US transducer. The position of the spherical inclusion, as reported by the USGRT device, was used to update the position of the 6MV x-ray beam aperture (multi-leaf collimator) and enable the calculation of system latency and geometric accuracy.

Results: The developed liver blood vessel template matching algorithm produced improved accuracy over a naïve incremental template matching approach (mean absolute and 95% errors were reduced from 6.2 and 9.1 mm to 1.6 and 1.4 mm, respectively for the training data). The mean absolute and 95% errors for the validation data were 0.8 and 1.5 mm, respectively. For the clinical USGRT device, the overall system latency ranged from 400 ms (for 2d imaging) to 1000 ms (for 3d imaging i.e. with mechanical sweep of 3.6 to 20.8°). The latency-corrected geometric accuracy ranged from < 1 mm (for 2d imaging) and < 2 mm (for 3d imaging).

Conclusions: Ultrasound-based motion estimation has potential to monitor liver motion over long time periods relevant to EBRT delivery. The algorithm could be extended to 3d and incorporate information on liver deformation e.g. strain. For tracking respiratory-induced motion *in vivo* the clinical USGRT device would need to provide faster position updates and include prediction methods to account for long system latencies. A matrix array transducer (with no mechanical sweep) would reduce the imaging rate contribution to overall latency.

Acknowledgements: This work was supported by Cancer Research UK Grant No. C33589/A19727. The authors acknowledge NHS funding to the NIHR Biomedical Research Center at The Royal Marsden and The Institute of Cancer Research.

References: O'Shea, T.P., Bamber, J.C. and Harris, E.J., 2016. Temporal regularization of ultrasound-based liver motion estimation for image-guided radiation therapy. Medical physics, 43(1), pp.455-464.

Fast, M.F., O'Shea, T.P., Nill, S., Oelfke, U. and Harris, E.J., 2016. First evaluation of the feasibility of MLC tracking using ultrasound motion estimation. Medical Physics, 43(8), pp.4628-4633.

034 **EXPERIMENTAL AND NUMERICAL STUDY OF CIRCUMFERENTIAL AND AXIAL CYLINDRICAL WAVES IN PVA PHANTOMS SURROUNDED BY WATER OR EMBEDDED INTO SOFTER PVA MATERIAL.**

DA. Shcherbakova[1], N Debusschere[1], M Kersemans[2], A Caenen[1], M Pernot[3], P Segers[1], A Swillens[1].*
[1]IBiTech - bioMMeda, Department of Electronics and Information Systems, Ghent University, 9000 Ghent, BELGIUM; [2]Faculty of Engineering and Architecture, Ghent University, 9000 Gent, BELGIUM; [3]Institut Langevin, ESPCI ParisTech, CNRS UMR 7587, INSERM ERL U979, 10 rue Vauquelin, 75231 Paris Cedex 05, FRANCE.

Background: Shear wave elastography (SWE) in arteries is traditionally applied along the artery's main axis to measure the shear wave propagation speed (SWS) during the cardiac cycle [1]. However, the blood pressure exhibits load mostly applied perpendicular to the vessel's wall and due to the artery's anisotropic properties. This leads to more stiffness variation in the cross-sectional view [2]. Moreover, as collagen fibers are circumferentially oriented, investigating changes in their structure (e.g. collagen remodeling) would be more obvious in that view [2]. Therefore, it is relevant to study SWE imaging and circumferentially propagating shear waves (SWs).

Aims: To investigate SWs in thin-walled (3 mm) linear elastic tubular phantoms using both experiments and computational modeling, two types of boundary conditions (BCs) were considered, with the tube phantoms embedded in water or a softer medium.

Methods: 2 PVA phantoms (2 freeze-thaw cycles, 10% PVA; SWS_{Bulk} in plates were 6.6 and 7 m/s, respectively; Fig. A, E) were constructed with one phantom as a single tube and another tube surrounded by softer PVA medium (SWS_{Bulk}=5.3m/s). SWE measurements were performed with phantoms pressurized under a water column with pressure ranging from 0 mmHg to 70 mmHg with a step of 10 mmHg. The tube surrounded by water was axially prestretched to 1.4 mm/mm. SWE was studied in both longitudinal and cross-sectional views. Afterwards, a single 3 mm tube at 0 mmHg pressure was modeled numerically in Abaqus (Simulia, Dassault Systemes, USA) taking into account surrounding water.

Results: Derived SWS results were calculated based on the time-of-flight algorithm (Fig. B,F). In the tube surrounded by water, pressurizing the phantom led to an increase in SWS in the cross-sectional view, while it decreased in the axial direction. A similar trend was observed for the embedded tube in the cross-sectional view. The reference value (SWS_{Bulk}) was in between the values obtained from both views. In Fig. C, G complex SWs patterns are shown at 0.5 ms with downward velocities smaller in the embedded tubular phantom. In Fig. D numerical results are shown, revealing patterns similar to the experimental SWs patterns of Fig. C, with a SWS of 4.8 m/s.

Conclusions: SWS values measured in tubes at different pressure levels demonstrate different behavior for different views and BCs. Though the material is linear elastic, such behavior could be partially due to the acoustoelastic effect related to internal stresses and waves being guided inside the wall. Moreover, post-processing SWS data in such thin phantoms is a challenging task and a proper approach has to be followed. Numerical simulations with a known ground truth will allow for a better understanding of SWs propagation in such complex settings and minimize the influence of the post-processing methods.

Acknowledgements: Darya Shcherbakova and Abigail Swillens are Ph.D. and Postdoctoral Fellows of the Research Foundation-Flanders (FWO-Vlaanderen). The authors gratefully acknowledge the financial support of the CWO, Faculty of Engineering and Architecture, Ghent University.

References: [1] Couade, Pernot, Prada, et al. Ultrasound Med & Biol 36, pp. 1662 – 1676, 2010. [2] Gasser, Ogden, Holzapfel. J. R. Soc. Interface, vol. 3, pp. 15–35, 2006.

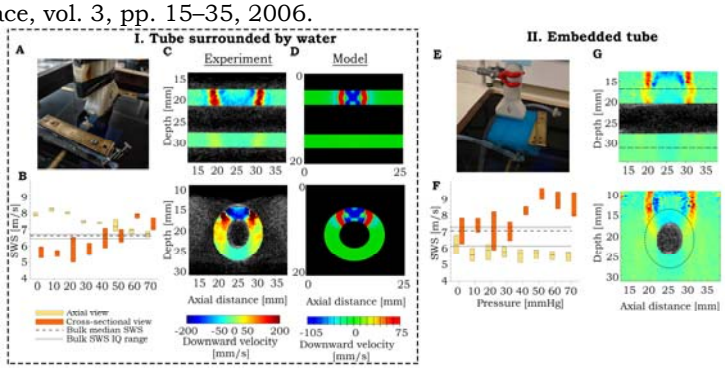

017 **HIGH FRAME RATE ACCURATE TRACKING OF TISSUE MOTION AFTER VALVE CLOSURE.**

HJ Vos [1,2], M Strachinaru [1], BM van Dalen [1], I Heinonen [1], J Bercoff [3], JG Bosch [1], AFW van der Steen [1,2], N de Jong [1,2].*

[1]Thorax Center, Erasmus MC, Rotterdam, THE NETHERLANDS; [2]Acoustical Wavefield Imaging, Delft University of Technology, Delft, THE NETHERLANDS; [3]Supersonic Imagine, Aix en Provence, FRANCE.

Background: The propagation velocity of shear-like waves in the heart is expected to relate to local tissue stiffness. However, the conversion from propagation velocity to actual shear (or Young's) modulus depends on the physics of the wave in the confined cardiac septal wall. The possible wave types (bulk shear, Rayleigh, or Lamb waves) all have a different theoretical relation between wave propagation and shear modulus of the material. Moreover, when studying the physiological waves after valve closures, the sensitivity of tissue Doppler to trace such waves depends on the angle between exact tissue motion and the beam axis; this means that the echographic view (apical, parasternal, trans-esophageal) may affect the sensitivity of tissue Doppler to track the waves.

Aims: To identify the wave mode or modes that are present in the septal wall after valve closure, we studied the wave mechanics from several echocardiographic views in open-chest porcine animal models.

Methods: We recorded the wave motion in the ventricular septal wall of four Göttingen minipigs with open chest. Data were acquired with an Aixplorer system (Supersonic Imagine, France) in research mode with an L10-2 probe at a framerate of 1000 frames per second (FPS). The data were acquired in a view corresponding to the apical and lateral views of the heart. We recorded 10 movies on average per animal, of which about half were in apical-like views, and half in parasternal-like views. Data analysis was done with two different methods:
(1) Axial tissue motion was extracted from IQ-based frames by a one-lag autocorrelation and smoothed with a spatial moving average filter. The tissue motion along a virtual M-mode line was analyzed by a normalized Radon transform to reveal the propagation velocity of the shear waves;
(2) The speckle pattern in the frames was tracked with 2D autocorrelation and subsample displacement estimation to obtain local tissue displacement in axial and lateral direction after valve closure.

Results: After aortic valve closure, the axial tissue motion analysis showed, in parasternal view, wave propagation throughout the entire length of the septal wall, whereas the apical view showed propagation in a confined area nearby the annular ring of the aortic valve. Yet, no significant difference in the propagation velocity was observed in these views. On the other hand, the standard deviation of measured velocities is smaller in a parasternal view, most likely caused by the longer visible propagation path in this view, leading to longer measurement interval. The speckle tracking confirmed the motion results, as the tissue motion nearby the annular ring showed a component both along the septal wall and perpendicular, whereas the tissue near the apex showed only motion perpendicular to the wall.

Conclusions: The results show that the waves after valve closure exhibit a complex nature, and are not pure shear waves, which explains why they can be viewed both in an apical and parasternal view.

Acknowledgements: This research was financially supported by the Netherlands Organisation for Scientific Research (NWO, ZonMW, Heartin4D) and The European Commission FP7-Health-2010 grant MEDIA-261409. The position of I.H. and the animals were financially supported by the Academy of Finland (251272), Finnish Diabetes Research Foundation, and the Finnish Foundation for Cardiovascular Research.

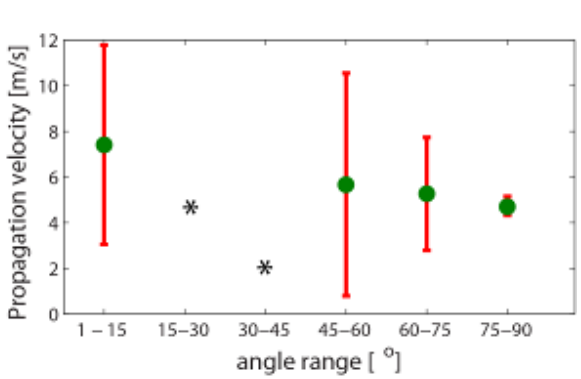

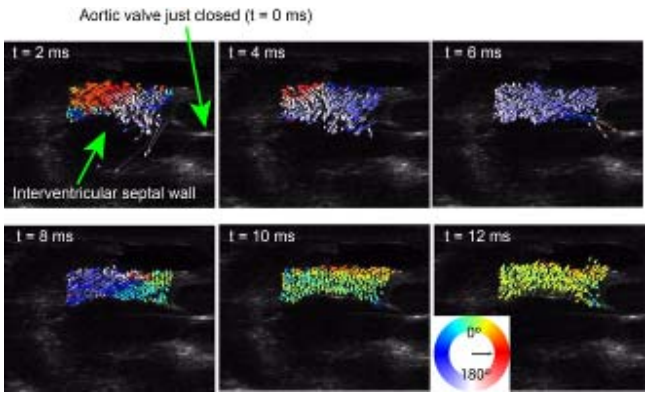

010 **EVALUATE CAROTID ARTERY ANISOTROPY USING PRINCIPAL STRAIN ELASTOGRAPHY.**

R Nayak[1], G Schifitto[2], MM. Doyley[1].*

[1]University of Rochester, Dept. of Electrical & Computer Engineering, Rochester, New York, USA;
[2]University of Rochester Medical Center, Dept. of Neurology, Rochester, New York, USA.

Aims & Background: The carotid artery (CA) exhibits transversely isotropic mechanical behavior; however, most vascular elastography techniques assume vessels are isotropic. Such an assumption can degrade (a) diagnostic performance, and (b) accuracy of the modulus and stress recovery process. In this study, we assessed the feasibility of estimating fractional anisotropy (FA) -- a metric for assessing anisotropy within vascular tissues -- using principal strains. We performed (a) simulations with isotropic and transversely isotropic vessel models, and (b) a pilot study with 10 healthy volunteers to demonstrate its efficacy in identifying isotropic and anisotropic components in vessels. We believe this non-invasive technique could improve the diagnostic performance of ultrasound (US) based vascular elastography.

Methods: We used two finite element (FE) vessel models with identical geometry (Fig 1.a), having inner and outer radii of 1.5 and 6 mm, respectively, but different mechanical behavior (isotropic vs. transversely isotropic) -- to visualize how well FA maps can identify vessel anisotropy. The arterial wall, lipid-core, and fibrous cap of the isotropic vessel model were assigned a stiffness of 45 kPa, 1 kPa, and 700 kPa, respectively, and a Poisson's ratio of 0.495. The transversely isotropic vessel model was assigned an arterial wall and fibrous cap stiffness of 45 kPa, and 700 kPa, respectively, Poisson's ratio of 0.01 along radial direction, and 450 kPa and 7000 kPa, respectively and Poisson's ratio of 0.27 in the circumferential directions [1]. The plaque was modeled as an isotropic material with Young's modulus of 1 kPa and Poisson's ratio of 0.495. The compounded plane wave US images were synthesized for 15 transmissions (-14° to 14°, in increments of 2°) using Field II [2]. The simulated US system was equipped with a 128-element linear transducer array operating at a center frequency of 5 MHz. Gaussian noise of 20 dB was added to the simulated RF channel to mimic transducer noise. We conducted an *in vivo* study with 10 healthy volunteers between ages 50-60 years, to evaluate the FA maps acquired with a clinical prototype system. The *in vivo* echo imaging was performed using a commercial US scanner (Ultrasonix RP, Analogic Corp., MA, USA) that was equipped with a 5 MHz, 128-element transducer array and a parallel data acquisition system (Sonix DAQ, Analogic Corp., MA, USA). Beamforming was performed off-line using the delay-and-sum technique. Displacement elastograms were computed by applying a 2D cross-correlation-based echo-tracking technique to the echo frames. FA was estimated using the principal strains estimated from Eigen decomposition of the 2D strain tensor [3]. Root mean square error (RMSE) between the simulated and the FE estimates were computed to evaluate the accuracy of the FA maps.

Results: Fig. 1 (b, c) shows FA maps obtained from simulated vessels. FA varied between 0 (isotropic) and 1 (completely anisotropic). Fig. 1 (b) shows the FA map for the isotropic model; FA in the vessel wall and the lipid pool were similar (≈0.33). Fig. 1 (c) shows the corresponding FA map for the transversely isotropic vessel with an isotropic plaque, showing low FA in the isotropic lipid pool (≈0.35) and high FA (>0.8) in the vessel wall. Isotropic and anisotropic vessel components were discernable in FA maps. Further, there was good agreement between FE-derived FA maps and those estimated from noisy principal strains, with RMSE error < 10%. Figure 1 (d,f) & (e,g) show B-mode and the corresponding FA elastograms associated with two healthy volunteers, respectively. The mean FA of the patient elastograms were > 0.6 which corroborates that the CA shows transversely isotropic mechanical behavior. More specifically, localized areas of low FA values were apparent in the anisotropic maps. Although these results are encouraging, we plan to conduct further studies with *ex vivo* tissue samples and histological analysis to validate our *in vivo* findings.

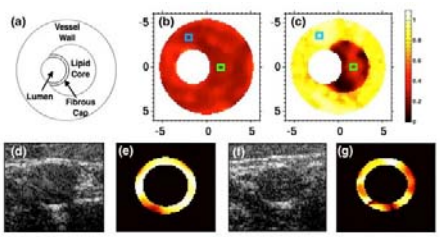

Fig. 3 (a-c) show the geometry and the estimated FA of the simulated vessels. The bottom row (d-g) shows the B-mode and FA maps of the two healthy volunteers, respectively.

Conclusions: This study shows that besides providing coordinate independent strain estimates, principal strain elastography can be used to assess the degree of anisotropy within vascular vessels.

Acknowledgement: This work was supported by the National Heart and Lungs Research: R01 HL123346.

References: [1] Finet G., et. al "Biomechanical interaction between cap thickness, lipid core composition & blood pressure in vulnerable coronary plaque: impact on stability or instability." *Cor. Art. Dis.* 15.1 (2004): 13-20.
[2] Jensen, JA et. al. "Calc. of pressure fields from arbitrarily shaped, apodized, & excited US transducer." *IEEE UFFC.* 39.2 (1992): 262-267.
[3] Alexander, AL., et al. "Diffusion tensor imaging of the brain." Neurotherapeutics 4.3 (2007): 316-329.

001 **HOW DOES ULTRAFAST IMAGING AFFECT SHEAR WAVE VISUALIZATION?**

A. Caenen[1], M. Pernot[2], D.Shcherbakova[1], I. K. Ekroll[3], P. Segers[1], A. Swillens[1].*
[1]Ghent University, Ghent, BELGIUM; [2]Institute Langevin, Paris, FRANCE; [3]Nowegian University of Science and Technology, Trondheim, NORWAY.

Background: In Shear Wave Elastography (SWE), the acoustically excited shear waves can only be captured at high frame rates (~ kHz), as achieved using dedicated single or compounded plane wave imaging. However, it is unclear to what extent this ultrafast image acquisition affects SW visualization, especially when complex wave phenomena such as dispersion occur.

Aims: To investigate whether ultrafast imaging affects SW visualization and derived mechanical properties in the left ventricle (LV) via experiments and multiphysics modeling. The latter allows us to generate virtual SWE images with the true biomechanics behind the image fully known.

Methods: *Experiments:* SW's were excited in an LV phantom (cfr. fig. A) with a frequency of 8 MHz and voltage of 50 V, using the Aixplorer system. Next, SW's were imaged using ultrafast scanning without (0°) and with (-2°, 0°, 2°) plane wave compounding, as shown in fig. C. The phantom's stiffness was determined via uniaxial mechanical tensile tests.
Simulations: The SW propagation of the experiment was mimicked in the finite element software Abaqus (fig. D) [1]-[3]. Next, two ultrafast imaging setups were modeled in Field II, i.e. plane wave imaging with and without compounding. The LV phantom was represented by point scatterers upon which the ultrasound waves reflect and further propagated during scanning according to the tissue displacements of the finite element model (fig. E).

Results: Wave dispersion is obviously present for the experimental and simulated SW (left panels of fig. C and F), imaged without compounding: we clearly see two downward velocity wave fronts (red zones) surrounding the tissue relaxation (blue). Compound imaging conceals dispersion both in model and experiment, cfr. right panels of fig. C and F. In practice, different shear modulus estimators are applied for dispersive and non-dispersive regimes: time-of-flight method vs. phase speed analysis. This leads to shear moduli of 16.5 kPa for compounding (~ no dispersion) and 26.2 kPa for non-compounding (~ dispersion), even though both images have the same mechanical ground truth (24.3 kPa).

Conclusions: The multiphysics simulations confirm that the applied imaging set-up might affect the observed SW patterns. Therefore, caution is advised when choosing a tissue characterization method based on visualized SW physics, as this might give an erroneous stiffness estimate.

Acknowledgements: This research is supported by the Flemish government agency for Innovation and Entrepreneurship (VLAIO) and Research Foundation Flanders (FWO).

References: [1] Palmeri et al, *IEEE Trans. Ultrason. Ferroelectr. Freq. Control*, 52:1699-1712, 2005. [2] Lee et al, *Int. J. Numer. Methods. Biomed. Eng.*, 28:678-696, 2012. [3] Caenen et al, *IEEE Trans. Ultrason. Ferroelectr. Freq. Control,* 62:439-450, 2015.

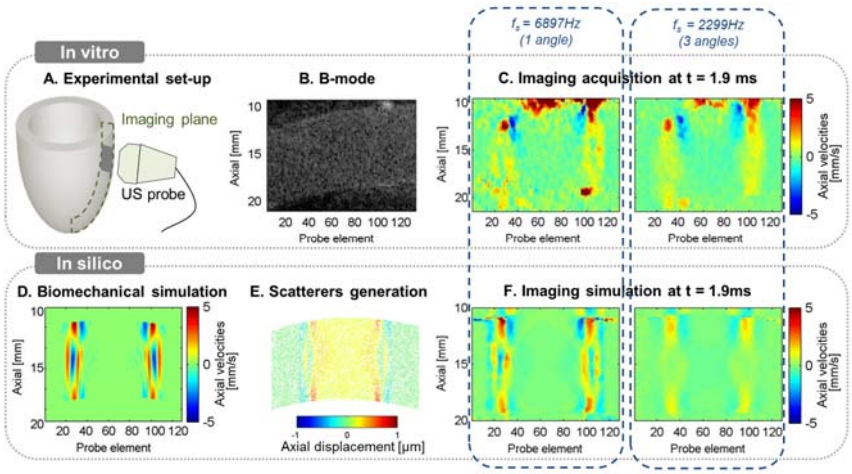

028 **SHEAR WAVE SPEED ESTIMATES WITH VELOCITY AND DISPLACEMENT DATA: THEORY, SIMULATIONS, AND EX VIVO APPLICATIONS IN THE CERVIX OF THE RHESUS MACAQUE.**

IM Rosado-Mendez [1], LC Drehfal[1], ML. Palmeri[2], H Feltovich[1,3], TJ. Hall[1].*

[1]Department of Medical Physics, 1111 Highland Ave., Rm. 1005, Madison, Wisconsin, 53705 USA; [2]Biomedical Engineering Department, Hudson Hall, Rm. 136, Durham, North Carolina, 27708, USA; [3]Maternal Fetal Medicine Department, Intermountain Healthcare, Provo, Utah, 84604, USA

Background: Shear Wave Elasticity Imaging involves estimating the shear wave speed SWS using particle displacements (disp) or velocities (vel). Under a purely elastic model, both estimates are expected to agree. Viscous components introduce an increasing dependence on SWS with increasing frequency. As a result, SWS(vel) are larger than SWS(disp) since the former contain higher frequencies than the latter.[1]

Aims: Here we investigate the discrepancy between SWS(vel) and SWS(disp) under different viscoelastic configurations using theoretical and simulated shear wave propagation. This analysis is extended to *ex vivo* samples of the Rhesus Macaque cervix that are known to be highly dispersive.[2]

Methods: Particle displacements and velocities produced by an Acoustic Radiation Force Excitation (0.5ms duration) induced shear waves in a Zener (three-parameter) viscoelastic solid were simulated using a finite-element method.[3] SWS(disp) and SWS(vel) were estimated with a RANSAC estimator [4] and a Radon Sum estimator[5] for comparison. The ratio R=SWS(vel)/SWS(disp) was studied under two scenarios. First, the transient and equilibrium elastic shear moduli were kept constant (G_I=2kPa, G_0=20kPa, respectively) while varying the viscous modulus (0.7<η<7 poise). Second, G_I, G_0, and η were increased proportionally (8.3< G_I <225kPa, $G_0=10G_I$, η/GI=0.4ms). Simulations were compared to predictions from a theoretical model. [1] R was also computed in ARFI data acquired from *ex vivo* hysterectomy cervix samples from Rhesus Macaques following a previously described procedure.[5] Viscosity was assessed by through the slope of the phase velocity versus frequency between 0.4—1.0kHz.

Results: In Figure (a), theoretical prediction and simulations show that R increases as a function of the viscous modulus from 1 at low viscosity (η/G_I=0.3ms) up to 3.5 (theory) and 2.5 (simulations) for η/G_I=3.3ms. Fig. (b) shows that, regardless of η, R remains constant as long as η/G_I is constant. No differences were found between the RANSAC and the Radon Sum estimators. The analysis of *ex vivo* Rhesus macaque cervix shows that R increases as a function of the phase velocity vs. frequency slope as 0.96exp(0.08×slope).

Conclusions: Three-fold differences between SWS(vel) and SWS(disp) were found under important viscous conditions, including an animal model of the cervix. This discrepancy can be a confounding factor when interpreting SWS in tissues with a significant viscous component.

Acknowledgements: This work was supported by National Institutes of Health Grants R21HD061896, R21HD063031 and R01HD072077 from the Eunice Kennedy Shriver National Institute of Child Health and Human Development. We are also grateful to Siemens Healthcare Ultrasound division for equipment loan and support.

References: [1] Rouze, NC et al., "An analytic Fourier domain description of shear wave propagation in a viscoelastic medium using asymmetric Gaussian sources," JASA,139(2): 1012-1022, 2015. [2] Rosado-Mendez, IM et al., "Viscoelasticity of the rhesus macaque uterine cervix assessed through SWEI: An Ex Vivo study," submitted to UMB, 2016. [3] Palmeri, ML et al., "A finite-element method model of soft tissue response to impulsive ARF," IEEE TUFFC, 52(10): 1699-1712, 2005. [4] Wang MH, et al., "Improving the robustness of time-of-flight based SWS reconstruction methods using RANSAC in human liver in vivo," UMB, 36(5): 802-813, 2010. [5] Rouze NC, et al., "Robust estimation of time-of-flight SWS using a Radon Sum transformation," IEEE TUFFC 57(12): 2662-2670, 2010.

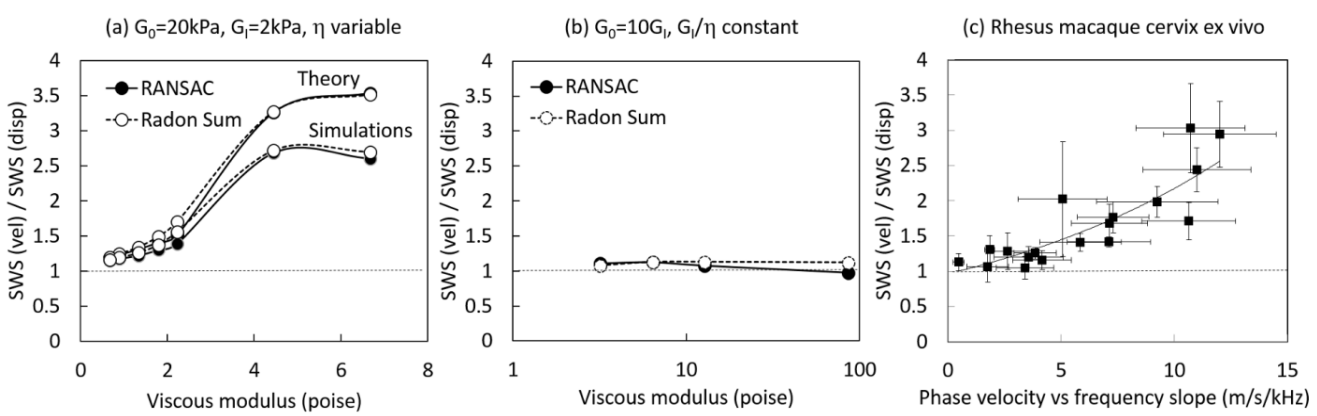

052 **STRATEGIES FOR QUALITY ASSESSMENT OF SHEAR WAVE SPEED ESTIMATES: *EX VIVO* APPLICATION IN THE RHESUS MACAQUE CERVIX**

IM Rosado-Mendez [1], LC Drehfal[1], ML. Palmeri[2], H Feltovich[1,3], TJ. Hall[1].*

[1]Department of Medical Physics, 1111 Highland Ave., Rm. 1005, Madison, Wisconsin, 53705 USA; [2]Biomedical Engineering Department, Hudson Hall, Rm. 136, Durham, North Carolina, 27708, USA; [3]Maternal Fetal Medicine Department, Intermountain Healthcare, Provo, Utah, 84604, USA.

Background: The clinical value of Shear Wave Elasticity Imaging (SWEI) depends on the accuracy and precision of the shear wave speed (SWS) estimates. Common criteria for rejecting unreliable SWS estimates are a minimum peak particle displacement caused by the shear wave and the goodness of fit of the SWS estimate to a model [1]. However, these criteria might reject otherwise good data and not reject unreliable estimates thereby affecting the detection or diagnosis power for a particular SWEI application.

Aims: We performed a systematic analysis of the SWS estimate quality in terms of the consistency and the goodness of fit of the estimates and created a quality index to study the performance of conventional threshold approaches to reject unreliable estimates. This analysis was performed on SWEI data acquired from ex vivo samples of a Rhesus macaque non-human primate (NHP) model of the uterine cervix.

Methods: Acoustic Radiation Force Impulse-based SWEI was applied to 28 NHP necropsy cervix specimens using a Siemens Acuson S2000 and 9L4 transducer that was aligned parallel to the cervical canal. Further data acquisition details are described in [1]. Displacements were calculated using the Loupas' routine.[2] Shear wave speed (SWS) was estimated using a RANSAC algorithm [3] (12 iterations with independent seeds) and a Radon Sum algorithm [4]. The difference between SWS obtained with these methods quantified estimate consistency. The percentage of time-to-peak points lying on the fitted RANSAC plane quantified goodness of fit. A quality index, defined as the ratio of the percent of inliers and the absolute difference of the two estimators' SWS values, was computed for each data set totaling 1213 SWS estimates. The discrimination of good vs. bad data is based on maximum displacement of 0.5μm and a percent of inliers<40% [1; referred to as MDPI] is compared to the new Quality Index.

Results: The figure below shows the Quality Index as a function of the mean RANSAC SWS estimate. Estimates with QI>10 are uncorrelated with SWS. Estimates with low QI (<10) are found mostly when SWS > 10m/s (because of the discrepancy between the two estimators). Thus QI=10 is used as a threshold between good and bad data. From the total of 141 estimates with QI<10, the MDPI criterion identified only 16. A total of 110 estimates with QI<10 were misclassified by the MDPI criterion as being of good quality.

Conclusions: Conventional MDPI criteria are found to be incorrectly SWS estimate reliability in some cases. We propose the use of the quality index defined here as a better criterion for SWS estimate reliability. We are currently studying the factors contributing to the reduction of the quality of the SWS estimates, and developing strategies to circumventing them.

Acknowledgements: This work was supported by National Institutes of Health Grants T32CA009206, R21HD061896, R21HD063031 and R01HD072077 from the Eunice Kennedy Shriver National Institute of Child Health and Human Development. We are also grateful to Siemens Healthcare Ultrasound division for equipment loan and support.

References: [1] Huang B, et al., "Estimation of Shear Wave Speed in the Rhesus Macaques Uterine Cervix," IEEE TUFFC, in press. [2] Loupas, T, et al. IEEE TUFFC 42(4): 689-699, 1995. [4] Wang MH, et al., UMB, 36(5): 802-813, 2010. [4] Rouze NC, et al., IEEE TUFFC 57(12): 2662-2670, 2010.

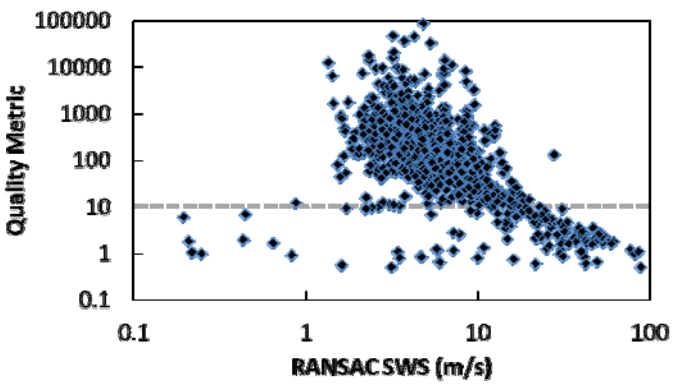

013 **ESTIMATION OF PULSE WAVE VELOCITY IN ARTERIES: A NEW METHOD BASED ON CROSS-CORRELATION.**

P. Nauleau[1], IZ. Apostolakis[1], MDJ. McGarry[1], EE. Konofagou[1,2].*

[1]Department of Biomedical Engineering, Columbia University, New York, NY, USA; [2]Department of Radiology, Columbia University, New York, NY, USA.

Background: The progression of cardiovascular diseases has been shown to be associated with changes in vascular stiffness [1]. The pulse wave velocity (PWV) is accepted as a surrogate of the vessel stiffness [1]. The method of estimation of the PWV currently used clinically consists in measuring the time-of-flight of the pulse wave between two distant sites (e.g. the carotid and the femoral arteries) and the distance between those sites. Our lab developed a non-invasive ultrasound-based technique of pulse wave imaging (PWI). This method allows for a regional assessment of the PWV [2-3]. PWI calculates the displacements of the wall through a cardiac cycle in a field of view defined by the ultrasonic probe, creating an image of the propagation: the spatio-temporal map. The tracking of the 50% upstroke of the wavefront yields an estimation of the PWV [4]. However, this tracking may be biased by the presence of reflections (e.g. from the carotid bifurcation) and only uses a few points of the waveforms. We hypothesize that critical additional information could potentially be retrieved by analyzing the entire signals.

Aims: In this study, we present a new method of estimation of the PWV based on the cross-correlation study of the spatio-temporal maps. We investigate the potential of the technique in phantoms and evaluate initial in vivo feasibility in healthy subjects.

Methods: A cylindrical phantom was generated with one half of soft material (silicone gel, Factor II-Inc) and another half of a stiffer material (a mixture of silicone gel and silicon elastomer in a 7:3 ratio, Factor II-Inc) twice stiffer than the soft part. The compliance of the two materials were characterized through static testing: E_{soft} =3.2x10^{-9} m^2/Pa, E_{stiff} = 1.5x10^{-9} m^2/Pa. Different concentrations of scatterers were used in order to see the interface between the two parts. Three experiments were conducted: 1) the soft part was imaged in a region without reflections, 2) in a region with reflections and 3) the transition between the stiff and the soft areas was imaged. A single pulse was emitted by manually releasing the inlet of the phantom. Each experiment was repeated 5 times. Healthy human carotids were imaged to evaluate the feasibility of the method in vivo. Channel data were acquired with a linear array L7-4 (Philips Healthcare, Andover, MA) and a research scanner (Verasonics Inc., Redmond, WA). Compounding imaging sequences were used to achieve a high frame rate (2650 fps) with a good spatial resolution. The axial displacements at the walls were estimated by the normalized 1D cross-correlation with a window size of 10λ and 95% overlap. The PWV was then estimated from the calculated spatio-temporal map using both the conventional and the new cross-correlation methods. The cross-correlation method consists in tracking a peak of the cross-correlation between the displacement of the wall observed with the element #n of the array and the displacements observed with the other elements of the array.

Results: In the ideal case (no reflections), the cross-correlation method yields as accurate PWV values as the conventional method: $PWV_{50\%up}$=2.52±0.56 m/s *vs* PWV_{corr}=2.51±0.29 m/s, with the value obtained with static testing equal to 2.41±0.31 m/s. The new correlation-based method can provide an unbiased estimate when reflections are present: $PWV_{50\%up}$=1.70±0.17 m/s *vs* PWV_{corr}=2.14±0.21 m/s. The study of the transition soft/stiff showed that the area under the cross-correlation curve can locate accurately the interface. The new proposed processing has a success rate of 90% for the classification of the soft and the stiff parts, while the conventional processing presents a success rate of 20%. The proposed method was shown feasible in healthy subjects: the area under the cross-correlation curve identified, as expected, the carotid as one homogeneous area. The values obtained are realistic compared to the existing literature (range between 2 and 4 m/s) and are in good agreement with values estimated with the conventional PWI methodology.

Conclusions: A new method of estimation of PWV is hereby proposed. Its abilities were investigated through a series of experiments with an artery mimicking phantom. The in vivo feasibility was shown in healthy subjects and findings indicated a higher robustness of the correlation-based method especially in presence of strong reflections.

Acknowledgements: Funding NIH R01 HL114358

References: [1] Laurent et al. Expert consensus document on arterial stiffness: methodological issues and clinical applications. Eur Heart J. 27, 2006.

[2] Luo et al. Pulse wave imaging of normal and aneurysmal abdominal aortas in vivo. IEEE Trans Med Imaging. 28, 2009.

[3] Luo et al. Pulse wave imaging of the human carotid artery: an in vivo feasibility study. IEEE Trans Ultrason Ferroelectr Freq Control. 59, 2012.

[4] Li et al. Performance assessment of pulse wave imaging using conventional ultrasound in canine aortas ex vivo and normal human arteries in vivo. Arte Res. 11, 2015.

005 **A NOVEL METHOD TO ENHANCE THE CONTRAST TO NOISE RATIO OF ACOUSTIC RADIATION FORCE IMPULSE (ARFI) IMAGING**.

M Vejdani-Jahromi[1], J Freedman[1], PD. Wolf[1].*
[1]Duke University, Durham, NC, USA.

Background: Acoustic Radiation Force Impulse (ARFI) Imaging is an ultrasound elastography technique for assessing mechanical properties of the tissues and is being used for detecting malignancies in different tissues including liver and prostate. ARFI uses an acoustic wave to push the tissue and the displacements are tracked. Generally, a single point of the time-displacement curve is used to construct the ARFI image. This point is chosen based on methods including maximum displacement, displacement at a fixed post push interval, or time to peak method. These methods could be affected by noise and jitter.

Aims: In this research, we propose to use the area under the displacement curve (AUC-ARFI) to include a higher number of points and to reduce noise and enhance the contrast and CNR for ARFI Imaging. A similar concept may be utilized by summation or averaging multiple points.

Methods: Soft tissue reaches maximum displacement faster and takes longer to return to baseline, therefore, the AUC of the soft tissue is larger than the AUC of stiff tissue. A phantom with a background stiffness of 8 ± 2.5 kPa and a stiff lesion of 24 ± 4 kPa was imaged. Contrast and CNR were calculated for boxes, 1.5*0.86 mm^2, inside and outside lesion, at the same axial depth. The displacement at 0.36 mS after the push, the maximum displacement, the sum of the displacements over 0.79 ms, and the area under the curve (AUC-ARFI) for 0.79 ms were calculated.

Results: Phantom results are shown in the following figure and table. These images are normalized to the maximum value at each axial depth. AUC-ARFI improved the normalized CNR by 61%.

Conclusions: Preliminary results also showed increased CNR in detecting ablation lesions in vivo. AUC-ARFI results in increased quality of ARFI imaging with no change in imaging methods or parameters.

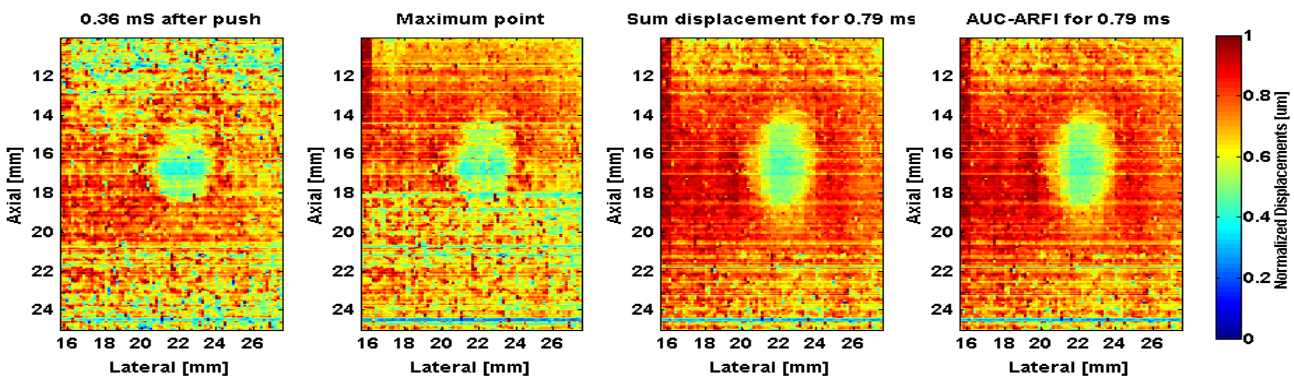

	Fixed Time	Maximum	Sum	AUC-ARFI
Contrast	0.35	0.36	0.42	0.43
CNR	2.21	3.19	6.56	6.76
Contrast-Normalized	0.35	0.36	0.42	0.43
CNR Normalized	2.20	3.05	4.69	4.92

051 **ACCURACY ASSESSMENT OF TIME DELAY ESTIMATION IN ULTRASOUND ELASTOPGRAPHY.**

M Ghasemi Amidabadi[1], O Ahmad[1], H Rivaz[1,2.]*

[1]Department of Electrical and Computer Engineering, Concordia University, De Maisonneuve Blvd. W, Montreal, Quebec, CANADA, H4B 1R6

[2] PERFORM center , Concordia University, 7141 Sherbrooke St. W, Montreal, Quebec, CANADA.

Background: Ultrasound elastography entails time-delay estimation (TDE) between ultrasound radio frequency (RF) data as the tissue undergoes deformation. TDE is utilized to calculate mechanical properties of tissue, which are often correlated with pathology [1]. The accuracy of TDE is usually measured by calculating the value of normalized cross correlation (NCC) at the estimated displacement [2]. NCC, however, can be very high at a displacement estimate with large error, a well-known problem in TDE referred to as peak-hopping [3].

Aims: TDE is challenging due to the signal decorrelation between the two ultrasound frames. Failure in TDE creates artifacts which can adversely affect the diagnosis or surgical operation. Accuracy assessment of TDE is important for several reasons: (i) To mask erroneous areas of the elasticity image, (ii) To obtain a weighted averaged of elasticity images, and (iii) To train sonographers to take high-quality elastograms.

Methods: Let I_1 and I_2 be pre-and post-compressed images [4]. In order to quantify accuracy of the displacement map, previous work only calculates NCC at the estimated time delay in I_2. In this work, we also calculate four neighboring NCC values around the estimated one to investigate the behavior of the similarity metric in the neighborhood of the estimated pixel. After obtaining these five NCC values for each pixel in I_1, a binary classifier (SVM) is used to evaluate the accuracy. Training the aforementioned model is done in two steps. First, according to the available ground truth for simulated data, we calculate five NCC values for all pixels in I_1 as a true set. Second, a random noise is added to the ground truth, and then five NCC values are calculated as a false set. Trained model with a large number of samples can be utilized to show accuracy map of the important regions in the strain image.

Results: Field II [4] and ABAQUS (Providence, RI) software are used for ultrasound simulation and for finite element simulation. The probe frequency is 7.27MHz, the sampling rate is 40MHz and the fractional bandwidth is 60%. These parameters are set to mimic commercial probes. Pre-and post-compressed images are of size 1041×250 and maximum axial and lateral displacements are 10 and 1 samples in displacement field. The proposed method has been applied to the aforementioned data wherein the number of training and validation samples are 62690 and 6269, respectively. Classification accuracy for using one NCC is 71.8% and using 5 NCC values is 84.56 %. Accuracy map of the tumor region using 1 NCC and 5 NCC values has been shown below for NP (Negative Prediction) class. NP class addresses the output of the classifier that must be recognized as negative set. Failed pixels are shown in Figs c and d in black. It is clear from this image that the number of failed pixels using 5 NCC values is much less than using 1 NCC value in Figs c and d. These results show that the proposed method substantially outperforms traditional techniques. We have also validated our method on phantom and in-vivo data.

References:

[1] Ophir, J., et al. " Elastography: ultrasonic estimation and imaging of the elastic properties of tissues." Proceedings of the Institution of Mechanical Engineers, Part H: Journal of Engineering in Medicine 213.3 (1999): 203-233.

[2] Viola, Francesco, and William F. Walker. "A comparison of the performance of time-delay estimators in medical ultrasound." *IEEE transactions on ultrasonics, ferroelectrics, and frequency control* 50.4 (2003): 392-401.

[3] Walker, William F., and Gregg E. Trahey. "A fundamental limit on delay estimation using partially correlated speckle signals." *IEEE Transactions on Ultrasonics, Ferroelectrics, and Frequency Control* 42.2 (1995): 301-308.

[4] Rivaz, Hassan, et al. "Real-time regularized ultrasound elastography." *IEEE transactions on medical imaging* 30.4 (2011): 928-945.

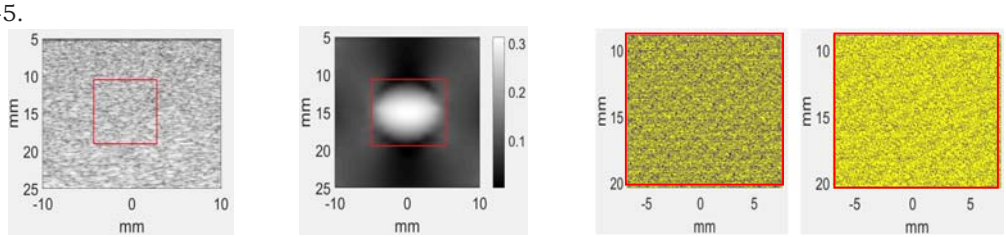

Left to right (a-b-c-d) : (a) B-mode image, (b) Strain image, (c) Accuracy map using 1 NCC value for NP class, (d) Accuracy map using 5 NCC values for NP class. Black pixels in figures c and d show failed pixels in the area within the red square.

012 **LINEAR ACTUATOR-ASSISTED TRANSDUCER TO OBTAIN SUB-PITCH RESOLUTION FOR ELASTOGRAPHY.**

S Selladurai[1], AK Thittai[1].*

[1]Indian Institute Of Technology Madras, Chennai, Tamil Nadu, INDIA.

Background: In elastography, Conventional Linear Array (CLA) based RF data acquisition can only provide accurate displacement measurements in the direction of beam propagation (axial direction) compared to the perpendicular direction (lateral). For high-precision Lateral Displacement Estimation (LDE), one of the popular methods is by interpolating additional A-lines in between neighboring RF A-lines [1]. However, utilizing actual data from sub-pitch location, if available, will yield fundamentally better estimation. In this paper, we describe a method of acquiring and augmenting true RF A-lines, instead of interpolating the data, by translating the US linear array transducer in sub- pitch range using a linear actuator and analyze the resulting improvements in LDE. Note- eventually the actuator can be integrated inside the transducer casing to form one unit, but it is not the case in the current study. While mechanical translations have known-limitations, it may provide an opportunity to improve the LDE quality in a relatively inexpensive manner. Improving the LDE is necessary for obtaining reliable rotation elastograms, accurate inverse solution, total shear strain elastogram, poroelastograms, etc. Broadly, there are two ways to utilize the data obtained from the sub-pitch location, 1. Stagger the raw RF data and then perform beam forming or 2. Obtain beamformed RF data and then stagger it. While the former is expected to yield fundamental improvements, at this preliminary stage we report the results by implementing the latter. Work on implementing the former approach is currently underway.

Methods: Fig. 1a shows the SPRAT (Sub Pitch Resolution Ultrasound Array Transducer) configuration. Simulation study consisted of two components, (1) Finite Element Simulation of 2D plane-strain model using COMSOL® software and (2) Field II [2] for simulating CLA, SPRAT and pre-&post-compression RF data. Experimental setup consisted of a linear array transducer (pitch of λ) that was connected to a linear actuator (Fig. 1c). In the SPART approach a first set of RF data was acquired at one transducer location and subsequently a second set was obtained after translating the array by a distance of λ/2 using the actuator. These RF data were merged together to form the SPRAT. For elastography experiments a compression of 2% was applied from the top and the LDE were obtained by using the pre- and post-compression SPRAT data. In simulation, the performance improvement of LDE was estimated using the sum of squared error metric by taking the ideal displacements predicted from COMSOL as reference. For experimental data, the SNR of the lateral strain estimates were compared.

Results: A comparison of the lateral PSF obtained using CLA and SPRAT configuration along with the FWHM (full width half maximum) is shown in Figure1 (d) &1(e). Results from simulation and experiments are listed in table 1.

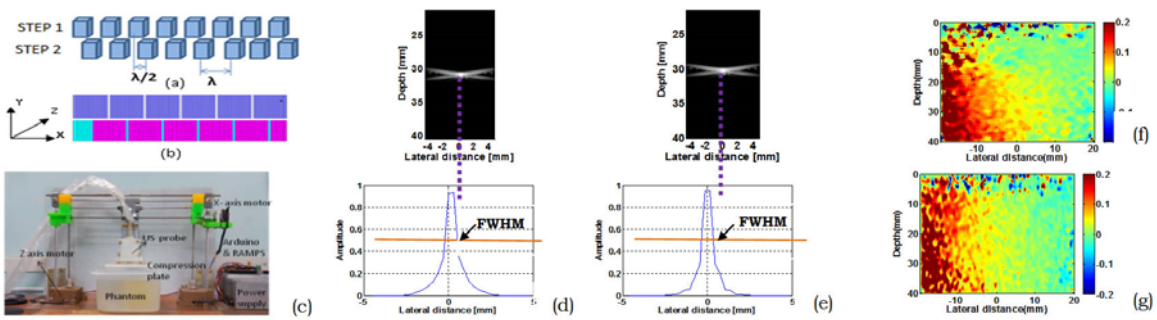

Figure1:(a)Schematic of SPRAT, (b) SPRAT simulation in field II, (c) Experimental setup, simulation of point scaterrer using (d)Linear array and (e)SPRAT, Experimentally obtained LD using (f) linear array and (g)SPRAT.

Table1: Quantitative analysis of CLA and SPRAT technique.

Configuration	Parameters		
	FWHM in mm(simulation)	Mean Square error(simulation)	Lateral Strain SNR(db)(experiment)
CLA	0.78	5.142*10^-4	8.2
SPRAT	0.65	2.264*10^-4	8.6

Conclusions: The simulation and experimental results clearly demonstrate an improvement in precision of LDE obtained from SPRAT compared to CLA method where sub-pitch data were obtained from interpolation.

Acknowledgement: This work was funded by MHRD, Govt. of India.

References:

[1] Elisa Konofagou and J Ophir. "A New Elastographic Method for Estimation and Imaging of Lateral Displacements, Lateral Strains, Corrected Axial Strains and Poisson's Ratios in Tissues", Ultrasound in Med. & Biol., Vol. 24,1998.

[2] Jensen JA. Field: A Program for Simulating Ultrasound Systems. In10TH NCBI, VOL. 4, 1996.

044 **PLURAL SPECTRAL FREQUENCY DIVISIONS FOR HIGH FRAME RATE ULTRASONIC TISSUE DISPLACEMENT VECTOR MEASUREMENT.**

Chikayoshi Sumi. [1]*

[1]Sophia University, 4 Yonban-cho, Chiyoda-ku, Tokyo, 102-0081, JAPAN.

Abstract Body For achieving a human tissue displacement vector and/or strain tensor measurement with a high frame rate, the plural spectral frequency division method (PSFDM) is presented. The effectiveness of processing is demonstrated by performing the measurements on an agar phantom interrogated by wideband ultrasonic (US) single beam scanning and compounding of steered plane wave or spherical wave transmissions.

Background: A high frame rate is required to achieve measurements of a high speed tissue motion or a shear wave propagation, which can be performed using a plane [1,2] or spherical [2] wave transmission, for instance. For a displacement vector measurement, a lateral modulation can be used together with the multidimensional autocorrelation method (MAM) [1]. Alternatively, the spectral frequency division method (SFDM) can also be performed with MAM (e.g., [3,4]). For increasing a lateral spatial resolution imaging, the coherent compounding can be performed on steered plane or spherical wave transmissions, which can also achieve a high frame rate [2,4].

Aims: For achieving a high accuracy tissue displacement vector and/or strain tensor measurement with a high frame rate, the plural spectral frequency division method (PSFDM) is presented.

Methods: The original spectral frequency division method (SFDM) is effective on large bandwidth spectra [4,5]. In this report, a laterally wideband single beam scanning is generated by performing a rectangular apodization on a single beam scanning [5] and a compounding of plural plane wave transmissions [4], on which reception beamforming can be performed once [2]. Specifically, (i) a vertical (axial) or beam direction and (ii) a horizontal (lateral) direction or a direction orthogonal to the vertical (axial) or beam (axial) direction; and (iii) disregarding low frequency spectra (HPF) in the horizontal (lateral) direction or the direction orthogonal to the vertical (axial) or beam (axial) direction. The degree of the effects depends on the respective spectra. (iv) Moreover, disregarding the low frequency spectra in the vertical (axial) or beam direction can also be effective similarly and particularly effective in decreasing calculations of the Fourier's transform. The SFDMs of (i) to (iv) can be performed on such beamformings in two fashions, specifically AND or OR operations. We refer to such methods using plural (or multiple) spectral frequency divisions as the plural spectral frequency division method (PSFDM). Thus, with respect to a single beam scanning, original SFDM is (i), which is performed once for a single spectra to yield two quasi steered beams or waves (i.e., two simultaneous Doppler multidimensional equations), whereas PSFDM yields more quasi-steered beams or waves than the unknown displacement vector components (i.e., ODS).

Results: For instance, on the lateral strain measurement on an agar phantom compressed in a lateral direction [5], SDs were obtained, i.e., original SFDM, 6.39; PSFDM, 6.18 (single beam) and 2.92 (plane waves) $\times 10^{-3}$. However, too many divisions on (i) and (ii) decreased the measurement accuracy in a contrary due to decreasing an independency of generated quasi-beams or waves.

Conclusions: Using PSFDM, the single beam scanning allows the useful and high accuracy measurement/imaging of a displacement vector and/or a strain tensor by simple beamforming with a conventional effective aperture width and no apodization rather than the original SFDM, whereas the compounding of steered plane waves or spherical waves achieves a high frame rate and much higher measurement accuracy, which will enable us to perform high accuracy observations of heart (sector or spharial wave scanning) and liver motions or various blood flows etc. In this report, a 2D displacement vector measurement case is explained and SFDM and PSFDM are significantly effective in a 3D displacement vector measurement case using a finite aperture size and channels of a 2D array transducer. The spectral divisions in the 3D case can be similarly performed and the divisions are explained in ref. 5.

Acknowledgements: This research has been partially supported by the Precise Measurement Technology Promotion Foundation, JAPAN.

References: [1] C. Sumi, Int Ultrasonics Symp, pp. 1771-1776, 2005, [2] C. Sumi, Proc of 14th ITEC (Full paper version), ID: 039 (2015). [3] C. Sumi, Proc of 10th ITEC, ID: 064 (2011). [4] C. Sumi, Proc of 11th ITEC (Full paper version), ID: 068 (2012). [5] C. Sumi, Rep Med Imag, **5**, 58-101 (2012).

006 **THE EFFECTS OF TENDINOPATHY AND EXERCISE INTERVENTIONS ON MULTIAXIAL STRAINS IN THE ACHILLES TENDON INSERTION.**

RL. Chimenti[1,2], M Kelly[1], M Bucklin[1], JP. Ketz[1], AS. Flemister[1], MS. Richards[1], MR. Buckley[1].*
[1]University of Rochester, Rochester, NY, USA; [2]University of Iowa, Iowa City, IA, USA.

Background: Insertional Achilles tendinopathy (IAT), a painful condition that affects 5% of the general population and up to 20% of the athletic population, is challenging to treat non-surgically. We have previously used ultrasound elastography to measure multiaxial strains in the Achilles tendon insertion of healthy individuals during weight-bearing activities [1]. But how these strains are altered by IAT or by exercise protocols used to treat IAT is unknown.

Aims: The aims of this study were to 1) examine the effects of IAT and tendon region on tendon strains in the Achilles tendon insertion; and 2) assess the effect of an exercise protocol aimed at treating IAT on Achilles tendon strains.

Methods: A Sonix Touch L9-4/38 ultrasound transducer (Ultrasonix, British Columbia, Canada) was positioned over the Achilles tendon insertion during weight-bearing dorsiflexion tasks, which included standing and partial squat (Figure 1). The ultrasound images were collected with a center frequency of 10 MHz, a sampling frequency of 40 MHz, a depth of 3 cm and at a frame rate of 128 Hz. A non-rigid image registration-based algorithm [2] was used to estimate transverse compressive and axial tensile strains in the tendon. Strains in healthy (n=20) and IAT (n=24) individuals were measured and compared across pathological state (healthy versus IAT) and region (superficial versus deep). In addition, strains in IAT individuals were compared before and after a 12-week physical therapy protocol that combined isometric and eccentric loading exercises.

Results: For transverse compressive strain, there were significant main effects of pathological state and tendon region. That is, the magnitude of transverse compressive strain was reduced by IAT and was greatest in the deep tendon. However, there were significant interactions between these factors for both dorsiflexion tasks, because IAT reduced transverse compressive strain magnitude more in the deep tendon region than in the superficial tendon. For axial tensile strain, the IAT group demonstrated a main effect of lower tensile strain than the control group. There was also a main effect of greater tensile strain in the superficial region of the tendon compared to the deep during standing but not during partial squat. Completion of the physical therapy protocol resulted in increased transverse compressive strain magnitude in the superficial Achilles tendon compared to the pre-therapy value when standing and when performing a partial squat. Moreover, there was a decrease in axial tensile strain in the deep portion of the tendon in response to physical therapy.

Conclusions: Reduced magnitudes of transverse compressive and axial tensile strains in the IAT group indicate altered mechanical properties specific to the region of IAT pathology. Additionally, these patterns of strain are consistent with the theory of calcaneal impingement against the deep tendon region leading to increased tendon stiffness and to IAT pathology. Importantly, increased transverse compressive strain magnitude in the superficial region following 12 weeks of exercise suggests partial reversal of IAT-associated changes with this intervention.

Acknowledgements: This study was supported by the National Institute of Arthritis and Musculoskeletal and Skin Diseases (NIAMS) of the National Institutes of Health (NIH) under Award Number R03 AR067484 and by a pilot grant funded by NIH/NIAMS Award Number NIH P30 AR061307.

References: [1] Chimenti et al., 2016. Ultrasound strain mapping of Achilles tendon compressive strain patterns during dorsiflexion. J Biomech 49:39-44. [2] Richards et al., 2013. Non-rigid image registration based strain estimator for intravascular ultrasound elastography. Ultrasound Med Biol 39: 515-533.

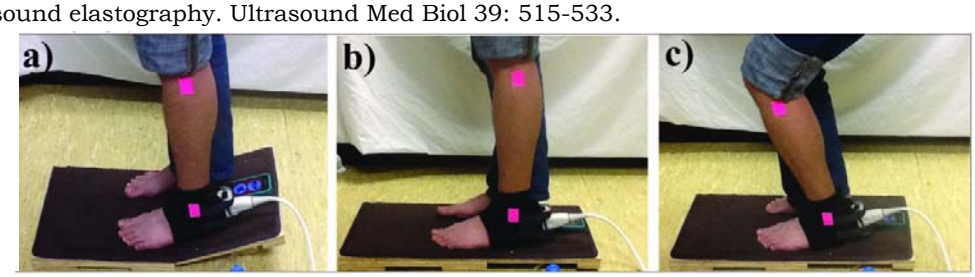

FIGURE 1. Dorsiflexion tasks starting with the heel in an inclined position (**a**) on a platform raised to a 17° inclination to plantarflex the ankle. The two tasks include: (1) standing (**a** to **b**), and (2) partial squat (**a** to **b** to **c**). The tape indicates the location of the fibular head and the lateral malleolus.

054 **FUNCTIONAL CHANGES IN CORTICAL STIFFNESS OBSERVED WITH MAGNETIC RESONANCE ELASTOGRAPHY.**

S Patz[1], N Nazari[2], PE. Barbone[2], R Sinkus[3].*
[1]Harvard Medical School and Brigham and Women's Hospital, Boston, MA, USA;
[2]Boston University, Boston, MA, USA; [3]Kings College London, London, UK.

Aim: To evaluate a new contrast mechanism to measure brain function. Specifically, Magnetic Resonance Elastography (MRE) is used to measure changes in the brain's shear modulus due to functional stimuli.
Methods: A spin-echo MRE sequence [1] was modified to allow two interleaved functional paradigms: P1/P2 for stimulation/no stimulation, respectively. To avoid neuronal habituation, a paradigm is only active for 10s before switching to a different paradigm. The k-space data acquisition was segmented into 10s blocks to be compatible with this approach. For each k-space segment, P1 and P2 are applied sequentially before advancing to the next k-space segment. After each paradigm switch, a period of 1.8s is allowed for hemodynamic equilibrium to be re-established. 8 wave phases in x, y, and z, 2 paradigms, and 9 slices account for 432 images, acq. time= 58 min.
Animal: 6 healthy black mice were studied. Each was anesthetized with isoflurane with the level adjusted for a respiratory rate of ~40/min. During P1, the hind limb was stimulated electrically through two 30 gauge needles inserted in a hind limb. A constant current was supplied: ~1mA, 3Hz, pulse width ~250μs. A control scan was also performed where no stimulus was applied for either paradigm. The MRE apparatus was modified from an earlier version [1]. The modification uses a cage assembly that clamps the mouse head and is mounted on pivots. Vibration frequency=1kHz.
Results: The Figure shows an example of mouse brain data. A 20% increase in |G*| was observed for stimulation (a) in the somatosensory and motor cortex areas, whereas no difference was observed in the control scan (b). (c) & (d) show ROI placement; (e) shows corresponding anatomical scans for the MRE maps, which are averaged over slices 4-6. (f) shows a corresponding cross section from a mouse atlas [2] with the contralateral somatosensory cortex shown in red and the bilateral primary (M1) and secondary (M2) motor cortex shown in blue and green, respectively. Note |G*| is 10% lower in (b) than the "no stimulus" (a) scan, possibly due to incomplete hemodynamic relaxation in (a). Similar changes in |G*| ranging from 10-40% were seen in 5 of 6 mice studied.

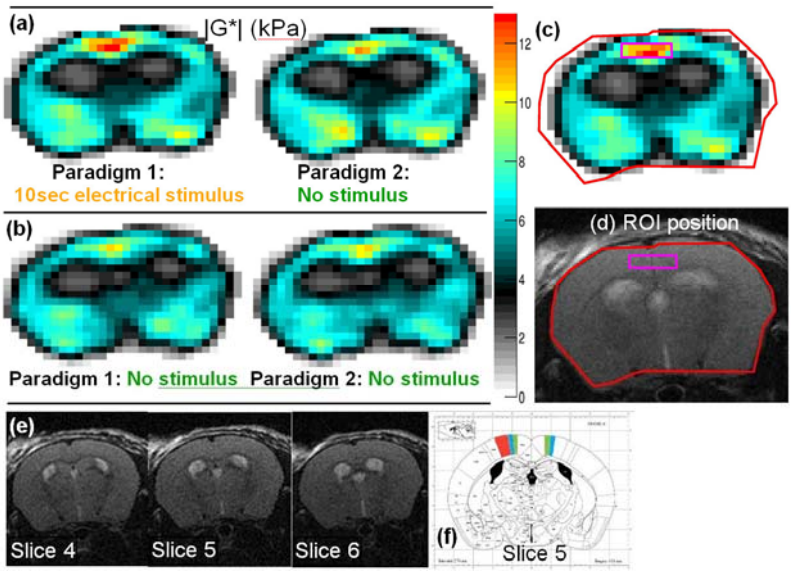

Conclusion: The shear modulus of the brain cortex is shown to be dependent on its functional activity. This is a direct observation of the relationship between structure and function. The mechanism responsible for this observation is currently unknown, but is likely vascular related.
Acknowledgements: Support is gratefully acknowledged from NIH 1R21EB020757; NSF grant No. 1148124; a European Union Horizon 2020 research and innovation grant No. 668039; and from Boston University and Brigham and Women's Hospital.
References:
1. Schregel K, Wuerfel E et al., Proc Natl Acad Sci USA, 6650-6655, 2012.
2. Paxinos G & Franklin KBJ. The Mouse Brain in Stereotaxic Coordinates. 2001: Academic Press.

040 **REAL-TIME HARMONIC MOTION IMAGING FOR FOCUSED ULTRASOUND FOR ABLATION MONITORING OF HIGH-INTENSITY FOCUSED ULTRASOUND TREATMENT *IN VITRO* AND *IN VIVO*.**

Y Han[1], S Wang[1], T Payen[1], EE Konofagou[1].*
[1]Columbia University, New York, NY, USA.

Background: The successful clinical application of High Intensity Focused Ultrasound (HIFU) ablation depends on reliable monitoring of the lesion formation. Harmonic Motion Imaging for Focused Ultrasound (HMIFU), as an all-ultrasound-based elasticity imaging technique, monitors HIFU liver, breast or pancreatic ablation based on the stiffness change of the tissue rather than the echo intensity change in conventional B-mode monitoring, potentially rendering it more sensitive to lesion development.

Aims: In this study, the feasibility of HMIFU for real-time monitoring of the lesion formation during HIFU treatment is explored.

Methods: The HMIFU setup consists of a 93-element, 4.5-MHz HIFU transducer confocally aligned with a 64-element 2.5-MHz phased array or a 104-element 7.8-MHz phased array (for small animal) to transmit and receive through a Verasonics Vantage system. All HIFU channels were excited by amplitude modulated signals to vibrate the tissue at 100 Hz. A GPU-based, fast image reconstruction method was used to monitor lesion development in real-time. *In vitro* experiments were performed on 6 canine liver specimens. The acoustic power and ablation duration varied within the range of 6-8 W and 90-120 s, respectively. *In vivo* experiments were performed on a mouse with a pancreatic tumor. Peak-to-peak HMI displacement maps were generated with the displacement estimates obtained using a 1D cross-correlation method. The first displacement frame was used as a reference and subtracted from the subsequent frames the HMIFU lesion maps during ablation.

Results: In real-time monitoring, the displacement map and lesion map were streamed onto a computer screen at a display frame rate of 2.4 Hz during treatment without interruption (Figure 1(a)). The dimensions (Figure 1(d)) of each lesion (n = 13) measured by HMIFU were compared against corresponding gross pathology. Excellent agreement in lesion depth (r^2 = 0.81, slope = 0.90), width (r^2 = 0.85, slope = 1.12) and area (r^2 = 0.75, slope = 0.58) against pathology showed that HMIFU can successfully monitor thermal lesion development in real time. *In vivo* lesion monitoring exhibited stiffening within the tumor after a 59s-ablation with a displacement reduction rate of 43.3% indicating lesion formation confirmed by pathology.

Conclusions: We concluded that HMIFU has the potential of providing the capability for real-time HIFU monitoring by depicting the formation of the lesion during ablation in soft tissue in vitro and in vivo.

Acknowledgements: Supported by NIH R01EB014496-01.

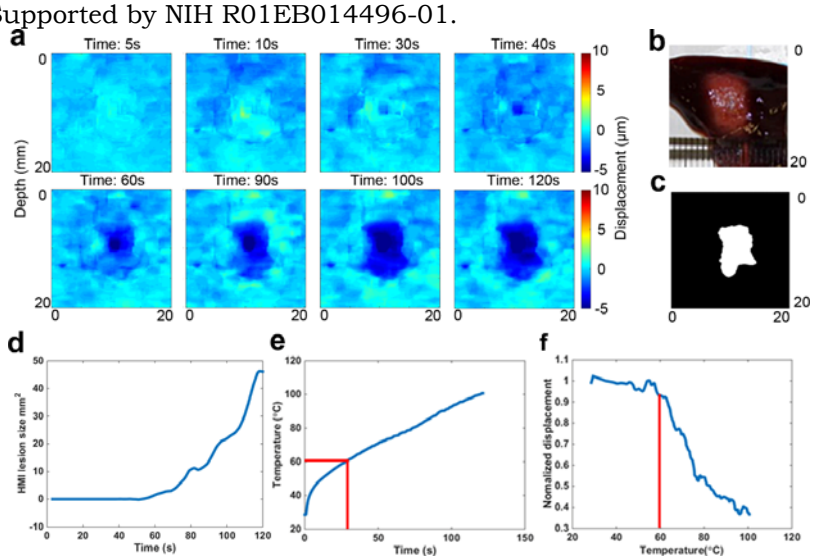

Figure 1. Example case of HMIFU lesion monitoring on 120s ablation. Lesion developing overtime is shown in (a) with blue indicating the formation of the lesion in the liver. Gross pathology of the lesion (b) is shown along with the HMI lesion map at the end of the treatment (c). (d) HMI lesion size development overtime. (e) Temperature measurement from thermocouple. (f) HMI displacement change during the ablation.

029 **SHEAR WAVE ASSESSMENT OF CERVIAL SOFTENING IN PREGNANT RHESUS MACAQUES: *IN VIVO* COMPARISON OF EARLY VS LATE PREGNANCY.**

IM. Rosado-Mendez [1], QW. Guerrero[1], LC. Drehfal[1], AP. Santoso[1], S Kohn[1], M Shotzko[2], ML. Palmeri[3], H Feltovich[1,4], TJ. Hall[1].*

[1]Department of Medical Physics, 1111 Highland Ave., Rm. 1005, Madison, Wisconsin, 53705 USA; [2]Wisconsin National Primate Research Center, University of Wisconsin-Madison, Madison, WI, 53715, USA; [3]Biomedical Engineering Department, Hudson Hall, Rm. 136, Durham, North Carolina, 27708, USA; [4]Maternal Fetal Medicine Department, Intermountain Healthcare, Provo, Utah, 84604, USA.

Background: Vaginal birth, either at term or preterm, is preceded by cervical softening. We are investigating the use of Shear Wave Elasticity Imaging (SWEI) to track cervical softening during pregnancy, with special focus on abnormally rapid changes that could result in spontaneous preterm birth. The Rhesus macaque cervix comprises an interesting animal model to perform *in vivo* longitudinal studies of the progression of cervical changes during pregnancy due to its shorter pregnancy duration and the rate of pregnancy complications similar to humans.

Aims: This work presents a comparison of cervical stiffness assessed *in vivo* through SWEI at early and late pregnancy, as well as before pregnancy and after delivery, in the Rhesus macaque non-human primate (NHP) model.

Methods: Acoustic Radiation Force Impulse (ARFI) based SWEI is being applied to twenty-five NHP subjects before mating, at various time points during the ~ 24-week long pregnancy, and two weeks after delivery. A linear array transducer on a Siemens Acuson S2000 system (Siemens Healthcare, Mountain View, CA, USA) is used to ARFI-induce shear waves and to track them within 25mm^2 regions of interest (ROI) placed at various locations in the anterior and posterior halves of the cervix. Displacements are calculated using phase-correlation techniques[2]. Shear wave speed (SWS) is estimated using a RANdom SAmple Consensus (RANSAC) algorithm [3] as well as with a Radon-sum method [4] to assess the consistency of the estimates. SWS estimates for each time point, each ROI location (anterior vs. posterior), and each subject were compared in terms of their goodness of fit and their consistency to choose the most reliable estimate. The statistical significance of SWS differences (ΔSWS) in pre-pregnancy, early-pregnancy (4 weeks), late pregnancy (20 weeks) and post-delivery for each subject was assessed with a Wilcoxon-paired test with a significance level of $p<0.05$. Here we report inter-subject medians and interquartile ranges (IQR) of ΔSWS.

Results: Eight of the 25 subjects that have been recruited have successfully completed the study. The remaining 17 subjects are at various pregnancy stages and will have completed the study in early September. For these 8 subjects, no significant differences were observed when comparing SWS values obtained before pregnancy and early pregnancy. SWS values at late pregnancy were smaller than those at early pregnancy by ΔSWS=1m/s (ΔSWS IQR: 0.3-2.4m/s) and ΔSWS=2.5m/s (ΔSWS IQR: 1.0-4.8m/s) in the anterior and posterior sides of the cervix, respectively. Statistical significance of ΔSWS between early and late pregnancy was observed only in the posterior side. This has practical importance as pre-pregnancy SWS estimates will not be available in the clinical setting. Post-delivery values were not significantly different from pre-pregnancy or early pregnancy values, suggesting structural recovery.

Conclusions: Our preliminary results support the use of SWEI to track cervical softening during pregnancy. The results from the study with the NHP animal model will be compared to those from an ongoing longitudinal *in vivo* study in humans.

Acknowledgements: This work was supported by National Institutes of Health Grants R21HD061896, R21HD063031 and R01HD072077 from the Eunice Kennedy Shriver National Institute of Child Health and Human Development. We are also grateful to Siemens Healthcare Ultrasound division for equipment loan and support.

References: [1] Huang B, et al., "Estimation of Shear Wave Speed in the Rhesus Macaques Uterine Cervix," IEEE TUFFC, in press. [2] Loupas, T, et al. "Experimental evaluation of velocity and power estimation for ultrasound blood flow imaging, by means of a two-dimensional autocorrelation approach," IEEE TUFFC 42(4): 689-699, 1995. [4] Wang MH, et al., "Improving the robustness of time-of-flight based SWS reconstruction methods using RANSAC in human liver in vivo," UMB, 36(5): 802-813, 2010. [4] Rouze NC, et al., "Robust estimation of time-of-flight SWS using a Radon Sum transformation," IEEE TUFFC 57(12): 2662-2670, 2010.

060 **MONITORING GLIOMA PROGRESSION IN MOUSE BRAIN WITH MRE.**

N Nazari[1], M Nowicki[2,4], S Lawler[2,4], R Sinkus[3], PE. Barbone[1], S Patz[2,4].*
[1]Boston University, Boston, MA, USA; [2]Harvard Medical School, Boston, MA, USA;
[3]Kings College London, London, UK; [4]Brigham and Women's Hospital, Boston, MA, USA.

Background: Glioma is a primary brain malignancy with one of the highest rates of mortality, growth and invasion rates [1]. Ullrich et al. [2] have demonstrated that the mechanical environment strongly regulates glioma cell proliferation and migration rates in culture. MRE provides a means to image elastic properties of the brain, and hence can be used to monitor the mechanical environment of glioma tumors in vivo.

Aims: Use MRE to monitor longitudinal changes of the mechanical properties of glioma and surrounding tissues in mouse brain, and correlate with histology.

Methods: This study included 12 nu/nu athymic mice, divided in 2 groups, which were injected with a human glioblastoma (GBM) stem cell line in the right hemisphere of the brain. MRE was performed on one group of mice weekly over a 4-week period. Each week, 2 mice were sacrificed: one from each group. Brains were fixed immediately after the experiment in order to minimize deviation of histology slides from the MRE and MRI images. Tissue sections were labeled with (1) DAPI (DNA stain) to detect the density of cell nuclei, (2) anti-CD31 antibody to detect blood vessels, and (3) anti-vimentin staining to detect glioma cells and distinguish them from mouse tissue.

Results: MRE images show the tumor as a soft mass, the location of which was verified by histology of the respective brain slices. Both MRE and histology show the tumor grows in size with clear boundaries. Tumor growth in the MRE scans is also seen as a shape distortion of the surrounding soft tissue structures in the intracranial cavity. Histology, but not MRE, shows a dramatic decrease in blood vessel density within the tumor as well as regions of high nuclear density and necrosis.

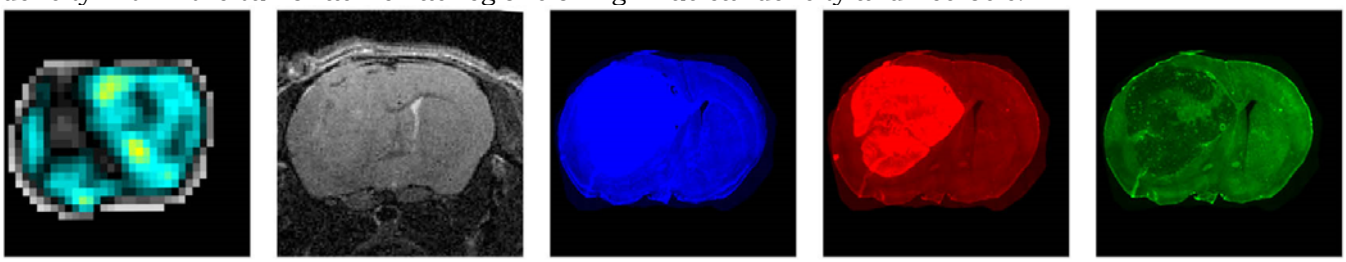

clusions: By measuring the shear modulus, MRE offers a non-invasive imaging modality to provide insight into brain malignancies. Compared to histology, our MRE data did not distinguish between different regions of the tumor implying that it is not sensitive to changes in nuclear density or necrosis within the tumor. The vascularity, as shown by histology, however, did correlate well with the MRE results. Since vascularity or angiogenesis is a known marker of tumors and response to therapy, we conclude that MRE may have an important role to play in the diagnosis and follow-up of brain tumors.

Acknowledgements: Support is gratefully acknowledged from NIH 1R21EB020757; NSF grant No. 1148124; a European Union Horizon 2020 research and innovation grant No. 668039; and from Boston University and Brigham and Women's Hospital.

References:

1) Hess, Kenneth R., Kristine R. Broglio, and Melissa L. Bondy. "Adult glioma incidence trends in the United States, 1977–2000." *Cancer* 101.10 (2004): 2293-2299.
2) Ulrich, Theresa A., Elena M. de Juan Pardo, and Sanjay Kumar. "The mechanical rigidity of the extracellular matrix regulates the structure, motility, and proliferation of glioma cells." *Cancer research* 69.10 (2009): 4167-4174.

078 **INVESTIGATING SKIN MECHANICAL ANISOTROPY USING SHEAR WAVE ELASTOGRAPHY UNDER MULTI-DIRECTIONAL TENSILE STRAIN**

EG Simon[1,2], JC Bamber[1].*

[1]Joint Department of Physics and Cancer Imaging Centre, the Institute of Cancer Research and Royal Marsden Hospital, Sutton, London, UK; [2]François Rabelais University, Inserm UMR U930 and University Hospital Center of Tours, Tours, FRANCE

Background: Previous studies of skin stiffness using tensile strains have suggested that mechanical anisotropy that is present in normal skin could be collapsed in the case of breast cancer related lymphedema (BCRL), even in early stages of the condition [1]. The force-extension curves observed for skin are non-linear, due especially to the progressive recruitment of collagen fibers during stretching, but the previous studies investigating skin anisotropy by tensile tests did not fully explore this non-linear behavior, choosing instead to avoid it as a confounding factor by studying an approximately linear region of the force-extension curve [1,2]. One previous study has suggested that skin anisotropy could also be detected by shear wave elastography (SWE) [3], but the tensile state of the skin in this study was not characterized. Here we explore a hypothesis that taking into account the nonlinear behavior of the skin under tensile strain could improve the detection of anisotropy by SWE.

Aims: To investigate skin mechanical anisotropy using SWE under multi-directional tensile strain.

Methods: The tensile strains were applied with a skin stretching device, the uniaxial extensometer (Cardiff-Biometrics Ltd, Cardiff, Wales), which registered the force-displacement response of the skin. Meanwhile, SWE measurements (Young's modulus E and shear wave speed c_s) of the skin were obtained from the Aixplorer® system (Supersonic Imagine, Aix-en-Provence, France) by positioning an ultrasound transducer L10-5 over the extensometer brackets (Figure 1). The experiment was repeated in two orthogonal directions on the same skin area: across and along the volar forearm. SWE measurements were made in the relaxed position (E1, c_s1), and then in the stretched position (E2, c_s2), during 5 extension-relaxation cycles. Meanwhile, the extensometer provided stiffness values (S) in the relaxed and stretched positions (S1 and S2 respectively). The following ratios were calculated in each direction: E2/E1, c_s2/c_s1, S2/S1.

Results: In healthy volunteers, the force-displacement response of the skin was nonlinear, with a significant correlation between E, c_s, and S (Spearman rank correlation, $r_s=1$, p-value = $4.96e^{-05}$) (Figure 2). Relations between the ratios E2/E1 and S2/S1 are illustrated in Figure 3. The ratio E2/E1 was significantly higher in the stiffest direction (along volar forearm) and depended on the tensile strain (Figure 4).

The application of tensile strain made it possible to observe significant changes E, and in E2/E1 according to the direction, compared to the absence of strain. These directional variations in E2/E1 seemed to be emphasized by the extension.

Conclusions: The application of multi-directional tensile strains probably improves the ability of SWE to detect skin anisotropy, and could be relevant for clinical use in case of BCRL. Further work is required to evaluate this behavior over many individuals and in patients suffering BCRL.

References:

[1] Coutts LV, et al., J Biomech 49, pp94–99, 2016.
[2] Coutts L, et al., Skin Res Technol 19, e37–44, 2013.
[3] Luo C-C, et al., Med Phys., pp 4106–4115, 2015.

Fig 1: SWE scanning of the skin under tensile strain

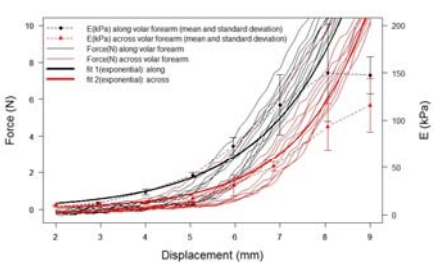

Fig 2: Force and Young's modulus versus tensile extension (one volunteer)

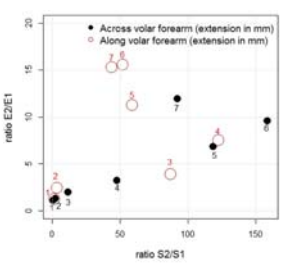

Fig 3: Detection of non-linearity for one volunteer

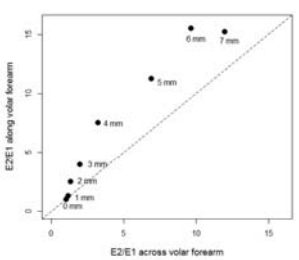

Fig 4: Ratio E2/E1 in two orthogonal directions for one volunteer

065 **MAXIMAL SHEAR STRAIN ESTIMATION FOR IMPROVED BREAST CANCER DETECTION IN Automated BREAST VOLUME SCANNING.**

GAGM Hendriks[1], C Chen[1], HHG Hansen[1], CL De Korte[1].*
[1]Medical UltraSound Imaging Center, Radboud university medical center, Geert Grooteplein 10 Nijmegen, THE NETHERLANDS

Background: Ultrasound imaging is used for breast cancer detection as alternative for mammography which has reduced sensitivity for women with dense breasts. As hand-held ultrasound imaging is clinician depended, the automated breast volume scanner (ABVS) was introduced which consist of a linear transducer translating over the breast while collecting ultrasound data to reconstruct volumetric breast image. Although this scanner shows high sensitivity, clinicians report high recall-rates due to detection of many lesions of uncertain malignant potential. Since malignant compared to benign lesions are often more firmly-bound to its surrounding tissue and stiffer, discrimination and so specificity might be improved by estimating the maximal shear strain as measure for lesion binding.

Aim: To verify whether it is feasible to estimate the maximal shear strain as measure for lesion binding by implementing quasi-static elastography and plane-wave imaging method on an ABVS-like system.

Methods: In this study, two block phantoms containing a loosely- or firmly-bound lesion (both same stiffness) were scanned by an ABVS-mimicking device that consisted of a transducer (L12-5, ATL) mounted on a translational stage to allow axial and elevational translation. While the transducer translated with constant speed (40 mm/s) over the phantom in elevational direction, ultrasound data were collected every 0.5 mm. Acquisition was repeated after lowering the transducer 0.5 mm axially. To reduce acquisition times within one breath-hold, plane-wave acquisitions were used. Thereafter, RF-data at each position were reconstructed by delay-and-sum beam-forming and displacements calculated by two-step coarse-to-fine 3-D cross-correlation of pre- and post-deformation RF-data. The strain components of the 3-D strain tensor were estimated by a least-square strain estimator. The eigenvalues and eigenvectors of this tensor were derived as they represent the maximal strain values and directions. As measure for lesion binding, the maximal shear strain can be calculated by the differences between the minimal and maximal eigenvalues.

Results: The 3-D maximal shear strain results of both phantoms are visualized in figure 1. The maximal shear strains appeared to be increased and more directly distributed around the loosely-bound lesion, whereas they were more globally distributed into the surroundings of the firmly-bound lesion. Shear strain was especially elevated in front and at top of the firmly-bound lesion and might be due to the elevationally translating transducer.

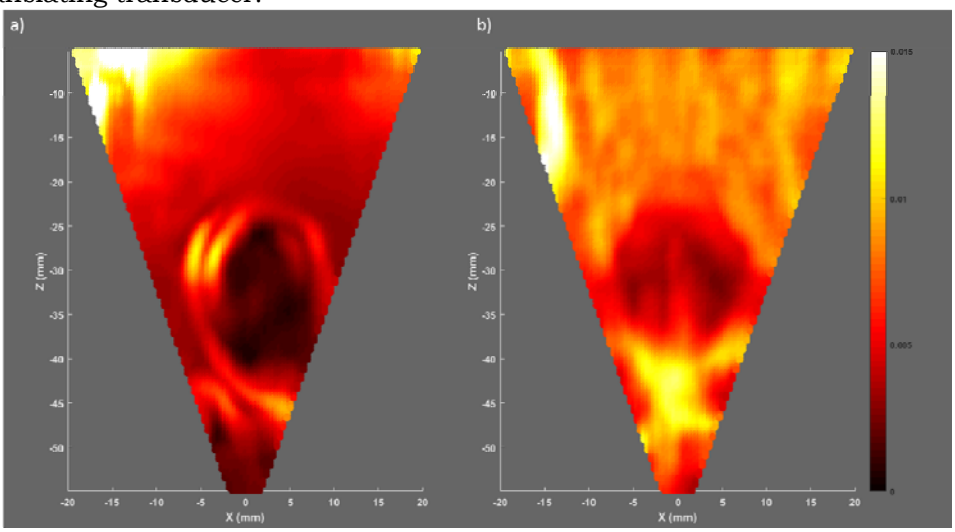

Figure 1 3-D visualization of the maximal shear strain of the phantom containing a loosely-bound (a) and firmly-bound lesion (b).

Conclusions: We conclude that it is feasible to derive the maximal shear strains by ABVS-like scanning which can be used to discriminate between lesions depending on their binding to their surroundings.

Acknowledgements: This research is supported by the Dutch Technology Foundation STW (NKG 13290), which is part of the Netherlands Organization for Scientific Research (NWO), and which is partly funded by the Ministry of Economic Affairs.

022 **MINIMUM VARIANCE BEAMFORMING WITH SPATIAL COMPOUNDING FOR IMPROVED PERFORMANCE OF PLANE WAVE VASCULAR ELASTOGRAPHY.**

P. Verma[1], MM. Doyley[2].*
[1]Department of Physics and Astronomy, University of Rochester, Rochester, NY, USA; [2]Department of Electrical & Computer Engineering, University of Rochester, Rochester, NY, USA.

Background: Plane wave (PW) imaging achieves narrow lateral beam width using boxcar apodization, but at the expense of high side-lobes. Combining spatial compounding (SC) with fixed or adaptive apodization reduces the side-lobe levels while improving the sonographic signal-to-noise ratio. For this study, we used modified sinh functions with parameter β for fixed apodization case. For β=1, this function closely resembles spheroidal wave functions that have been shown to produce lowest side-lobes [1]. For adaptive apodization, we employed minimum variance beamformer (MVB) with subarray averaging [2].

Aims: The aim of this study was to evaluate the quality of sonograms and elastograms produced with: (1) SC combined with fixed apodization (modified sinh functions); (2) SC combined with MVB.

Methods: We used the Field II ultrasound simulation program and finite element modeling as described in Korukonda et al., 2013 [3] to generate PW echo data. The simulated vessels were incompressible with Young's moduli of 41.6 kPa and 19.9 kPa assigned to vessel wall and plaque, respectively. A uniform pressure of 666.7 Pa was applied to the inner lumen. The imaging was performed at 5 MHz with transducer parameters chosen to represent the L14-5/38 probe used in our experimental ultrasound system. In case of fixed apodization, we used modified sinh functions with β=1.0, 1.5, 2.0 and 2.5 for comparison along with boxcar apodization. For MVB, we assessed the imaging performance for subarray lengths (L) of 1, 16, 32, 48 and 56 elements. The spatial compounding was performed over 1, 3, 5, 7 and 11 angles at the increments of 2 degrees.

Results: Figure 1 (a) and (b) shows the improvement in elastographic contrast-to-noise ratio (CNRe) obtained by combining SC with fixed apodization and MVB, respectively. CNRe increases with increase in number of angles for both cases except SC+sinh(β=1.0). For lower number of angles (≤5), the MVB method achieved the highest gain in CNRe (> 5 dB); whereas for higher angles (> 5) better performance was achieved using no apodization (boxcar). This occurred because echo data obtained at large beamsteered angles was highly decorrelated, which reduces the efficacy of the averaging process while computing the final covariance matrix.

Conclusions: In this study, we evaluated the combined effect of apodization and spatial compounding on the performance of sonograms and elastograms produced with PW imaging. Spatial compounding with both fixed apodization and MVB reduced clutter in the sonograms and improved their quality. However, SC+MVB demonstrated better performance for low sector angles.

References:

[1] K. J. Parker. Correspondence: Apodization and windowing functions. *IEEE Trans. Ultrason., Ferroelectr., Freq. Control*, 60(6):1263–1271, June 2013.
[2] J. F. Synnevag, A. Austeng, and S. Holm. Adaptive beamforming applied to medical ultrasound imaging. *IEEE Trans. Ultrason., Ferroelectr., Freq. Control*, 54(8):1606–1613, August 2007.
[3] S. Korukonda and M. M. Doyley. Visualizing the radial and circumferential strain distribution within vessel phantoms using synthetic-aperture ultrasound elastography. *IEEE Trans. Ultrason., Ferroelectr., Freq. Control*, 59(8):1639–1653, August 2012.

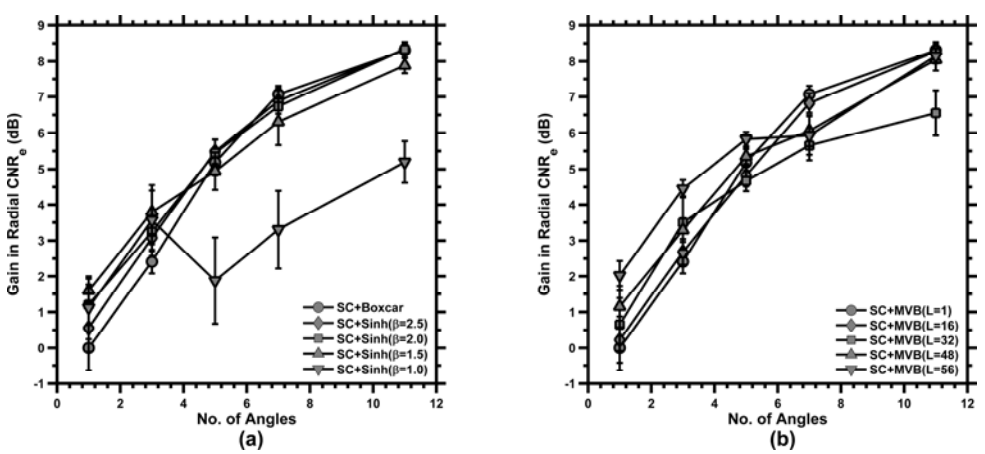

008 **IMPROVING ROTATION ELASTOGRAM QUALITY USING SYNTHETIC TRANSMIT APERTURE TECHNIQUE: EXPERIMENTAL RESULTS.**

Lokesh B[1], AK Thittai[1].*

[1]Indian Institute of Technology Madras, Chennai-600036, INDIA.

Background: It is well-documented in literature that benign fibroadenomas are loosely-bonded to its surrounding tissue and tend to slip under a small compression, while malignant lesions do not [1]. It has been shown specifically that when a loosely-bonded asymmetric lesion is oriented non-normally to the axis of compression, nonzero axial-shear strain values appear inside the lesion referred to as "fill-in" [2]. This fill-in feature observed in Axial Shear Strain Elastogram (ASSE) was thought to be a surrogate of the actual rigid-body rotation [3]. In order to directly image this rotation (Eqn. 1) it would be necessary to improve the lateral displacement estimates. Recently, Synthetic Transmit Aperture (STA) technique was adapted for improving lateral displacement estimation in elastography [4]. We had earlier reported a simulation study showing improvements in quality of Rotation Elastogram (RE) by extending the use of STA approach [5]. In this work, we report on the experimental validation of this approach using tissue-mimicking phantoms.

$$Wx,y(rotation) = 0.5\left(\frac{\partial v}{\partial x} - \frac{\partial u}{\partial y}\right) \qquad (1)$$

u-lateral displacements, v-axial displacements, x and y are the lateral and axial directions, respectively

Aims: Experimental validation of full Synthetic Transmit Aperture (STA) technique for improving the rotation elastogram quality.

Methods: Phantom was made using agar-gelatin-water mixtures containing three loosely-bonded inclusions whose sketch is shown in Figure 1(a). The cylindrical inclusions were 3 times stiffer than the background. The inclusion in the region-of-interest (shown in red box) is an ellipse with major to minor axis ratio of 0.7. Pre- and post-compressed (~2%) RF data were collected and stored using Conventional Focused Beamforming (CFB) technique and STA technique by SONIX TOUCH Q+® (Analogic Corp., MA, USA) scanner operating at 5 MHz center frequency. A multilevel 2-D displacement tracking algorithm [2] was used to obtain the axial and lateral displacement estimates. The RE was obtained using Eqn. 1. In order to quantitatively compare STA and CFB, Contrast to Noise Ratio (CNR) of RE was calculated. A total of 5 imaging planes separated by approximately 0.3 mm were acquired to calculate the mean and standard deviation of CNR value.

Results: Figure 1(b-e) demonstrates the improvement in lateral displacement estimates and image quality of RE obtained from STA technique over the CFB technique. The calculated value (mean ± std) of the CNR was 4.69 ± 2.32 and 2.35 ± 1.15 for STA and CFB, respectively.

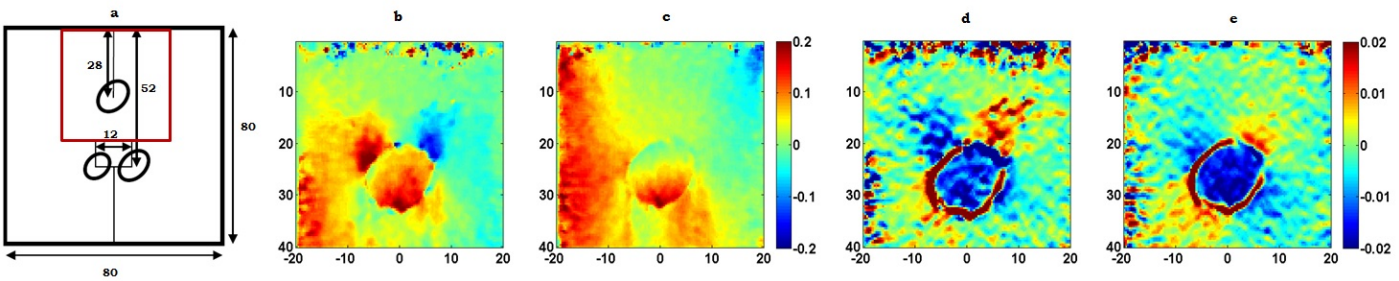

Figure 1: (a) Sketch of phantom geometry with the region bounded by red lines representing the ROI of acquired image. The lateral displacement estimates (b-c) and RE (d-e) obtained using CFB and STA technique are shown for comparison. Note: images shown are an average of 5 frames obtains at different planes. All dimensions are in mm.

Conclusions: The experimental results demonstrate that STA technique can be used to obtain improved-quality rotation elastogram. Current efforts are on to overcome some of the known limitation with STA technique to make it practically useful for this application.

Acknowledgements: Authors would like to thank Ministry of Human Resource Development (MHRD), Government of India, for financially supporting this work.

References:

[1] Ueno E et al. "Dynamic tests in real-time breast echography". Ultrasound in medicine & biology. 1988 Jan 1;14:53-7.
[2] A. K. Thittai et al. "Axial-shear strain distributions in an elliptical inclusion model: experimental validation and in vivo examples with implications to breast tumor classification" Ultra. Med. Biol., vol. 36, no. 5, pp. 814–20, May 2010.
[3] A. K. Thittai et al. "On the advantages of imaging the axial-shear strain component of the total shear strain in breast tumors" Ultra. Med. Biol., vol. 38, no. 11, pp. 2031–2037, Nov. 2012.
[4] S. Korukonda et al. "Estimating axial and lateral strain using a synthetic aperture elastographic imaging system" Ultra. Med. Biol., vol. 37, no. 11, pp. 1893–908, Nov. 2011.
[5] Lokesh B et al. "Improving rotation elastogram quality using synthetic aperture technique" 14th ITEC,Italy,p.81,2015.

064 **VASCULAR SHEAR WAVE ELASTOGRAPHY: COMPARING SHEAR WAVE VELOCITY IN THE LONGITUDINAL AND TRANSVERSE IMAGING PLANE.**

H.H.G. Hansen[1], M. Pernot[2], S. Chatelin[2], M. Tanter[2].*

[1]Radboud university medical center, Nijmegen, Geert Grooteplein 10, Nijmegen, THE NETHERLANDS; [2]Institut Langevin, École Supérieure de Physique et de Chimie Industrielles, Paris, FRANCE.

Background: Rupture of atherosclerotic plaques in carotid arteries is considered to initiate many strokes and transient ischemic attacks. Especially lipid-containing plaques with a thin fibrous cap are known to be dangerous, because of their high chance at sudden rupture. Ultrasound shear wave elastography (SWE) might provide a fast, patient-friendly and inexpensive means to detect lipids in the arterial wall. Several studies already showed that SWE enables detection of locally softer regions in vessel-mimicking phantoms and also in vivo shear wave velocities correlated with histology-derived plaque composition [1, 2]. However, studies only report SWE in a longitudinal imaging plane, while it is known that the induced waves also propagate in the circumferential direction [3]. These circumferentially traveling waves might also be used to quantify stiffness in other parts of the vessel cross-section.

Aims: To compare shear wave velocity estimation in transverse and longitudinal imaging planes.

Methods: A SuperSonic Imagine Aixplorer (Aix-en-Provence, France) equipped with an SL10-2 (f_c = 6 MHz) induced a single focused ultrasonic push (300 µs) in the center of the top wall of concentric homogeneous vessel-mimicking polyvinylalcohol phantoms of varying dimensions and Young's moduli. The push was followed by 100 plane wave acquisitions (PRF ≥ 10 kHz) for shear wave velocity assessment. The push-imaging sequence was repeated for longitudinal and transverse imaging planes. Axial phase shift maps were derived showing the axial motion as a function of time along longitudinal and circumferential propagation paths centered between the inner and outer wall boundaries. From these maps, shear wave velocities were determined. For the longitudinal map, velocity was estimated only in the top wall. For the circumferential map, it was estimated for each quadrant of the circumference.

Results: Shear modulus, dimensions, and estimated shear wave velocities (SWVs) for the phantoms are presented in table I. As can be observed the estimated velocities for the longitudinal direction are usually lower than for the circumferential direction. The difference is largest for the thick walled phantom. Overall, similar SWVs were estimated for the top-left, and top-right quadrant, and for the bottom-left and bottom-right quadrants. For the thick walled phantom, the SWV in the bottom quadrants was ~2.5 m/s lower than for the top quadrants. For the other phantoms differences between top and bottom were smaller, although a small systematic increase in SWV was observed from top to bottom for the intermediate phantom. The large differences for the thick walled phantom are due to the fact that the shear waves are less guided along the circumference and thus not exactly follow the defined propagation path. In the intermediate phantom, dispersion seems to cause the variation in SWV between top and bottom. Nevertheless, for all measurement locations SWV positively correlated with wall stiffness.

Table I: Phantom properties and estimated shear wave velocities (SWV) in the top wall of the longitudinal cross-section and the top, right, left and bottom wall of the transverse cross-section.

Phantom	µ(kPa)	Inner Ø	Wall thickness	SWV longitudinal	SWV top-right	SWV top-left	SWV bottom-right	SWV bottom-left
Thick	**75.5**	**0.7 cm**	**0.60 cm**	**6.8 m/s**	**10.2 m/s**	**10.1 m/s**	**7.6 m/s**	**7.5 m/s**
Intermediate	**7.8**	**0.7 cm**	**0.30 cm**	**2.7 m/s**	**3.2 m/s**	**3.3 m/s**	**3.8 m/s**	**3.9 m/s**
Thin	**24.0**	**0.6 cm**	**0.15 cm**	**4.1 m/s**	**4.8 m/s**	**4.7 m/s**	**4.7 m/s**	**4.3 m/s**

Conclusions: Shear wave elastography in transverse vascular imaging planes seems feasible, although an exact quantification of elasticity seems difficult because wave propagation highly depends on vessel geometry.

Acknowledgements: This research is supported by the Dutch Technology Foundation STW (NKG 12122), which is part of the Netherlands Organization for Scientific Research (NWO), and which is partly funded by the Ministry of Economic Affairs.

References:

[1] Maksuti E et al. Ultrasound Med Biol. 2016 Jan;42(1):308-21
[2] Garrard JW et al. Ultraschall Med. 2015 Aug;36(4):386-90.
[3] Couade M et al. Ultrasound Med Biol. 2010 Oct;36(10):1662-76.

033 **QUANTITATIVE OPTICAL COHERENCE ELASTOGRAPHY.**

L Dong[1], P Wijesinghe[2], J T. Dantuono[1], D D. Sampson[2], P.R.T. Munro[3], B. F. Kennedy[2], A.A. Oberai[1].*

[1]Rensselaer Polytechnic Institute, Troy, NY 12180, USA; [2]The University of Western Australia, Crawley, WA 6009, Australia; [3]University College London, WC1E 6BT, UK.

Background: Over the past 15 years, optical coherence elastography (OCE), based on optical coherence tomography (OCT), has gained attention as a means to generate images of mechanical properties of tissue at a finer resolution than ultrasound [1]. Applications of OCE in many areas, including breast cancer, ophthalmology and cardiology, are currently being considered. In this talk we will describe several new developments in OCE that have led to quantitative elastic modulus images with spatially adaptive resolution. First, we describe the solution of an inverse problem in the presence of a calibration layer that leads to quantitative modulus images with minimal assumptions about the stress state of the material [2]. Second, we describe a spatially adaptive approach to reconstructing the modulus that allows for reconstructions in three dimensions at high resolution.

Aims: Develop algorithms for generating quantitative images of elastic moduli using OCE with spatially adaptive resolution.

Methods: The axial displacements were obtained from an experimental set up described in [2] which probed the sample of interest placed under a calibration layer of known elastic properties. Using these displacements, an inverse problem was solved to determine the spatial distribution of the shear modulus. In order to make use of the prior information concerning the calibration layer, as well as to circumvent the difficulty of the incomplete and noisy displacement field, the inverse problem was solved as a PDE-constrained minimization problem, regularized by total variation to better reconstruct tissue heterogeneity. A gradient-based optimization algorithm, L-BFGS, was used to find the solution. In order to reduce the computational cost, adjoint equations were used to efficiently evaluate the gradient vector. Finally, an adaptive mesh strategy was used to optimally allocate computational resources, so as to better resolve the more heterogeneous regions of the sample.

Results: Our algorithm reconstructed the shear modulus distribution of a tissue phantom with a stiff inclusion with less than 15% error in both 2D and 3D, respectively (see Figures 1a and 1b). This algorithm was also used to map the elastic properties of ex-vivo tissue samples in two and three dimensions, respectively (see Figures 2a and 2b).

Conclusions: We have developed and validated a new approach to OCE to generate modulus images with minimal assumptions regarding stress state of the sample. We have applied this approach in conjunction with an adaptive resolution algorithm to generate modulus images in three dimensions.

Acknowledgements: LD and AAO are supported by US NSF grant #1148,111.

References:

[1] BF Kennedy, KM Kennedy, DD Sampson: A Review of Optical Coherence Elastography: Fundamentals, Techniques and Prospects. IEEE J Sel Topics Quantum Electron, 20(2), pp.272-288, 2014.

[2] L Dong, P Wijesinghe, JT Dantuono, DD Sampson, PR Munro, BF Kennedy, AA Oberai: Quantitative Compression Optical Coherence Elastography as an Inverse Elasticity Problem. IEEE J Sel Topics Quantum Electron, 22(3), pp.1-11, 2016.

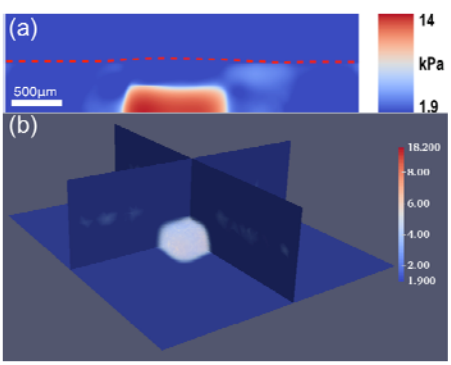

Figure 1: Shear modulus (kPa) reconstruction of a tissue phantom with a stiff inclusion in (a) 2D and (b) 3D.

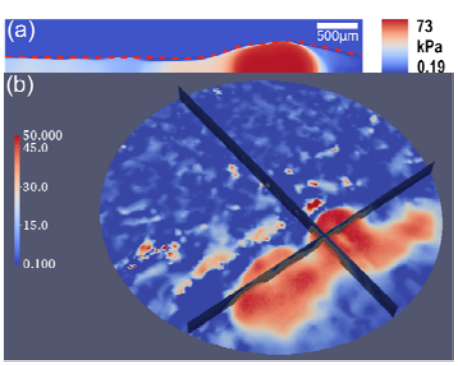

Figure 2: Shear modulus (kPa) reconstruction of (a) the equine bronchus in 2D and (b) the breast tumor tissue in 3D.

066 **ELASTOGRAPHY OF PORCINE CORNEA BY TRACKING THE PROPAGATION OF SURFACE ACOUSTIC WAVES USING OPTICAL COHERENCE ELASTOGRAPHY.**

F. Zvietcovich[1], J. Yao[2], M. Ramirez[3], M.R.Buckley[3], J.P. Rolland[2], K J. Parker[1].*

[1]Department of Electrical and Computer Engineering, [2]The Institute of Optics, [3]Department of Biomedical Engineering, University of Rochester, 500 Joseph C. Wilson Blvd., Rochester, NY, 14627, USA.

Background: Measuring the biomechanical properties of the cornea, such as shear modulus, is fundamental to better understanding, diagnosing, and monitoring degenerative ocular diseases [1]. Current clinically-available elastographic techniques for the cornea suffer from inaccuracy and low depth-resolved resolution. Optical coherence tomography (OCT) has being successfully applied to the study of the cornea structure due to its micro-scale resolution and its depth penetration in millimeters. The application of OCT in elastography can be used to calculate the speed of surface acoustic waves (SAW) in the cornea since it is related to the local shear modulus [2].

Aims: To estimate the depth-resolved shear modulus of the cornea in order to identify different elastic layers by tracking the propagation of SAW.

Methods: A fresh porcine cornea (Fig. 1a) was excited with a rod connected to a piezoelectric actuator in order to produce a tone-burst of 1 kHz propagating from left to right (Fig. 1b-d). The propagation of the waves was detected using a phase-sensitive OCT system implemented with a swept source laser (HSL-2100-WR, Santec, Aichi, Japan) with a center wavelength of 1318 nm. The tone was sent every 35 ms in order to acquire motion frames at a frame rate of 20 kHz. The region of measurement in the sample consisted of a rectangle 2.5 mm high x 15 mm wide. After the acquisition process was conducted, motion frames were acquired and stored as a video. Subsequently, space-time maps (Fig. 1e) were calculated for each propagation path. Herein, the slope of the main peak trajectory of the tone-burst represents the inverse of the SAW speed, which is related to the elasticity of the sample [3].

Results: Experiments with porcine cornea reveal differentiated layers as shown in the 2D SAW speed map (Fig. 1 f). Moreover, we found a decreasing tendency with a local maximum close to the cornea surface when a vertical depth-resolved speed profile was analyzed (Fig. 1g). The SAW speed values range from 1.10 m/s to 1.47 m/s, which produce shear moduli of 1.34 kPa and 2.39 kPa, respectively.

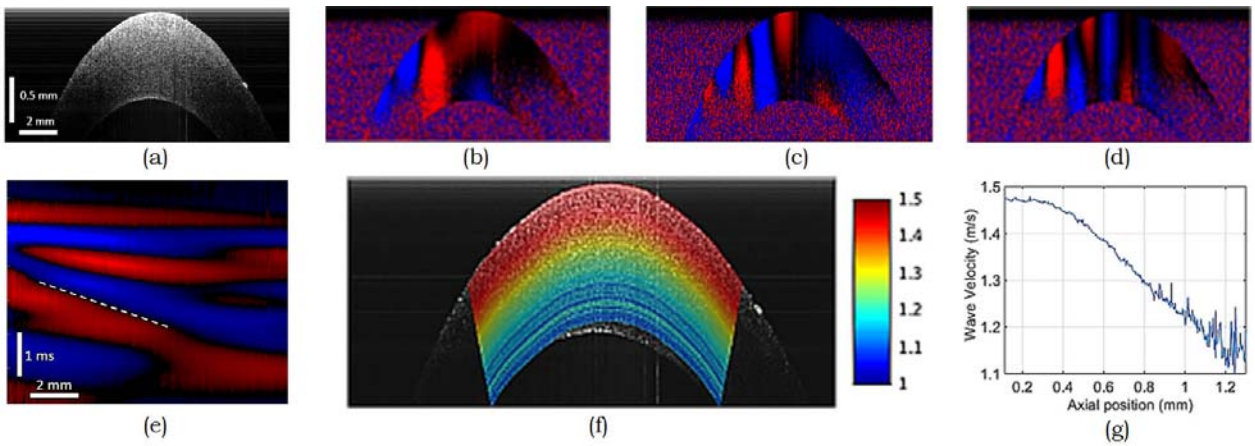

Fig 1. (a) B-mode structural image of a porcine cornea (b-d) Motion 2D snapshots of SAW propagation at various instants (needle located on the left side). (e) Space-time map of SAW propagation. (f) 2D SAW speed map depicting differentiated layers. (g) Depth-resolved SAW speed profile depicting a decreasing tendency.

Conclusions: SAW speed can be successfully measured for the identification of differentiated layers in *ex vivo* cornea using OCT. Further research related to the SAW dispersion is required for the estimation of viscoelastic parameters.

Acknowledgements: This research benefitted from support of the II-VI Foundation.

References:

[1] C. Edmund, "Corneal elasticity and ocular rigidity in normal and keratoconic eyes," *Acta Ophthalmol.* (Copenh.) **66**(2), 134–140 (1988).

[2] C. Li, G. Guan, Z. Huang, M. Johnstone, and R. K. Wang, "Noncontact all-optical measurement of corneal elasticity," *Opt. Lett.* **37**(10), 1625–1627 (2012).

[3] I. A. Viktorov, *Rayleigh and Lamb waves: physical theory and applications*, Plenum Press (1970).

071 **SIMULTANEOUS ACQUISITION OF MRE AND SLDV FOR COMPARISON OF MAGNETIC RESONANCE AND OPTICAL ELASTOGRAPHY.**

S Brinker [1], S P. Kearney [1,2], T J. Royston [1,3]. D Klatt[1,3].*
[1]Department of Mechanical & Industrial Engineering, University of Illinois at Chicago, Chicago, IL, USA; [2]Advanced Photon Source, Argonne National Laboratory, Argonne, IL, USA; [3]Richard and Loan Hill Department of Bioengineering, University of Illinois at Chicago, Chicago, IL, USA.

Background: Elastographic techniques are diagnostic tools based on the mechanical behavior of soft biological tissue that varies in health and disease. Typically the mechanical properties are calculated from measured tissue displacement fields that are externally introduced using a mechanical driver.

Aims: To compare the displacement fields and complex moduli in soft tissue-mimicking media acquired using two elastography imaging modalities, magnetic resonance elastography (MRE) and Scanning Laser Doppler Vibrometry (SLDV).

Methods: This work introduces a novel platform to concurrently measure both, internal and surface displacement fields using MRE and SLDV, respectively. Wave motion was induced into cylindrical soft tissue mimicking specimens of Plastisol and Ecoflex using geometric focusing actuation at 60, 100 and 150, and 250 Hz. Phantom stiffness was varied by adjusting the softener amount in each material. Complex shear moduli were derived in MRE and SLDV using 3D algebraic Helmholtz inversion [1] and averaged 1D curve fitting [2], respectively.

Results: It is visually perceptible from the wave images that internal and surface displacement fields show similarity in wave front geometry at all frequencies. Storage shear modulus was closest at 150 Hz with Plastisol G' (MRE) = 9.03 ± 0.43 kPa and G' (SLDV) = 8.82 ± 0.15 kPa while Ecoflex was G' (MRE) = 15.71 ± 0.95 kPa and G' (SLDV) = 14.3 ± 0.03 kPa. Generally, the SLDV-derived values were lower than the MRE-derived values. Correlation between MRE and SLDV complex shear moduli related by all 36 coupled scans yields a Pearson's correlation of $\rho = 0.88$ with $p < 0.001$ for G' (storage modulus) and $\rho = 0.85$ with $p < 0.001$ for G" (loss modulus).

Discussion: While a good correlation was observed between MRE and SLDV, there was the trend of underestimated moduli using SLDV compared to MRE. The observed similarity of the wave images using both methods indicates that the chosen actuation setup imposed the continuation of the body wave to the phantom surface. We speculate that differences observed in calculated moduli are due to the use of different wave inversion algorithms. Further study is needed.

Conclusions: The introduced platform can serve as a cross-validation method for MRE and SLDV. Also, the relationships between body and surface wave propagation in soft tissues can potentially be investigated using a different mechanical actuation setup.

References: [1] Manduca et al.; *Med Image Anal*; 5(4); 237-254 (2002); [2] Kearney et al.; *Phys Med Biol*; 60; 6975-6990 (2015).

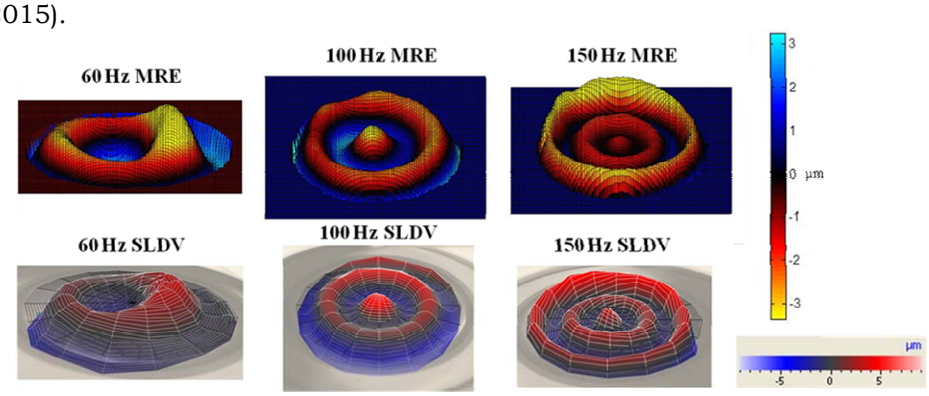

Comparison between surface and internal displacement fields (perpendicular to specimen axial plane) for the large Ecoflex specimen with increasing frequency acquired using SLDV and MRE, respectively. Data was collected simultaneously for both imaging modalities at each individual excitation frequency. MRE wave motion images are located ~2 mm below the specimen surface. SLDV wave images are acquired from the specimen surface.

045 **STUDY OF NONLINEAR INVERSION PARAMETERS FOR MR ELASTOGRAPHY ON PHANTOMS AND HUMAN BRAIN.**

AT Anderson[1], CL Johnson[2], L Solamen[3], MDJ McGarry[3], KD Paulsen[3], BP Sutton[1], EEW Van Houten[3,4], JG Georgiadis[1,5].*

[1]University of Illinois at Urbana-Champaign, Urbana, IL, USA; [2]University of Delaware, Newark, DE, USA; [3]Dartmouth College, Hanover, NH, USA; [4]Université de Sherbrooke, Sherbrooke, QC, CANADA; [5]Illinois Institute of Technology, Chicago, IL, USA.

Background: Magnetic resonance elastography (MRE) has emerged as a sensitive method for evaluating the mechanical properties of the human brain [1], and has shown significant promise in detecting disease [2]. However, the potential for observing meaningful regional mechanical property variations in the brain is dependent on the accurate estimation of material properties through inversion algorithms that rely on specific parameter choices.

Aims: This research investigates the effects of two nonlinear inversion (NLI; [3]) parameters on reconstructed material properties: number of conjugate gradient (CG) iterations and the subzone size.

Methods: External vibration was applied to a silicone phantom and the brain of a healthy human subject with a pneumatic actuator; MRE imaging captured the steady state displacement fields; and viscoelastic material property distributions were reconstructed via NLI. NLI was executed with varying two dominant parameters: CG iterations per subzone solution (range: 2 to 5 iterations) and subzone sizes (range: $L_s/4$ to L_s cubic edge length, where L_s is the average shear wavelength of the material).

Results: The NLI material property reconstructions for the phantom and human brain (Fig 1) show an absolute difference in the final reconstructed material properties and a relative contrast between features across the parameters. The extremes of the subzone size highlight problems with too little or too many elements involved in estimation of parameters. For the largest subzone, the model-data mismatch of the falx cerebri corrupts the reconstruction and the surrounding tissue. An increase in CG iterations increases the sharpness and contrast of features, but with a computational cost.

Conclusions: An accurate inversion from NLI is a balance of subzone size relative to material features and determining the number of sufficiently necessary CG iterations. The phantom allows for independent mechanical testing and direct comparisons can be made but the human brain will require new criteria for determining accurate solutions. The criteria for *in vivo* data will, most likely, build from understanding the determinability criterion of the material parameters from the Hessian matrix, or an approximation, for the well-understood case of the phantom and applying it the *in vivo* brain reconstructions.

Acknowledgements: Research partially supported by NSF CMMI-1437113 and NIH/NIBIB R01-EB018230. Computational resources provided by UIUC-NCSA Blue Waters and Calcul Québec's Mammouth parallèle 2. Imaging support from the Biomedical Imaging Center of the Beckman Institute at UIUC.

References: [1] C Johnson, M McGarry, et al. Local mechanical properties of white matter structures in the human brain. NeuroImage, 2013, 79:145-152. [2] I Sack, K Jöhrens, et al. Structure-sensitive elastography: on the viscoelastic powerlaw behaviour of in vivo human tissue in health and disease, 2013, 24:5672-5681. [3] M McGarry, E Van Houten, et al. Multiresolution MR elastography using nonlinear inversion. Med Phys, 2012, 39:6388-6396.

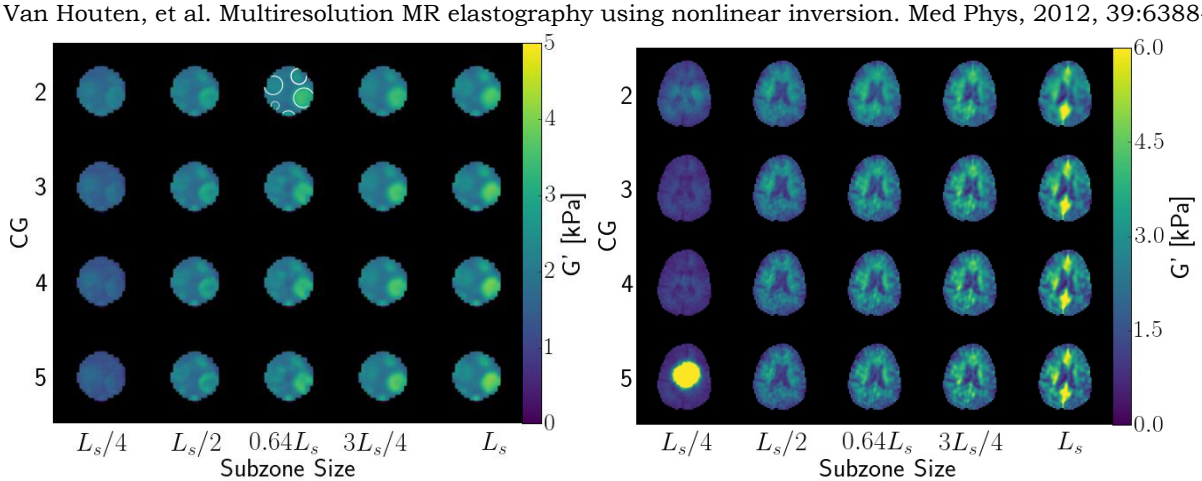

Figure 4: NLI reconstructions of G' (G'' not shown) for a silicon inclusion phantom (left) and for a human subject (right).

036 **LOW COST ALTERNATIVE FOR ULTRASOUND HARMONIC ELASTOGRAPHY.**

C F. Otesteanu, S J. Sanabria, O Göksel.*
Computer-assisted applications in Medicine, ETH Zurich, Zurich, SWITZERLAND.

Background: One elastography method for reconstruction of the visco-elastic parameters of tissue is the inverse problem (IP) formulation of the finite element method (FEM). Different techniques have been used in literature [1] as means of excitation (quasi-static, transient, harmonic), often requiring additional devices or tools that have to be integrated in the acquisition via hardware or software.

Aims: To develop a low cost alternative method as means of excitation for harmonic elastography, with readily available devices that do not require additional hardware or software integration.

Methods: Smartphones are commonly available devices nowadays, which can provide a means of harmonic excitation through vibration at frequencies between 120 – 210 Hz [2]. For our experimental setup (Fig. 1) we used a Samsung Galaxy S4 mini smartphone, attached to the ultrasound probe with a velcro band, to excite a 049 Elasticity QA phantom (CIRS Inc.). A precise alignment and fixation between probe and phone was not required. An 80 kPa inclusion of 1 cm diameter, located at 1 cm depth in a 23 kPa background was imaged. Ultrafast plane wave imaging (SonixDAQ) at 0° angle was used at 1 kHz frame-rate to image the deformations produced by phone vibrations. Axial tissue displacements were tracked using a time-domain cross-correlation method with displacement priors. Displacement phasors were computed and used as the input to the FEM inverse elasticity problem [3]. Fixed top and bottom boundary conditions and free lateral ones were chosen for the reconstruction on a 32-by-32 grid.

Results: Phone-induced displacements were seen to be small (~1 μm) and to exhibit a (harmonic but) non-sinosoidal nature, with multiple resonance peaks. Figure 2 shows the power spectral density of the induced displacements. Considering that cell-phone vibrators operate within 120–210 Hz [1], only the resonance peaks in this range were taken as candidates for solving the inverse problem. The dominating frequency peak (180 Hz) was chosen to compute displacement phasors for the FEM IP. The B-mode image with the reference inclusion location and the reconstructed elasticity image can be seen in Fig. 3. The position, shape (circular) and size (1 cm diameter) of the inclusion were clearly identified, with a mean elasticity value of 91 kPa in a background of 15 kPa, comparable to the 80kPa inclusion in a 23kPa background as stated by the manufacturer. The differences can be attributed to inaccurate boundary assumptions. The reconstructed image has a CNR of 24.9 dB and an RMSE of 1.4 kPa.
The displacements could be tracked accurately (>0.8 correlation factor) up to a depth of 3 – 3.5 cm. This limit is due to the small vibration amplitude and the damping at the given high vibration frequency. In comparison to previously used commercial exciter [4], the contact area of the smartphone is smaller (4.2 cm^2 compared to 25cm^2), hence the vibration amplitude is also expected to be smaller.

Conclusions: We showed that a smartphone used as a means of excitations is capable to produce displacements that can be tracked and used in the FEM IP for successful elasticity reconstruction of a stiff inclusion.

Acknowledgements: This work was supported by the Swiss National Science Foundation.

References: [1] Doyley, M.M.: Model–Based Elastography: A Survey of Approaches to the Inverse Elasticity Problem. Phys. In Med. and Biol., 57(3), pp. R35–73, 2012. [2] Yim, J., Myung, R. and Lee, B., 2007, July. The mobile phone's optimal vibration frequency in mobile environments. Int. Conf. on Usability and Internationalization pp. 646-652. [3] Goksel, O., Salcudean, S.E., Mesh Adaptation for Improving Elasticity Reconstruction Using the FEM Inverse Problem, IEEE Trans. Med. Imag., 32, pp. 408-418, 2013. [4] Otesteanu, C.F., Sanabria, S.J., Goksel, O., Analysis of excitation frequency in elasticity reconstruction using the FEM inverse-problem, ISBI July 2016, pp. 485-488.

Fig. 1. Experimental setup

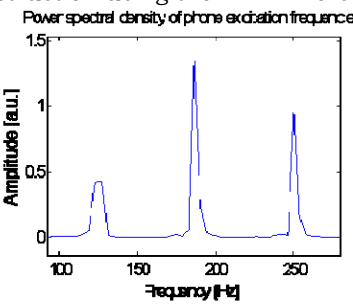

Fig. 2. Spectrum of excitation frequency

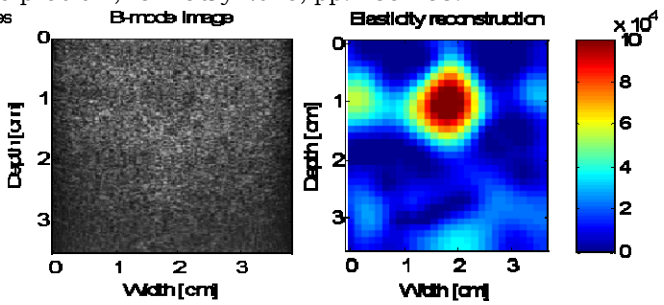

Fig. 3. B-mode and elasticity reconstructed image

027 **SINGLE TRANSDUCER LOVIT-ENABLED PHOTOACOUSTIC IMAGING: A FEASIBILITY STUDY.**

M Theodorou[1], M Jaeger[2], J Fromageau[1], T Petrosyan[2], M-X Tang[3], M Frenz[2], JC Bamber[1].*
[1]Joint Department of Physics and CRUK Cancer Imaging Centre, The Institute of Cancer Research and The Royal Marsden NHS Foundation Trust, Sutton, London, UK; [2]Division of Biomedical Photonics, University of Bern, Bern, Switzerland; [3]Department of Bioengineering, Imperial College London, London, UK.

Background: Freehand epiphotoacoustic (epiPA) imaging holds huge potential as a versatile non-invasive diagnostic tool [1] offering, within a routine ultrasound (US) examination, the ability to identify optically absorbing molecules in tissue by their optical absorption spectrum. Despite this potential, the imaging depth and clinical usefulness remain limited by clutter produced by PA waves generated at locations other than the imaged region. The use of an acoustic radiation force impulse (ARFI) for localized vibration tagging (LOVIT) of true PA signals provides efficient clutter reduction [2] but, to date, LOVIT has been demonstrated using separate US transducers for imaging and ARFI generation.

Aims: The aim of this study was to facilitate eventual clinical evaluation, by further develop, test and optimize LOVIT using a single transducer for US, PA and ARFI.

Methods: Experiments were performed using a pulsed laser (Quantel® Brilliant B, tuned to 800 nm, at 10 Hz repetition rate) connected to a Verasonics® US scanner (V-1-128). Line spreaders from a bifurcated fibre-optic bundle were attached to each side of a 5 MHz linear array transducer (HDI L7-4). Tissue-mimicking phantoms (optical μscattering= 1.25 ± 0.2 cm-1, μabsorption= 0.17 cm-1 [2]) made of gelatine, cellulose and titanium oxide powder were scanned via their upper surface. The phantoms contained seven hypoechoic, 2 mm diameter cylindrical gelatine inclusions positioned at 0.5 cm depth intervals. Each contained India ink to mimic the optical absorption coefficient of blood at 800 nm (μabsorption= 5 ± 0.1 cm-1 [2]). A 2 mm layer on the phantom surface contained India ink to mimic skin optical absorption. Conventional epiPA images were acquired before and at a time close to peak localized displacement induced by a 0.1 ms ARFI. A patch of a PA image with reduced clutter at the ARFI focus was obtained by subtracting the ARFI-PA image from a PA image without an ARFI. A complete clutter reduced image was then generated by electronically moving the ARFI focus to different locations and subsequently mosaicking the resulting clutter-reduced patches.

Results & Conclusions: Successful LOVIT-enabled epiPA was achieved using the same transducer for US imaging, epiPA imaging and ARFI generation, highlighting the possibility for clinical translation of the method. In tests on phantoms that mimic the acoustic and optical properties of breast tissue [3], single transducer LOVIT significantly improved the PA contrast of simulated blood vessels and doubled the useful imaging depth from about 15 mm to approximately 30 mm. Moreover, the performance of the method was quantified to identify the system variables for maximum clutter reduction and thus optimal recovery of the PA contrast deep within the samples. Further research should quantify the safety parameters and study the performance of the LOVIT epiPA imaging in vivo.

Acknowledgements: This research was funded by the Imperial Confidence in Concept Scheme, Imperial NIHR BRC/Imperial Innovations Funds, NIHR BRC at The Royal Marsden and The Institute of Cancer Research Funds 2015, and Chelsea & Westminster Hospital NHS Foundation Trust Funds 2015.

References: [1] Jaeger M, Birtill D, Gertsch A, O'Flynn E, Bamber J. Deformation compensated averaging for clutter reduction in epiphotoacoustic imaging in vivo. J Biomed Opt. 2012. 17(6), 066007, 1-8.
[2] Jaeger M, Bamber JC, Frenz M. Clutter elimination for deep clinical optoacoustic imaging using localised vibration tagging (LOVIT). Photoacoustics, 2013. 1(2):19-29.
[3] Durduran T, Choe R, Culver JP, Zubkov L, Holboke MJ, Giammarco J, Chance B, Yodh AG. Bulk optical properties of healthy female breast tissue. Physics in Medicine and Biology 2002; 47:2847–61.

003 **SOFT TISSUE VASCULARITY AND SHEAR WAVE SPEED.**

KJ Parker[1], J Ormachea[1].*
[1]University of Rochester, Hopeman Building 203, PO Box 270126, Rochester, NY, USA.

Background: The microchannel flow model (MFM) explicitly accounts for the effect of vascular and fluid channels on the stress-strain behavior of soft tissues [1-3]. The validity of the MFM is assessed by its ability to predict changes in stress-strain behavior due to swelling or vasoconstrictors.

Aims: To assess the effects of changes in vascularity on the biomechanical response of soft tissues, using experimental and theoretical approaches.

Methods: Experimental tests of the MFM were made on liver samples where changes in salinity (and therefore cellular swelling, which restricts small channels) were found to change the stress-relaxation curves. Cylindrical cores (approximately 25 mm in diameter and 60 mm in length) were acquired from fresh bovine livers using a custom coring tool, and stored at 4°C for 24 hours in either hypotonic (0.65%) saline, normal (0.9%) saline, or hypertonic (1.15% saline). The osmotic pressure difference can cause swelling or shrinking. In addition, the effect of a vasoconstrictor on living, perfused placentae was measured.

Results: The results show that the four parameter MFM model provides us with a prediction of change in shear wave speed and dispersion. For the liver, the elastic parameter A has a distinct trend as its value changes as a result of hypotonic swelling (highest, 4.1 kPa) vs. hypertonic swelling (lowest, 1.4 kPa). The power law parameter was in the range of 0.11 – 0.14 for all samples. Similar results were obtained in other soft tissues. For the placenta, the dispersion power law parameter increased from 1.4 to 1.6, and the stiffness increased following the administration of a vasoconstrictor.

Conclusions: The microchannel flow model predicts a number of ways in which a sample of normal soft tissue such as liver can be modified so as to be perceived as less compliant, or hardened. First, an increase in E may, for example, be achieved by soaking the specimens in formalin, which is known to harden and preserve samples. A second way to harden a sample is by increasing the viscosity of the fluids in the microchannels [2]. Finally, and even less obvious, is the hardening caused by constriction of the smallest microchannels. This has a double effect in modifying the relaxation spectrum, and shifting it to the right (longer time constants) according to the theory of the MFM [2,3]. The net result is a modification that makes the specimen feel more resistant or harder, over long time periods. This was experimentally approximated in liver and placenta; however, *in vivo*, this could be the net effect of inflammatory responses or edema. This could explain why inflamed regions of skin feel harder than the surrounding normal tissue.

Acknowledgements: This work was supported by the Hajim School of Engineering and Applied Sciences at the University of Rochester.

References:

[1] Parker KJ, "A microchannel flow model for soft tissue elasticity," *Phys Med Biol*, 59(15)4443-4457, 2014.
[2] Parker KJ, "Experimental evaluations of the microchannel flow model," *Phys Med Biol*, 60(11)4227-4242, 2015.
[3] Parker KJ, Ormachea J, McAleavey SA, Wood RW, Carrol-Nellenback JJ, Miller RK, "Shear wave dispersion behaviors of soft, vascularized tissues from the microchannel flow model," *Phys Med Biol*, 61(13)4890-4903, 2016

024 **ELASTIC PROPERTIES OF THE ANIMAL LENS AT DIFFERENT INTRAOCULAR PRESSURES.**

S Park[1], H Yoon[2], C Wu[3], K V. Larin[3,4], S Y. Emelianov[2,5], S R. Aglyamov[1].
[1]University of Texas at Austin, Austin, TX, USA; [2]Georgia Institute of Technology, Atlanta, GA, USA [3]University of Houston, Houston, TX, USA; [4]Baylor College of Medicine, USA; [5]Emory University School of Medicine, Atlanta, GA, USA.

Background: Accommodation is the ability of the human eye to change focus from far to near. Accommodation ability of the eye progressively decreases with age, leading to a condition known as presbyopia. Most of the current approaches for presbyopia correction are based on the assumption that presbyopia is due to a gradual age–related loss of flexibility of the crystalline lens of the eye [1]. However, the exact relation between mechanical properties of the lens and presbyopia remains to be established. Noninvasive measurements of the lens elastic properties will advance the understanding of the mechanism of presbyopia and developing new approaches for presbyopia treatment. In our previous studies, we have used optical coherence elastography approach to measure mechanical properties of the ocular tissues, specifically, the crystalline lens [2,3]. It is well known that mechanical characteristics of tissue significantly depend on the internal pressure. For example, recently, we have demonstrated how the speed of the elastic wave in the cornea increases with intraocular pressure (IOP) [4].

Aims: The major objective of this study is to measure speed of elastic wave propagation in the bovine crystalline lens *ex vivo* in response to the change of intraocular pressure.

Methods: Seven excised bovine eye globes of 25-30 months old animals (Sierra for Medical Science, Inc., Whittier, CA, USA) were used in experiments. Each eye globe was secured in a cuvette filled with saline solution, and cannulated with two needles inserted into the anterior chamber. One needle was connected to a saline-filled syringe via tubing to control the IOP in the eye globe. The other one was connected to a pressure transmitter (Keller AG, WinterThur, Switzerland) via tubing to measure the IOP. To image and generate acoustic radiation force in the samples, a V1 ultrasound imaging system (Verasonics Inc., Kirkland, WA, USA) with an L7-4v linear array transducer was employed. The ultrasound transducer was positioned at the top of the eyeball and aligned with both the cornea and the lens. A pushing pulse (600-μsec duration at 4.3 MHz) was used to remotely generate elastic waves in the cornea and the crystalline lens, and tracking pulses at the center frequency of 5.6 MHz were transmitted at 6 kHz frame-rate for imaging. A pushing pulse was transmitted at the left side of the cornea and the lens while the tracking pulses were transmitted on the right side of the pushing pulse. While the IOP in the eye was increased in the range from 5 to 50 mmHg with 5 mmHg interval, radio-frequency data were collected from the successive tracking pulses. For each eye globe, three measurements were acquired at each different IOP.

Results: As IOP increased from 5 to 50 mmHg, the shear wave speed in cornea increased from 1.0 m/s to 6.3 m/s. However, no significant changes in the shear wave speed (minimum 1.44 m/s at 5 mmHg and maximum 1.82 m/s at 20 mmHg) were found in the lens. A possible explanation is that the crystalline lens does not undergo significant deformation during IOP elevation as cornea, and, as a result, does not exhibit nonlinear elastic behavior.

Conclusions: The results of these studies show that shear wave elasticity imaging is a promising tool for noninvasive measurement of the mechanical properties of the lens. In addition, in contrast with cornea, the crystalline lens does not demonstrate significant changes in shear wave speed when IOP increases.

Acknowledgements: This study was supported by NIH grant EY022362.

References:

[1] Glasser A. Restoration of accommodation: surgical options for correction of presbyopia. Clin Exp Optom 2008; 91:279-95.
[2] Wu C et al. Assessing age-related changes in the biomechanical properties of rabbit lens using a co-aligned ultrasound and optical coherence elastography system. IOVS 2015; 56: 1292-1300.
[3] Aglyamov SR et al. The dynamic deformation of a layered viscoelastic medium under surface excitation. PMB 2015; 60:4295–4312.
[4] Li J et al. Revealing anisotropic properties of cornea at different intraocular pressures using optical coherence elastography. Proc. of SPIE 2016; 9710:97100T-97100T-7.

025 **ULTRASOUND SHEARWAVE ELASTOGRAPHY WITH FORCE SENSING – INTEGRATION DESIGN AND PRELIMINARY *EX-VIVO* RESULTS.**

M M. Nguyen[1], M A. Graule[2], A Y. Huang[2], V Shamdasani[3], B W. Anthony[2], H Xie[1].*
[1]Philips Research North America, 2 Canal Park, 3rd floor, Cambridge, Massachusetts, 02141, USA; [2]Massachusetts Institute of Technology, 77 Massachusetts Ave, 35-132, Cambridge, Massachusetts, 02139, USA; [3]Philips Healthcare, 22100 Bothell Everett Hwy, Bothell, Washington, 98021, USA.

Background: Ultrasound shearwave elastography is gaining wide acceptance in clinical practice as a quantitative diagnostic modality. Preload can impact stiffness measurement due to tissue nonlinear elasticity, especially in organs compressible by transducer (breast, thyroid, prostate, muscle, liver through subcostal scan) [1, 2]. In diffuse diseases, inter-user and intra-user measurement variations caused by pre-load can lead to difficulty in monitoring and longitudinal study of diseases or result in false positive diagnosis. In focal diseases, tissue non-linear elasticity can potentially improve lesion detection by increasing elasticity contrast when preload is applied [3].

Aims: The aims of this study include 1) integrating a force sensor to a commercial ultrasound transducer capable of shear wave elastography and 2) simultaneously recording preload and elasticity measurement.

Methods:
Force sensor integration: The one-axis load cell (FUTEK, LSB200/FSH00095) measures the force between the ultrasound transducer Philips C5-1 and the mechanically grounded outer shell, which was designed to fit both the force sensor and the transducer (Fig. A). The contact force between the transducer and the scanner tissue is measured in the direction along the axis normal to the face of the transducer. Raw load cell voltages are acquired using a National Instruments USB-6001 DAQ and the forces are calculated and displayed in LabVIEW.
Experimental setup: Bovine liver obtained from local grocery store, was degassed in a vacuum chamber for 3 hours before being imaged. The sensor-transducer module was rigidly attached to a linear stage with 1 degree of freedom (up-down) (Fig. B). As the module created preload from 0 to 3N on liver samples, with an increment of 1N, Young's moduli were measured by Philips ElastPQ feature (Elastography Point Quantification) on Philips EPIQ system (Fig. C). To take into account the transducer weight, zero Newton was calibrated at the point where the transducer-liver contact was first established, providing a good quality ultrasound image. Three measurements were made for each of the three tissue regions at every preload level.

Results: Fig. D plots the mean and standard deviation of Young's modulus as function of the preload. Increasing Young's modulus, by 247% on average, was observed in three liver samples as the preload increased from 0 to 3N.

Conclusions: While tissue biological state and constrained geometry in our ex-vivo experiment do not accurately represent normal in-vivo conditions, nonlinear elasticity of ex-vivo liver tissue was successfully captured. This property was not apparent in our similar experiments on liver-tissue-mimicking phantoms. Future work includes automated synchronization between preload and elasticity measurement, incorporation of shearwave imaging, and in-vivo studies.

References:
[1] Bell MA, et al. IEEE Trans Biomed Eng. 2016 Jul;63(7):1517-24. [2] Rotemberg V, et al. Phys Med Biol. 2012 Jan 21;57(2):329-41. [3] Krouskop TA, et al. Ultrason Imaging. 1998 Oct;20(4):260-74

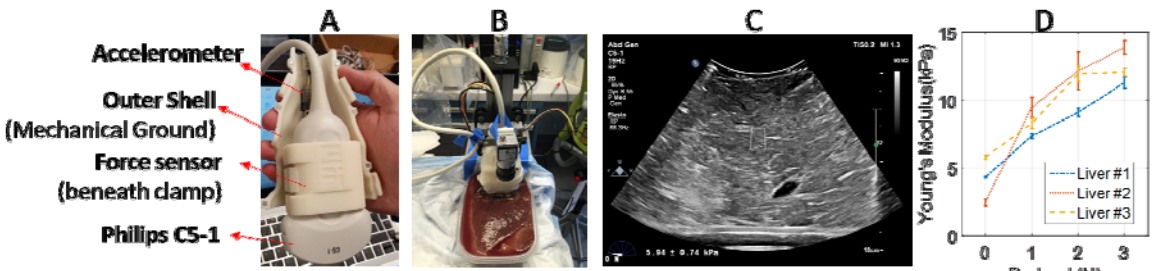

Figure. A) Integration of force sensor and Philips C5-1, B) Experiment setup with ex-vivo bovine liver C) B-mode from Philips ElastPQ D) Young's modulus of three liver regions at 0-3N preload

082 **PERMELASTOGRAPHY: QUANTITATIVE POROELASTIC PROPERTY IMAGING BY COMBINING SHEAR WAVE AND STRAIN ELASTOGRAPHY WITH A FORCE SENSOR.**

M Theodorou[1,2], J Fromageau[1,2], N deSouza[2,3], JC Bamber[1,2]*

[1]Joint Department of Physics, Sutton, London, UK; [2]Cancer Research UK Cancer Imaging Centre, Sutton, London, UK; [3]Royal Marsden NHS Foundation Trust, Sutton, London, UK.

Background: Poroelastic theory may be used to explain both cellular [1] and tissue rheology [2,3]. It describes the movement of fluid away from a region of (elastic) tissue during sustained compression. The resulting time- and spatially-varying deformation of the tissue matrix may be imaged as a change in ultrasound echo strain over time. Strain movies allow the quantitative imaging of the product of the tissue's aggregate modulus and fluid permeability, H_k, and its Poisson's ratio, ν (related to the volume of mobile fluid). We have successfully developed a novel ultrasound technique to measure tissue fluid permeability, k, independently of H, which we have assessed on tissue-mimicking phantoms.

Aims: To demonstrate in phantoms and volunteers the potential of combining simultaneous dynamic shear wave and strain elastography with a force sensor to separate the components of H_A and k, and therefore recover k, independently of ν and E.

Methods: In the new method, which we call permelastography, H is calculated from ν and the tissue's Young's modulus, E, where E is obtained from shear wave elastography [4]. This was tested on a series of agarose phantoms of varying matrix pore size, controlled by varying agarose concentration. Ultrasound measurements of k and magnetic resonance measurements of apparent diffusion coefficient (ADC) were made on each phantom.

Results & Conclusions: Both k and ADC varied systematically and reproducibly with matrix pore size. Intra-phantom variation in k was about 15% of the mean, and the mean values of k fell within about 28% of those measured using an independent but destructive method [5]. The non-invasive estimation of the biomechanical properties E, k and ν could be valuable clinically because cancer is associated with altered ability of fluid to move in tissue due to changes in the microenvironment such as increased collagen deposition in the extracellular matrix and the high density and leakiness of the microvasculature associated with angiogenesis. We have now adapted our experimental setup into a light, three-dimensionally printed hand-held design comprising one ultrasound transducer and one shear wave elastography transducer jointly held above a compressor plate, which contains load cells to provide force-feedback to the operator enabling a localized compression to be applied with a sustained constant force. The prototype is being evaluated in clinical breast imaging to characterize the poroelastic behavior of tumours, surrounding normal tissues and the post-irradiated breast.

Acknowledgements: This research was funded by the Cancer Research UK Imaging Centre grant and the Biomedical Research Centre (BRC).

References: [1] E Moeendarbary et al, Nature Materials, 12, 2013. [2] GP Berry et al, Ultrasound Med Biol, 32, 2006. [3] RL Liederman et al, Phys Med Biol, 51, 2006. [4] M Tanter et al, Ultrasound Med Biol, 34, 2008. [5] Johnson and Deen. AICHE J, 42, 1996.

002 **CONTROLLING THE SHEAR WAVE FIELD IN SOFT TISSUE USING VIBRATOR ARRAY.**

C Zemzemi[1,2], A Zorgani[1,2], S Catheline[1,2.]*
[1]LabTAU INSERM U1032, Lyon, France [2]Universtité de Lyon, France

Background: Improving cancer diagnostic is an important issue in oncology. Shear wave elasticity imaging techniques, known as elastography, have already shown their ability to locally retrieve the tissue elasticity and therefore suspicious cancerogenous nodules. A method for enhancing the signal-to-noise ratio is discussed in this presentation. To characterize the tissue elasticity, most of the current technics use a single active external source to generate shear waves. This limits the use of elastography to the diagnosis of superficial (shallow) organs. In order to improve the diagnostics of deeper organs, such as prostate, spleen, we propose multiple shear wave sources and the use of time reversal in order to improve the control of the shear wave field. As in echography where the implementation of the phase array improved the imaging quality, the source array that we propose may improve the quality of shear wave imaging by enhancing the signal-noise ratio.

Aims: This work aims to show the controlling of shear wave field by time reversal and its advantages for improving shear wave imaging.

Methods: The experiments are conducted on a Cirs[1] phantom. Multiple vibrators Cedrat[2] are placed around the phantom box. After each stimulation, the impulse response is measured inside the phantom by a 5MHz ultrasound probe connected to an ultrafast Verasonics Vantage ultrasound scanner[3]. We use a standard speckle tracking algorithm at 1000 Hz frame rate. The impulse responses are time-reversed and simultaneously sent back into the medium by their corresponding vibrators.
[1] : Elasticity QA Phantom Spherical, model 049A, CIRS, Virginia-USA
[2] : Piezoelectric Actuators APA600MML, Cedrat technologies, Meylon, France
[3] : Vantage 256, Kirkland, USA

Results: A displacement movie shows a shear wave focusing at the point where the impulse responses are chosen in the first step. The focusing is successful for different locations in our imaging field. We create focus spots in the center as well as in the corner.
The focus spot resolution depends on the number of sources used in the experiment; compared to an implementation of three sources, six sources yield a superior resolution.
The same relation is observed for the focusing amplitude. Hence, the implementation of more sources yields higher wave energy. This is also true for the focusing amplitude which is related to the energy. More sources are used, best is the focus spot resolution and amplitude. With this technique, simultaneous focus spot can also be generated as shown in fig.1.

Conclusions: This study shows that a shear wave field can be controlled with shear wave time reversal focusing. We can concentrate a maximum of energy in any region of interest. These results might bring significant improvement of the signal-noise ratio. Further mechanical parameters such as viscosity as well as non-linearity and anisotropy might profit of the technique.
How can this technique improve, in long-term, imaging at a shallow depth? At a deep depth? What is the best method?

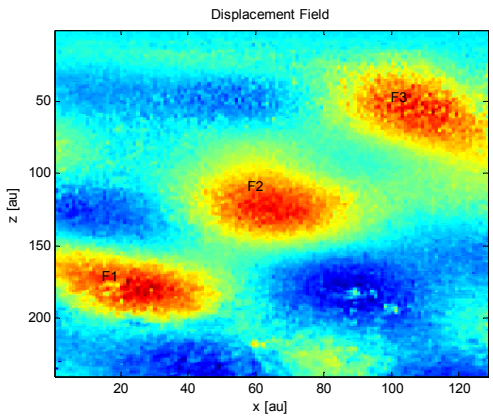

Fig.1: Field Control and shear waves focus in different points

019 **INTRAVASCULAR VS. INTRACARDIAC ARFI: A FINITE-ELEMENT SIMULATION OF CORONARY PLAQUE RESPONSE.**

CD Herickhoff[1], KT Looby[1], JR Doherty[2], JJ Dahl[1].*
[1]Stanford University, Palo Alto, CA, USA; [2]Kona Medical, Inc., Bellevue, WA, USA.

Background: Vulnerable intracoronary plaques, consisting of a soft, lipid-rich necrotic core and a thin, fibrous cap, are characteristic of coronary heart disease (CHD) and carry a high risk of heart attack. Our long-term goal is the development of an intravascular ultrasound (IVUS) probe capable of high-resolution acoustic radiation force impulse (ARFI) imaging in the coronary arteries, to identify and characterize vulnerable plaque.

Aims: In this work, we compare the ability of an IVUS transducer and an intracardiac echo (ICE) array [1] to create trackable, distinguishable displacements within coronary vessel and plaque structures.

Methods: Based on our previous experiments and prototype devices, we performed finite-element (FE) simulations of tissue response to an ARFI push from a 3.5-Fr, 1-mm long cylindrical IVUS transducer design, and we compared these to FE simulations using an ICE design composed of an 8-Fr, 7-mm long, 64-element linear array. A cylindrical FE mesh was created to simulate a 1.5-mm diameter coronary vessel surrounded by cardiac muscle. The FE mesh was defined as regions of background tissue, vessel media, and soft lipid plaque based on a scaled interpolation of segmented 3D MRI scans of carotid plaques; these regions were assigned a Young's modulus of 6 kPa, 1 MPa, and 25 kPa, respectively, corresponding to values reported in literature [2]. Field II was used to simulate an ARFI push excitation at 6 MHz from each transducer design with different orientations with respect to the FE mesh: the IVUS (within the vessel lumen) generated a broad, axisymmetric beam with peak intensity 1 mm from the vessel axis, and the ICE generated a beam focused on the vessel axis from a distance of 1.1 cm to mimic transmission through ventricular heart wall. The FE-simulated displacements from these ARFI excitations were then tracked in Field II using a 3.5-Fr, 0.75-mm long cylindrical phased array (Volcano Eagle Eye IVUS) and the ICE array, respectively.

Results: FE model output for the IVUS ARFI push shows highly precise and more localized displacements within the plaque's soft lipid core and the vessel media when compared to the ICE ARFI push (see figure). The IVUS displacements were also tracked more accurately than the ICE displacements.

Conclusions: Results of our finite-element simulations demonstrate that soft targets can be distinguished from a stiff background using a broad IVUS push beam, and that IVUS ARFI delineates soft plaques better than an ICE approach.

Acknowledgements: This work was supported by the National Institutes of Health (R01-EB013661-03).

References:

[1] Hsu, SJ, et al. "Challenges and implementation of radiation-force imaging with an intracardiac ultrasound transducer." IEEE transactions on ultrasonics, ferroelectrics, and frequency control (2007): 996-1009.
[2] Doherty, JR, et al. "Acoustic radiation force impulse imaging of vulnerable plaques: a finite element method parametric analysis." Journal of biomechanics (2013): 83-90.

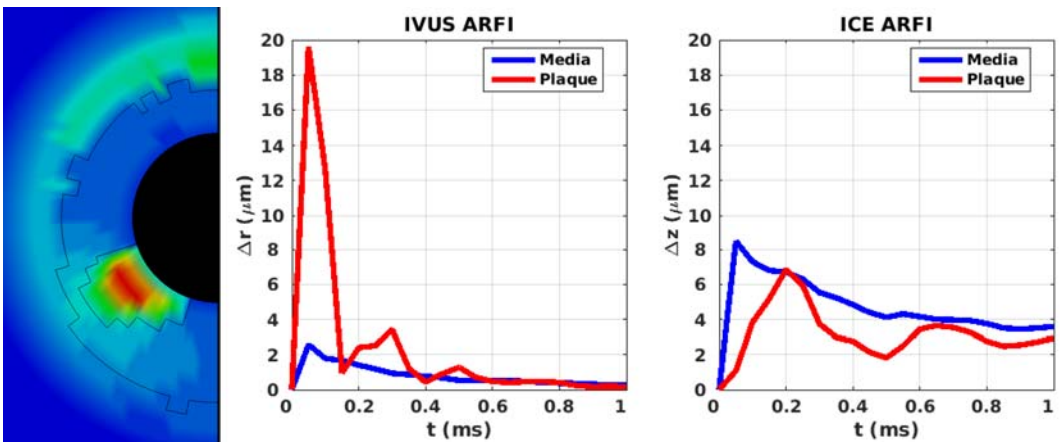

Figure: FE model output. (left, center) Radial displacement from IVUS ARFI push. (right) Axial displacement from ICE ARFI push.

058 **ACTUATION SYSTEM FOR LOW FREQUENCY ELASTICITY IMAGING.**

S W Gordon-Wylie[1], L Solamen[1], L Tan[1], M.D.J McGarry[3], E.E.W Van Houten[4], J.B Weaver[2], K D Paulsen[1,2].*

[1]Thayer School of Engineering, Dartmouth College, Hanover, NH, USA; [2]Geisel School of Medicine, Dartmouth College, Hanover, NH USA; [3]Columbia University, New York, NY, USA; [4]University de Sherbrooke, Sherbrooke Quebec, CANADA.

Background: Low frequency (~1 Hz) MR elasticity imaging (so called MRE) based on motion induced by cerebrovascular pulsation in the brain is particularly attractive because no external mechanical driver or device is required (allowing data collection to be added to any existing MRI protocol or patient population study merely as an another acquisition sequence) and patient compliance/acceptance is increased significantly (since discomfort/anxiety/risk associated with external vibration of the head is eliminated). However, technical validation, optimization and evaluation of this intrinsic actuation approach requires access to a controlled experimental environment where similar low frequency displacement fields can be induced in phantom systems.

Aims: The goal of this work was to develop a mechanical actuation system for low frequency (~1 Hz) MRE studies, first in phantoms, for validation, evaluation and optimization of the technical approach.

Methods: Modular solutions were developed to provide the necessary MRI triggering, motion, and signal vetting. In short, we triggered the magnet with an Arduino UNO by reading the analog output from an automotive pressure gauge and using it to drive a red LED which in turn triggered the PPU (peripheral pulse unit) on the magnet with an accuracy of about 1-2 ms. Pressure/flow waves were supplied by a Compuflow 1000 physiological pump. Plumbing connections were purchased “off-the-shelf” when possible and 3D printed when custom designs were necessary. A blood pressure cuff was used as an expandable diaphragm to compress/release a plastic plate simultaneously driving a block of tofu and a restoring force foam spring. Both mechanical and hydraulic forces were employed (so the tofu stays hydrated and/or simulates interstitial fluid flow). 3D Q Flow MRI methods (Phillips, 3T Achieva) were employed in each of 3 gradient encode directions to yield amplitude, phase and velocity data that was subsequently Fourier transformed to yield motion maps. Motion encode gradient directions were calibrated using a 3D flow phantom that displayed flow along each primary direction (+X, +Y, +Z) as well as a return path along the angle direction (-X-Y-Z).

Results: High quality motion maps were collected in multiple inclusion tofu phantoms with variations in scan acquisition parameters and slice selection directions. Example displacement data in coronal view of the real motion map at 1 Hz for tofu with three gelatin inclusions is shown below. Bright spots at 1 & 2 o'clock are motion artifact that is partially covering the 3rd inclusion. Hydraulic flow is evident at 6 o'clock.

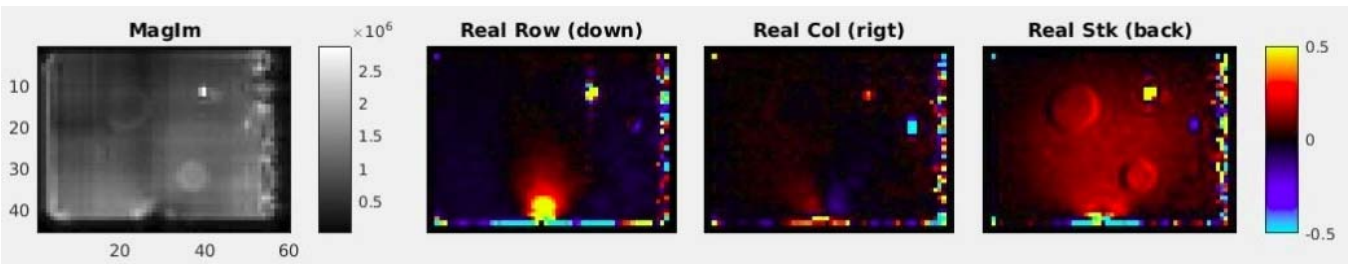

Conclusions: These initial results are a step towards realizing the full promise of 1 Hz elasticity based brain imaging[5].

Acknowledgements: This work was supported in part by NIH grant R01 EB018230 awarded by NIBIB

References:

[5]Weaver J, Pattison A, Brain mechanical property measurement using MRE with intrinsic activation, Physics in Medicine and Biology, 57(22); 7275-7287, 2012.

079 **A TOOL FOR SHEAR WAVE GERNERATION AND VISUALIZATION WITH THE VERASONICS RESEARCH ULTRASOUND SYSTEM.**

R Daigle[*1], *Y.-S Tung*[1].
Verasonics, Inc., 12016 115th Ave. NE, Kirkland, WA, 98034, USA.

Background: Shear waves generated by acoustic radiation force are used in several application areas and research studies. The acoustic pulse that generates the shear wave is often referred to as the 'push' transmit, while the high frame rate acquisitions that follow the propagation of the shear wave are referred to as 'detect' acquisitions. The push transmits have pulse durations in the range of 200 to 1000 usecs and require special considerations for the transmit circuitry. The detect acquisitions are typically plane wave acquisitions at frame rates of 1000-10000 frames per second. Tracking of the shear wave is typically performed by correlation of successive frame RF signal data that identifies small displacements in tissue with time.

Methods: A program tool has been developed for the Verasonics Research System for shear wave generation and visualization. The tool allows real-time adjustment of push parameters, including number of push elements, push duration, and focal point. A region of interest can be selected for the shear wave visualization, and the shear wave motion is detected using a 1-D autocorrelation method between IQ pixel values of adjacent frames. The processed frames can be played back in slow motion and saved as a movie file for reference

Conclusions: The tool has proved useful in evaluating the push capabilities of different transducers and analyzing the elastic properties of different phantom materials. In addition, the availability of the source programming script allows utilization of relevant portions of the code in custom shear wave studies.

004 **REVERBERANT SHEAR WAVE FIELDS IN TISSUES.**

K.J Parker[1], J Ormachea[1], F Zvietcovich[1], B Castaneda[2].*
[1]University of Rochester, Hopeman Building 203, PO Box 270126, Rochester, NY, USA; [2] Pontificia Universidad Católica del Perú, Av. Universitaria 1801, Lima 32, Perú.

Background: An inherent concern in many shear wave tracking approaches is the presence of reflected waves from organ boundaries and internal inhomogeneities. These reflections are responsible for modal patterns [1,2] in continuous wave applications and also for backwards traveling waves in transient experiments [3]. Directional filtering can be used to eliminate some types of reflection [4-8]. However, as the number of boundary reflections, internal reflections, and sources increases, a reverberant field can be created with unique properties.

Aims: In this work we apply the concept of a narrowband reverberant field of many waves within tissue. These are naturally established (even unavoidable) in practical situations, and can be reinforced by utilizing multiple sources near the tissues of interest. This particular approach leads to new estimators of local tissue shear wavelength or shear wave speed.

Methods: The complex pressure at a position in an acoustic reverberant chamber can be modeled as the superposition of plane waves incident from all directions [9-10]. We extend previous theory to the case of shear waves and integrate incident waves over 4π solid angle to obtain analytical solutions to the complex shear wave field.

Results: The new derivations suggest local shear speed estimators similar to conventional Doppler estimators. These can be applied to reverberant shear wave fields. Examples are given from simulations and from the CIRS breast cancer phantom.

Conclusions: The approach includes efficient Doppler estimators, takes advantage of internal reflections, and eliminates the need for ill-conditioned inverse solutions or directional filters.

Acknowledgements: This work was supported by the Hajim School of Engineering and Applied Sciences at the University of Rochester.

References: [1] Parker KJ, Lerner RM, "Sonoelasticity of organs," *JUM*, 11(8)387-392, 1992. [2] Taylor LS et al., "Three-dimensional sonoelastography," *PMB*, 45(6)1477-1494, 2000. [3] Ringleb SI et al., "Quantitative shear wave MRE," *Magn Reson Med*, 53(5)1197-1201, 2005. [4] Manduca A et al., "Spatio-temporal directional filtering," *Med Image Analy* 7(4)465-473, 2003. [5] McLauglin J, Renzi D, "Shear wave speed recovery," *Inverse Probl*, 22(2)681-706, 2006. [6] Deffieux F et al., "On the effects of reflected waves," *IEEE UFFC*, 58(10)2032-2035, 2011. [7] Hah Z et al., "Integration of crawling waves," *UMB*, 38(2)312-323, 2012. [8] Pengfei S et al., "Comb-push ultrasound shear elastography (CUSE): a novel method for two-dimensional shear elasticity imaging of soft tissues," *IEEE TMI*, 31(9)1821-1832, 2012. [9] Pierce D., "Acoustics," Chapter 6, New York: McGraw-Hill Book Co., 1981. [10] Parker KJ, Maye BA, "Partially coherent radiation from reverberant chambers," *JASA*, 79(1)309-313, 1984.

038 **GENERALIZED ADJOINT METHOD FOR POROELASTIC IMAGE RECONSTRUCTION.**

L Tan[1], M.D.J McGarry[3], E.E.W Van Houten[4], L Solamen[1], J B Weaver[2], K D Paulsen[1,2]*
[1]Thayer School of Engineering, Dartmouth College, Hanover, NH, USA; [2]Geisel School of Medicine, Dartmouth College, Hanover, NH USA; [3]Columbia University, New York, NY, USA; [4]University de Sherbrooke, Sherbrooke Quebec, CANADA.

Background: Poroelastic mechanical models provide access to hydrodyamical properties (in addition to traditional stiffness parameters) that may have particular importance and/or relevance to disease states in specific tissues which exhibit porous structural and physiological behavior, such as the brain, which has been mathematically described as a porous medium since the 70s [1]. Recent studies suggest that differences in the behavior of poroelastic and viscoelastic equations of motion, and how they represent and/or capture motion maps that occur in the brain, increase at frequencies approaching the heart rate because the fluid component of the mechanical system is able to oscillate more significantly over the period of harmonic excitation [2]. Thus, efficient computation methods for estimating mechanical and hydrodynamical properties in tissue based on low frequency motion maps such as those resulting from cerebrovascular pulsations [3] are of significant interest.

Aims: We have developed and implements an efficient gradient computation for solving inverse problems involving poroelastic equations of motion. The algorithm can be viewed as a generalized 'adjoint method' based on a Lagrangian formulation. The classic adjoint method requires self-adjoint properties of the stiffness matrix in the elasticity problem. In our new algorithm, this property is no longer a necessary, but the computational performance is as efficient as the classic method, which involves only two forward solutions and is independent of the number of parameters to be estimated.

Methods: The algorithm is developed and implemented for material property reconstructions from MRE displacement data using poroelastic modeling. Various gradient and Hessian-based optimization techniques have been tested in simulation, phantom and in vivo brain data to demonstrate the new approach is more efficient. The numerical results show the feasibility and the efficiency of the generalized adjoint scheme for gradient calculations based on poroelastic equations of motion.

Results: Computational costs per iteration are estimated for various gradient computational schemes (see table below, left) and compared as a function of increasing number of unknowns in Figure 1 (below middle) which demonstrates the generalized adjoint approach is comparable to the classic adjoint method. These efficiencies are also realized in practice as illustrated in Figure 1 (below, right). Repeatability tests of data collected in the brain of the same subject indicate the new method is robust and stable, is the preferred approach for poroelastic image reconstruction, at least from intrinsically actuated MRE displacement data.

method	computational cost
Gradient-based (classic adjoint)	$\mathcal{O}(N^{7/3}) + 2\mathcal{O}(N^{5/3})$
Gradient-based (generalized adjoint)	$2\mathcal{O}(N^{7/3}) + 2\mathcal{O}(N^{5/3})$
Gradient-based (straightforward)	$\mathcal{O}(N^{7/3}) + (M+1)\mathcal{O}(N^{5/3})$
Gauss-Newton	$\mathcal{O}(N^3) + \mathcal{O}(N^{7/3}) + (M+1)\mathcal{O}(N^{5/3})$

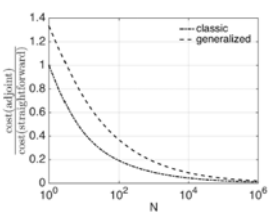

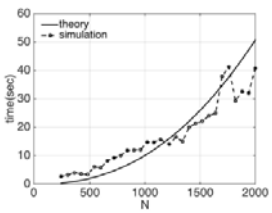

Conclusions: Efficient gradient computations for non-self adjoint poroelastic equations of motion can be realized through generalization of the classic approach. The method exhibits comparable computational performance and is similarly robust to image reconstruction for simulated and experimental MRE data.

Acknowledgements: This work was supported in part by NIH grant R01 EB018230 awarded by NIBIB

References:

1. Hakim S, Venegas J, The physics of the cranial cavity, hydrocephalus and normal pressure hydrocephalus; mechanical interpretation and mathematical model, Surgical Neurology 5(3); 187-210, 1976.
2. McGarry M, Johnson C, Suitability of poroelastic and viscoelastic mechanical models for high and low frequency MR elastography, Medical Physics, 42(2); 947-957, 2015.
3. Weaver J, Pattison A, Brain mechanical property measurement using MRE with intrinsic activation, Physics in Medicine and Biology, 57(22); 7275-7287, 2012.

041 **COMPLIANCE BOUNDARY CONDITIONS FOR ELASTICITY RECONSTRUCTION USING FEM INVERSE PROBLEM.**

E Ozkan[1], O Göksel[1].*

[1]Computer-assisted Applications in Medicine Group, ETH Zurich, Zurich, SWITZERLAND.

Background: Estimation of tissue stiffness for detecting tissue abnormalities has been a major research interest in the last decades. Some existing methods start with defining a region-of-interest (ROI) and formulating the elasticity reconstruction of ROI as an inverse problem (IP). These commonly utilize the Finite Element Method (FEM) and compute Young's modulus distribution in ROI from displacement field measurements in response to tissue excitations. For solving the FEM IP, boundary conditions at the outer boundaries of ROI are necessitated [1]. Conventionally, these are set arbitrarily, as zero-displacement or -force constraints at chosen ROI locations, which may lead to errors in IP solutions [2].

Aims: Our goal is to reconstruct accurate elasticity parameters with harmonic excitations by alternatively approximating boundary constraints from measured displacements.

Methods: Our proposed method starts with a displacement field tracking step obtained from harmonic excitation at angular frequency ω, using e.g. cross-correlation [3] or optical flow [4]. We then start our iterative process with an initial assumption for Young's modulus and estimate compliance boundary conditions (CBC) as proposed in [5]. Afterwards, we use estimated CBC to reconstruct Young's modulus using FEM IP [2]. We iterate this process until updated Young's modulus converges or maximum number of iterations is reached as shown in (a). Note that our method has two nested iterations: elasticity IP iteration for reconstructing Young's modulus with FEM IP, which checks convergence for displacements, and CBC update iteration to update CBC using estimated Young's modulus, which converges for change of Young's modulus.

Results: Simulations were performed using a 2D model with a circular inclusion embedded in a numerical phantom as in (b). Our simulation results over exterior iterations are demonstrated for $\omega = 2\pi f$ at f = 70 Hz in (c). Sensitivity of IP parameter reconstruction for two empirically-set baseline comparisons, bottom and all fix are compared to our method CBC for different f in (d). RMSE error of these are shown in (e).

Conclusions: The circular inclusion is recognizable for all angular frequencies and ROI choices using CBC, unlike empirically-set boundary conditions bottom and all fix. Our results show that using CBC as boundary conditions yields Young's modulus reconstruction outputs with less RMSE errors.

Acknowledgements: This work is supported by Swiss National Science Foundation (SNSF).

References: [1] Eskandari H, et al.: Phys. Med. Biol. 53, 2008. [2] Goksel O, et al.: IEEE Trans Med Imaging 32(2), 2013. [3] Ophir J, et al.: Proceedings of the Institution of Mechanical Engineers, 1999. [4] Poree J, et al.: IEEE Trans Med Imaging 34(12), 2015. [5] Ozkan E, et al.: Proceedings EMBC, 2015.

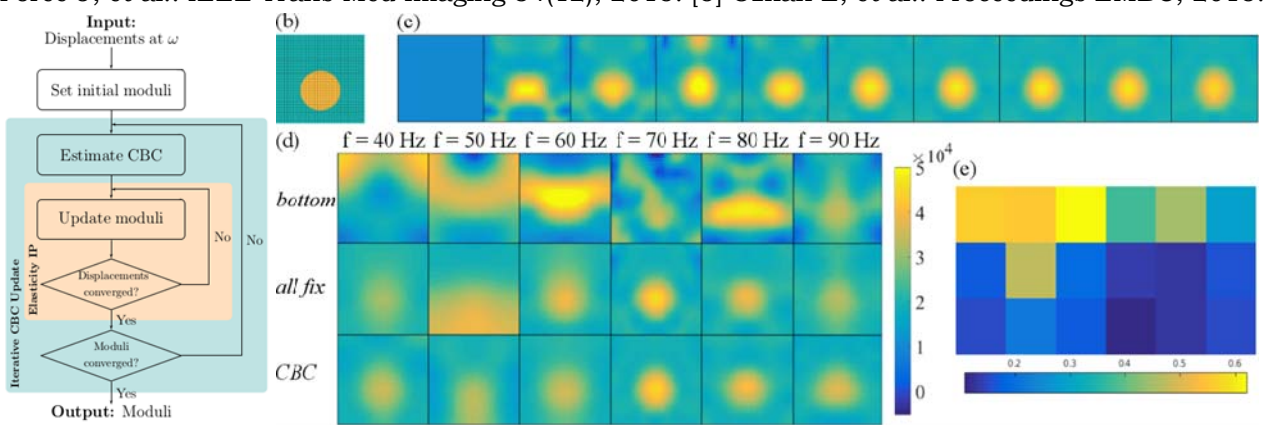

Figure 1: (a) Block diagram of our proposed technique. 2D model for experiments and simulation results over iterations are shown in (b) and (c). Baseline comparisons for different ω and RMSE errors are shown in (d) and (e), respectively.

047 **AN ANALYSIS OF INTRINSIC VARIATIONS OF LOW-FREQUENCY SHEAR WAVE SPEED IN A STOCHASTIC TISSUE MODEL: THE FIRST APPLICATION ON LIVER FIBROSIS.**

Y Wang[1], Min Wang[1], J Jiang[1].*
Michigan Technological University, 1400 Townsend Drive, Houghton, MI, 49931, USA.

Background: Ultrasound shear wave elastography (SWE) is increasingly being used to noninvasively stage liver fibrosis. Recent validations of SWE by QIBA [1] showed that uncertainty of SWE cannot be neglected, even in tissue-mimicking phantom materials. In order to accurately stage liver fibrosis based on cutoff values of shear wave speed (SWS), it is important to understand the accuracy and precision of SWS measurements.

Aims: In addition to measurement errors, SWS estimation is also subject to intrinsic variations due to tissue heterogeneity, analogous to intrinsic spectral broadening in Doppler measurements. Toward this end, this is a theoretical study aiming at quantitatively investigating the aforementioned intrinsic variations among SWS measurements using a stochastic tissue model.

Methods: Using the principle of Maximum Entropy (ME) [2], a probability density function (PDF) of the SWS distribution in a random multi-phase stochastic model was derived. In order to evaluate the performance, we compared the derived PDF with other commonly used statistical PDFs using simulated transient elastography data (50 Hz, 100 Hz and 150 Hz). We further simplify fibrotic liver tissues without steatosis as a two-phase model, which was used to generate shear wave data. Without loss of generality, four models (see Figure 1(a)) were created in this study. Models 1-3 were stochastic material models with three different inclusion geometries (*i.e.* circle, rectangle and arbitrary shape), whereas Model 4 was designated to mimic spatial (histological) characteristics of fibrosis under the METAVIR classification [3]. All simulations were performed using an open-source wave simulator, K-WAVE [4].

Results: Based on statistical evaluation criteria (*e.g.* Bayesian Information Criterion), initial results showed that the derived PDF out-performed three commonly used PDFs (see Figure 1(b)-(c)). Through multiple realizations of the stochastic tissue model, we found that, based on elastic wave propagation theory, shear wave fronts experience initial dispersion but quickly stabilize after a short (as compared to its wavelength) distance. The above-mention distances required to stabilize the shear wave propagation were not correlated to the traveling wavelengths in the Rayleigh scattering regime.

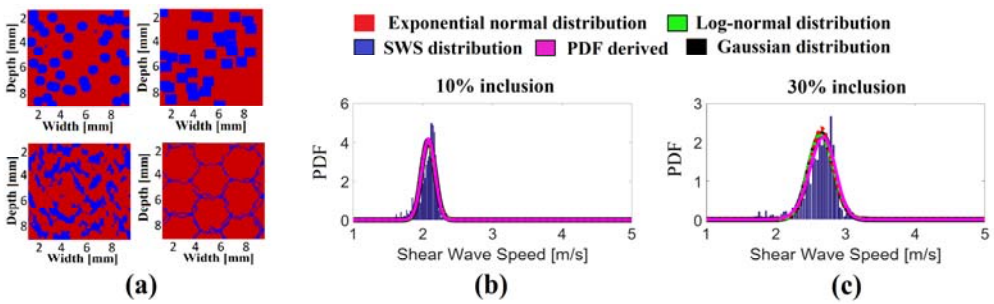

Figure 1. (a) Four different two-phase models. (b)-(c) Histogram distributions of K-WAVE simulated SWS (50 Hz) from two different volume fractions of inclusions: (a) 10% and (b) 30%. Four PDFs were overlaid with the histogram on each plot.

Conclusions: Our preliminary results showed that the proposed PDF function can quantitatively represent intrinsic variations in the simulated SWS measurements. Parameters of the derived PDF connected to the well-known effective medium theory of composite materials. We envision that, in the future, the derived PDF can be used as an integral component in a theoretical framework for statistical quantifications of the uncertainty of SWS in heterogeneous liver tissues, given further validations.

Acknowledgements: This study was partially supported by a NIH grant R15CA179409. The computing time for K-WAVE simulations was provided by a grant from Michigan Tech's Superior HPC cluster.

References: [1] T. J. Hall, 2013 IEEE International Ultrasonics Symposium (IUS), 2013, pp. 397-400. [2] E.T. Jaynes, Phys. Rev., 1975, pp. 620–630. [3] Bedossa P, The METAVIR Cooperative Study Group Hepatology 24 289-93. [4] www.k-wave.org.

048 **BUILDING AN OPEN-SOURCE SIMULATION PLATFORM OF ACOUSTIC RADIATION FORCE-BASED BREAST ELASTOGRAPHY.**

Y Wang[1], B Peng[1], J Jiang[1].*

[1]Michigan Technological University, 1400 Townsend Dr, Houghton, MI, 49931, USA.

Background: Ultrasound-based elastography techniques including quasi-static strain elastography (SE), acoustic radiation force Impulse (ARFI) imaging, point shear wave elastography (pSWE) and supersonic shear imaging (SSI) have been used to differentiate breast tumors among other clinical applications [1].

Aims: The objective of this study is to extend a previously published virtual simulation platform for ultrasound quasi-static breast elastography [2] (UQBE) toward acoustic radiation force-based breast elastography. Consequently, the extended virtual breast elastography simulation platform can be used to improve confidence of imaging interpretation in complex, heterogeneous but known media.

Methods: The extended virtual breast elastography system leverages four existing open source packages: Field II (ultrasound simulator), VTK (geometrical visualization and processing), FEBio (finite element [FE] analysis) and Tetgen (mesh generator). All acoustic radiation force based simulations involved three steps. First, acoustic radiation forces were used to excite soft tissue and generate tissue deformation using FEBio (an open-source FE solver). The aforementioned acoustic radiation force inputs were determined by pressure fields simulated using Field II. Second, Field II ultrasound simulations using a series of deformed numerical breast phantoms were used to obtain a series of pre-deformation and post-deformation ultrasound radio frequency (RF) data. In the third step, speckle tracking was performed on these RF data to estimate the tissue deformation and subsequently infer mechanical properties of the virtual tissues being imaged (*e.g.* shear wave speed [SWS], time-to-peak, normalized displacement, *etc.*). Examples involving three different numerical breast models with increasing complexity – one uniform model, one simple inclusion model and one virtual complex breast model derived from MRI data, were used to demonstrate capabilities of this extended virtual simulation platform.

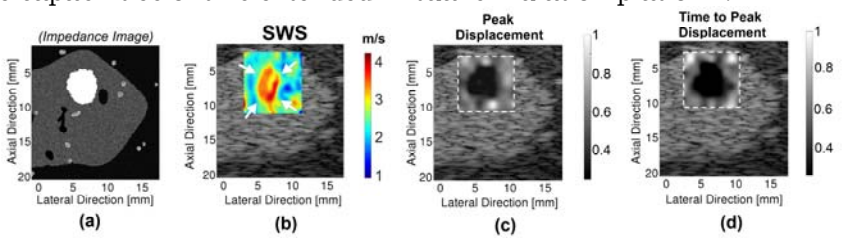

Figure 1. Results of SSI and ARFI for virtual complex breast model. (a) A simulated impedance image. (b) An estimated SWS image by SSI. The color bar represents the SWS in m/s. The white arrows represent a reconstructed lesion. (c) A simulated normalized peak displacement image by ARFI. (d) A simulated normalized time-to-peak-displacement image by ARFI. The color bars in (c) and (d) represent normalized values from 0 to 1.

Results: In all three models, elastographic simulation results were consistent with the published results [3-5]. More specifically, in the uniform model, the estimated SWS values were within 4% compared to known values. In the simple inclusion and the virtual breast models, SWS values estimated from all hard inclusions in soft background materials were underestimated by around 20%, similar to what has been reported. One example is shown in Figure 1.

Conclusions: In summary, initial results obtained by the proposed virtual simulation platform were consistent with our expectations and what have been reported on the literature [6].

Acknowledgements: This study is funded by a grant from NIH (R15-CA179409).

References: [1] Palmeri, M. L., Interface Focus 2011, 1:553-564. [2] Wang, Y., Medical Physics 2015, 42:5453-5466. [3] Nightingale, K., Curr Med Imaging Rev 2011, 7:328-339. [4] Palmeri, M. L., 2010 IEEE IUS, 13-16. [5] Bercoff, J., UFFC 2004, 51:396-409. [6] Bamber J, Ultraschall Med 2013, 34:169-84.

055 **FULL WAVE INVERSION APPROACH FOR ULTRASOUND ELASTOGRAPHY.**

O A. Babaniyi[1], M Bayat[2], M Fatemi[2], W Aquino[1].*
[1]Duke University, Durham, NC, USA; [2]Mayo Clinic College of Medicine, Rochester, MN, USA.

Background: Ultrasound shear wave elastography imaging has emerged as a promising modality to visualize local tissue mechanical properties. The majority of the established techniques, however, rely on a pointwise measurement of the speed of induced waves based on a localized planar wave propagation assumption [1]. It is further assumed that medium is purely elastic. While these assumptions can result in acceptable performance in experimental setup, appropriate performance in more realistic situations, such as in tissues, rely on enforcing a more general framework to deal with complex wave interactions due to complex geometry and heterogeneity in mechanical properties.

Aims: The goal of this work is to develop a full-wave inversion approach, that accounts for general wave propagation, to reconstruct shear modulus distribution from ultrasound measurements. We will compare the results from this model with more physics to the results from the popular model with less physics.

Methods: We achieve the goal by formulating a nonlinear PDE-constrained optimization problem to solve for the complex shear modulus distribution. We used both an elastic [2], and viscoelastic constitutive equation [3]. The objective of the optimization problem is to find the complex elastic modulus distribution that minimizes a modified error in constitutive equation (MECE) functional that contains both a data misfit term and an error in constitutive equation term [2] subject to satisfying a linear wave equation. This formulation allows us to accommodate incomplete, and corrupted data, and also unknown boundary conditions [3].

Results: We reconstruct the shear modulus distribution from displacement data obtained from a tissue mimicking phantom that contains stiff inclusions. Our experiments were performed using acoustic radiation force excitation and fast ultrasound tracking. We demonstrate that our full-wave inversion technique based on the MECE functional can successfully reconstruct elastic and viscoelastic properties. Furthermore, we compared our results using MECE to those obtained using conventional shear wave elastography and found that the former produces more consistent and accurate results across different excitation and acquisition conditions.

Conclusions: We have developed a full-wave inversion technique for elastography and demonstrated its feasibility through experiments in tissue mimicking phantoms. Our technique significantly relaxes the assumptions of plane waves usually made in conventional shear-wave elastography methods.

Acknowledgements: The authors will also like to acknowledge the support of the National institutes of Health through award R01CA174723.

References:

[1]. Ferraioli, Giovanna, et al. "Accuracy of real-time shear wave elastography for assessing liver fibrosis in chronic hepatitis C: A pilot study." *Hepatology* 56.6 (2012): 2125-2133.

[2]. Banerjee, Biswanath, et al. "Large scale parameter estimation problems in frequency-domain elastodynamics using an error in constitutive equation functional." *Computer methods in applied mechanics and engineering* 253 (2013): 60-72.

[3]. Diaz, Manuel I., Wilkins Aquino, and Marc Bonnet. "A modified error in constitutive equation approach for frequency-domain viscoelasticity imaging using interior data." *Computer methods in applied mechanics and engineering* 296 (2015): 129-149.

053 **THE COUPLED ADJOINT-STATE EQUATION IN FORWARD AND INVERSE ELASTICITY.**

D. T Seidl[1], P E. Barbone[2], A A. Oberai[3].*

[1]Sandia National Laboratories, Department of Optimization and Uncertainty Quantification, NM 87123, USA; [2]Boston University, Department of Mechanical Engineering, MA 02215, USA; [3]Rensselaer Polytechnic Institute, Department of Mechanical, Aerospace, and Nuclear Engineering, Troy, NY 12180, USA.

Background: The quasi-static inverse elasticity problem can be formulated as an optimization problem constrained to satisfy the equilibrium equation. At each iteration one solves a state problem and its adjoint and then computes the objective function and its gradient in order to determine a new material property iterate via a gradient-based optimization routine [1]. The objective function is proportional to the mismatch between the experimentally observed and computationally predicted displacement fields.
The success of this approach hinges on the ability to accurately simulate the experimental conditions. Displacement data obtained using ultrasound image registration techniques contains a mix of accurately (the axial component) and poorly (the lateral and elevational components) characterized measurements. This aspect of the data is problematic as the state equation requires sufficient boundary conditions to be well-posed. An approach that has been successful in practice involves using the axial component of the measured displacement field as Dirichlet data while imposing homogenous Neumann (i.e. traction-free) conditions on the lateral and elevational components [2]. The traction-free assumption introduces a bias into the reconstructed material property fields that can in some situations be a significant source of reconstruction error.

Aims: Design a forward elasticity formulation that does not assume displacement or traction boundary conditions. Evaluate this formulation as the forward model within an inverse elasticity optimization algorithm.

Methods: We derive a system of partial differential equations from a Lagrangian that contains a weighted data match term and an equilibrium equation constraint. The system looks like a coupled version of the normally decoupled state and adjoint equations. Finite elements are used to numerically approximate these variational forms. The use of piecewise linear shape functions yields an unstable numerical formulation. We stabilize the discrete system using residual-based stabilization.

Results: We show results obtained from simulated displacement data that mimics ultrasound elastography compression experiments. We then discuss two and three dimensional shear modulus reconstructions from tissue mimicking phantoms. Finally, we present reconstructions of benign and malignant breast masses.

Conclusions: Our approach is capable of producing material property reconstructions free of the bias induced by assumed boundary conditions. While the results presented here have been obtained from ultrasound displacement data, this technique is equally applicable to displacement fields estimated from MRI or OCT images. This formulation could be extended to nonlinear and time-dependent constraint equations.

Acknowledgements: We gratefully acknowledge support from the NIH (Grant No. NCI-R01CA140271) and the NSF (Grant Nos. 1148124 and 1148111). We thank T.J. Hall (University of Wisconsin) and J.C. Bamber (ICR London) for providing the displacement data analyzed in this work. Sandia National Laboratories is a multi-program laboratory managed and operated by Sandia Corporation, a wholly owned subsidiary of Lockheed Martin Corporation, for the U.S. Department of Energy's National Nuclear Security Administration under contract DE-AC04-94AL85000.

References: [1] A.A. Oberai, N.H. Gokhale, and G.R. Feijóo, Inverse problems, 2003, 19.2, 297.
[2] M. S. Richards, P.E. Barbone, and A. A. Oberai, Physics in medicine and biology, 2009, 54.3, 757.

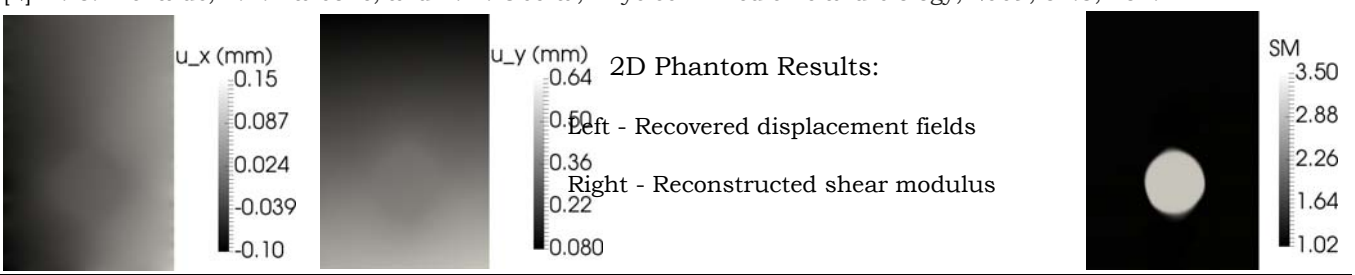

030 **SPATIALLY VARYING COMPLIANCE ESTIMATED THROUGH THE PULSE WAVE INVERSE PROBLEM: REPEATABILITY IN HEALTHY CAROTID ARTERIES.**

MDJ McGarry[1,2], IZ Apostolakis[1], P Nauleau[1], EE Konofagou[1].*
[1]Columbia University, New York, NY, USA; [2]Dartmouth College, Hanover, NH, USA.

Background: The mechanical properties of arteries are relevant to a range of conditions and diseases, including atherosclerosis, aneurysms, hypertension and aging[1]. Noninvasive measurements of vessel stiffness using ultrasound will allow efficient diagnosis and monitoring of these common conditions. Tonometry can estimate a global average of the compliance by recording the arrival time of the arterial pulse wave at two locations and computing the pulse wave velocity (PWV), which is related to the compliance through the Bramwell-Hill equation. Ultrasound-based wall displacement images obtained with our Pulse Wave Imaging methodology can also compute the PWV at smaller scales, although reflections can cause issues[2]. We have demonstrated a pulse wave inverse problem (PWIP) which accounts for reflections by fitting unknown parameters of a computational model of the governing 1D pulse wave equations to the measured data. The PWIP accurately recovered the compliance distribution of heterogeneous phantoms with stiff inclusions as small as 7 mm[3].

Aims: Recover spatially varying compliance of the carotid artery through the pulse wave inverse problem[3], and determine repeatability in healthy volunteers.

Methods: The PWIP uses a finite difference implementation of the partial differential equations governing pulse wave propagation in heterogeneous flexible tubes. The model is parameterized by a piecewise linear vessel compliance distribution and a number of discrete cosine transform (DCT) components of the inlet pressure boundary condition (BC). Starting from an initial guess, the parameters are updated using gradient descent optimization to minimize the difference between wall displacements predicted by the model and the wall displacements of the physical system measured via ultrasound[3].
Five 19-32 y/o healthy male volunteers with no known pre-existing cardiovascular disease were enrolled in the study. RF data was collected over 2 seconds in an imaging plane along the axis of the common carotid artery, approximately 20mm below the carotid bifurcation, using a clinical Ultrasonix Touch system with 32 scan lines and 505Hz framerate. Each subject was imaged 5 times in one session, with repositioning of the subject and ultrasound probe between each acquisition. The incremental displacements of the top and bottom wall were computed using 1D cross-correlation. This data was supplied to the pulse wave inverse problem, which estimated a 10-segment piecewise linear compliance distribution along the imaged length (~35mm), and 16 DCT components of the inlet pressure BC for each of the two main pulse waves and the dicrotic notch. The distance from the end of the imaged region to the carotid bifurcation was measured and used as the primary source of reflection in the finite difference model through a resistance outlet BC. The local pulse wave velocity (PWV) was computed from the compliance distribution and the vessel area using the Bramwell-Hill equation.

Results: All subjects showed a gradual increase of compliance along the artery approaching the bifurcation. The average intra-subject coefficient of variation was 38% for compliance and 20% for PWV. The repeatability is negatively influenced by occasional issues with false solutions, which capture the forward and reflected waves with one wide, fast pulse rather than a narrower wave which is reflected back into the imaging plane at the carotid bifurcation.

Conclusions: The PWIP is able to image spatially varying compliance along a section of the carotid artery. Future work will improve the modeling of the reflected wave and validate the in vivo compliance distributions using a pressure catheter. More accurate modeling of the source and nature of the downstream reflected waves (such as a Windkessel outlet BC) may be required. Some promising applications are in focal arterial diseases such as atherosclerosis, and aneurysms, where the compliance images may help to predict vulnerable cases at risk of rupture.

Acknowledgements: Funding from NIH R01HL098830

References: [1] SJ Zieman, M Vojtech, and DA Kass. "Mechanisms, pathophysiology, and therapy of arterial stiffness." *Arteriosclerosis, thrombosis, and vascular biology* (2005).
[2] I Apostolakis , S Nandlall and E Konofagou. "Piecewise Pulse Wave Imaging (pPWI) for detection and monitoring of focal vascular disease in murine aortas and carotids in vivo." *IEEE Transactions on Medical Imaging* (2015).
[3] M McGarry, R Li, I Apostolakis, P Nauleau, E Konofagou. “An inverse approach to determining spatially varying arterial compliance using ultrasound imaging”. *Physics in Medicine and Biology* (2016)

009 **EXPERIMENTAL RESULTS ON THE IMPROVEMENTS IN ROTATION ELASTOGRAM QUALITY USING SPATIAL COMPOUNDING APPROACH.**

A Arshad Kothawala[1], A.K. Thittai[1].*
[1]Indian Institute of Technology Madras, Chennai, India.

Background: Most elastography methods provide information related to the stiffness of the underlying tissue. Few others give information about the state of bonding of a tumor with its surrounding tissue [1],[2] .However, no approach exists for directly visualizing the local rigid body rotation undergone by a asymmetrically oriented loosely-bonded benign lesion when subjected to a small quasi-static compression. Inherent limitation in lateral US resolution makes it difficult to estimate and visualize this rotation. Spatial compounding (SC) method has been shown to improve the quality of lateral displacement estimates [3],[4].

$$Wx,y(rotation) = 0.5\begin{pmatrix} \delta v & \delta u \\ \delta x & \delta y \end{pmatrix} \quad (1)$$

u - lateral displacement, v - axial displacement.

Aim: To experimentally validate the simulation study reported earlier [5] that demonstrated an improvement in Rotation Elastogram (RE) quality using spatial compounding technique.

Methods: A phantom (dimension of 75 x 80 x 80 mm) prepared using agar- gelatin- water mixture was used for this experimental study. A cylindrical inclusion that was 3 times stiffer than the background having an elliptical cross section (12mm×8.5mm) was inserted at a depth of 25mm. This inclusion was oriented at ~45˚ to the axis of compression. The inserting mechanism ensured a loosely-bonded condition for the inclusion. Axial compression of 2% was provided using a controlled compression setup. Pre- and post - compressed RF data were collected from a linear array transducer operating at 5MHz from different insonification angles (L14-5/38, SONIX TOUCH Q+® ,Ultrasonix, Analogic Corporation) . A multilevel 2-D displacement tracking algorithm [1] was used to obtain the axial and lateral displacements. The RE was obtained using Eqn. (1). To investigate the improvement in quality, CNR was estimated for RE without compounding (0 ˚ view) and three different compounded RE (obtained with max steering angle(MSA) of ± 5 ˚,± 10 ˚ and ±15 ˚) , respectively. The step size was set to 1 ˚ for this analysis. Another analysis involved varying of step size at fixed MSA of 15 °.

Results: The results shown in Fig.1 (a, b) demonstrate RE of non-compounded (0°) RE and compounded RE (MSA=15˚). Plot in Fig.1(c) shows improvement in CNR with increase in MSA. The step size was 1˚ for this analysis. Fig.1 (d) depicts CNR v/s step angle for a fixed MSA of 15˚.

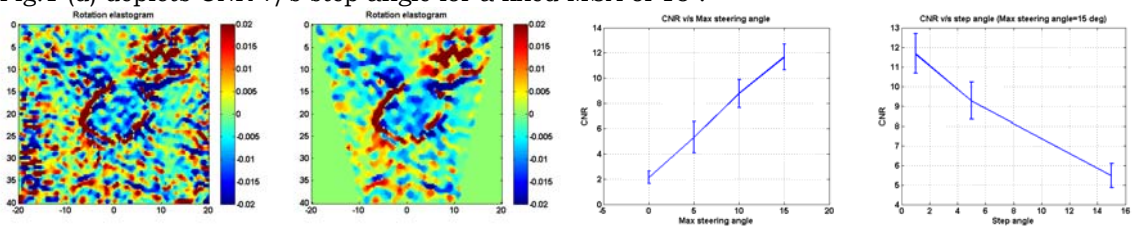

(a) (b) (c) (d)

Fig.1: (a) Non-compounded Rotation Elastogram (0˚),(b) Compounded Rotation Elastogram with maximum steering angle of ±15 ˚and step size of 1˚,(c) Plot of CNR v/s maximum steering angle,(d) Plot of CNR v/s step angle at a maximum steering angle of 15 ˚.

Conclusions: It can be concluded that spatial compounding technique can be utilized to improve the quality of RE.MSA and step size are two parameters of interest and the contribution of MSA to the quality of RE is high compared to step size. The compromise on CNR is low due to increase in step size from 1° to 5 °. The choice of 15° as MSA is acceptable for depth ranges typically encountered for breast lesions.

Acknowledgement: This work was funded by MHRD, Government of India.

References:

[1] A. K. Thittai et al."Axial-shear strain distributions in an elliptical inclusion model: experimental validation and in vivo examples with implications to breast tumor classification." Ultra. Med. Biol., vol. 36, no. 5, pp. 814–20, 2010.
[2]A. K. Thittai et al."On the advantages of imaging the axial-shear strain component of the total shear strain in breast tumors.," Ultra. Med. Biol., vol. 38, no. 11, pp. 2031–2037, Nov. 2012.
[3]Techavipoo et al."Estimation of displacement vectors and strain tensors in elastography using angular insonifications," IEEE Trans. Med. Imag.23(12), 1479-1489 (2004).
[4] H H G Hansen et al. "Full 2D displacement vector and strain tensor estimation for superficial tissue using beam-steered ultrasound imaging". Phys. Med. Biol. 55 3201–3218(2010).
[5] Sowmiya C et al."Rotation Elastogram:A Novel method to visualize local rigid body rotation under quasi- static compression", SPIE Medical Imaging Conference 2016 (San Diego).

021 **GENERATION OF SHEAR WAVES BY LASER IN SOFT MEDIA IN THE ABLATIVE AND THERMOELASTIC REGIMES..**

P. Grasland-Mongrain[1], Y. Lu[1,2], F. Lesage[2,3], S. Catheline[4], G. Cloutier[1,2,5]*

[1]Laboratory of Biorheology and Medical Ultrasonics, University of Montreal Hospital Research Center (CRCHUM), Montreal (QC), CANADA; [2]Institute of Biomedical Engineering, École Polytechnique and University of Montreal, Montreal (QC), CANADA; [3]Department of Electrical Engineering, École Polytechnique of Montreal, Montreal (QC), CANADA; [4]Laboratory of Therapeutic Applications of Ultrasound, Inserm u1032, Inserm, Lyon, FRANCE; [5]Department of Radiology, Radio-Oncology and Nuclear Medicine,, University of Montreal, Montreal (QC), CANADA

Background: Shear wave elastography relies on the detection of a shear wave throughout the studied medium. To induce the shear wave, most techniques imply either an external shaker [1] or a focused acoustic beam [2]. Alternatively, in photoacoustics, acoustic waves are induced with a laser [3]. A laser might thus be able to induce shear waves, to provide an alternative method for shear wave elastography.

Aims: The goal of the study was to demonstrate that a laser could induce shear waves in soft solids, and to study the underlying physical mechanism.

Methods: A Nd:YAG 532 nm laser beam was emitted on a gelatin phantom filled with graphite particles (see figure 1). Displacements were tracked with an ultrasound probe at 2000 frames per second. Theoretical displacements as given by the Navier equation were computed, and compared quantitatively and qualitatively to the experiments.

Results: Experiments showed two different regimes depending on the laser energy (figure 2). Physical modeling of the underlying phenomena revealed a thermoelastic regime caused by a local dilatation resulting from the temperature increase, and an ablative regime caused by a partial vaporization of the medium by the laser. Computed theoretical displacements are close to experimental measurements. Propagation patterns given by the numerical study are comparable to those generated experimentally.

Conclusions: These results provide a physical basis for the feasibility of a shear wave elastography technique (a technique which measures tissue elasticity from shear wave propagation) by using a laser beam.

Acknowledgements: Pol Grasland-Mongrain holds a post-doctoral research scholarship from the Natural Sciences and Engineering Research Council of Canada.

References: [1] L. Sandrin, B. Fourquet, J. Hasquenoph, S. Yon, C. Fournier, F. Mal, M. Beaugrand, *Transient elastography: a new noninvasive method for assessment of hepatic fibrosis*, Ultrasound Medicine & biology (2003), 29(12), 1705-1713.

[2] J. Doherty, G. Trahey, K. Nightingale, M. Palmeri, *Acoustic radiation force elasticity imaging in diagnostic ultrasound*. IEEE transactions on ultrasonics, ferroelectrics, and frequency control (2013), 60(4), 685-701.

[3] M. Xu, L. Wang, *Photoacoustic imaging in biomedicine*, Review of scientific instruments (2006), 77(4), 04110.

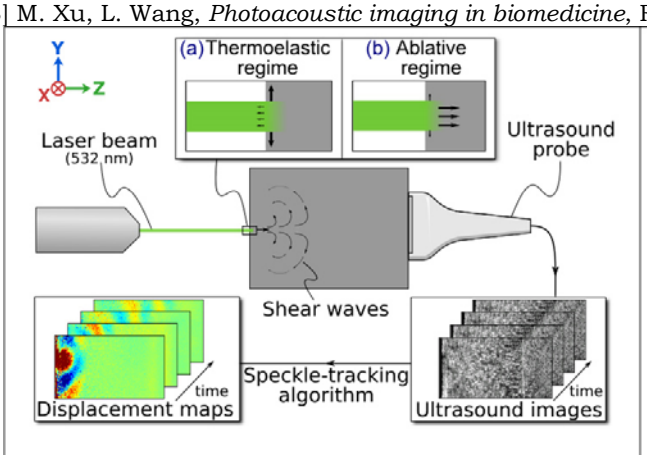

Figure 1: Scheme of the experiment: a laser beam is emitted in a medium observed by an ultrasound probe. Absorption of the laser by the medium gives rise to shear waves according to two physical phenomena: a thermoelastic dilatation or a medium partial ablation.

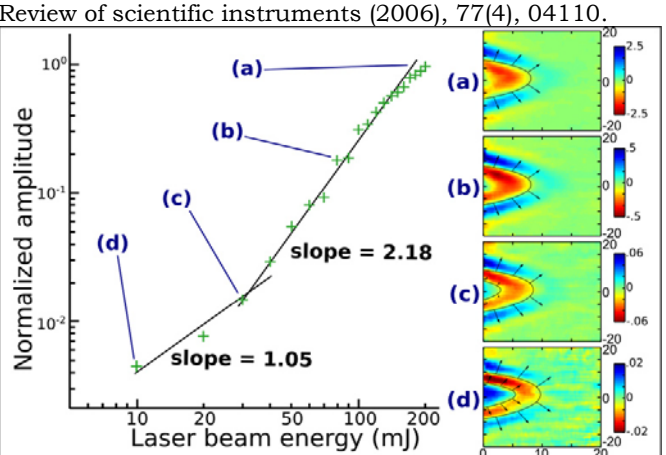

Figure 2: Transition between the thermoelastic (slope = 1.05) and the ablative (slope = 2.18) regimes, depending on the laser beam energy.

023 **BI-PLANE ARTERIAL WALL STIFFNESS ESTIMATION USING SHEAR WAVE IMAGING: A SIMULATION AND PHANTOM STUDY.**

Y Guo[1], H Yuen Lo[1,2], W-N Lee[1,2]*

[1]Department of Electrical and Electronic Engineering, The University of Hong Kong, Hong Kong; 2Medical Engineering Programme, The University of Hong Kong, Hong Kong.

Background: The feasibility of shear wave imaging (SWI) for quantitatively assessing the mechanical properties of the arterial wall has been demonstrated mainly in the longitudinal view based on both group (vg) and phase (vph) velocities [1, 2] but only recently in the transverse view in the mid wall through vg [3]. Whether the geometrical differences between these two orthogonal planes impact the accuracy of SWI-derived stiffness remains unknown. The transmural distribution of the stiffness in the cross section of the arterial wall has not yet been reported, either.

Aims: This study thus aims to investigate and compare the SWI-estimated stiffnesses through both vg and vph between two orthogonal views in finite element models (FEM) and tissue-mimicking phantoms of hollow cylinders with various geometrical and material properties.

Methods: Four linearly elastic, homogeneous, and isotropic hollow cylinders were simulated with finite-element modeling using COMSOL Multiphysics (Comsol Inc. Burlington, MA, USA). Model I had an inner and an outer radius (rin, rout) of (5, 10) mm and a shear modulus of 16kPa, whereas models II-IV had a shear modulus of 34 kPa [4] and (rin, rout) of (5, 7), (9, 11), and (13, 15) mm, respectively, to mimic the human aorta. An acoustic excitation of 1000kPa and 100 μs was applied within a wall region of h*π*12 m3, where h is the wall thickness, to generate shear waves. One hollow cylindrical phantom was made of 10% polyvinyl alcohol (PVA) and 1% silicone dioxide in deionized water, undergoing 3 freeze/thaw cycles). Its stiffness was confirmed by tensile testing and its dimension was designed, matching the FEM settings. The shear modulus of the PVA phantom was assessed at three different locations. A Vantage system (Verasonics Inc., Kirkland, WA) with an L7-4 probe (fc = 5.2 MHz) was used to remotely generate shear waves by an ultrasonic beam of 100 μs focused at the posterior wall of the PVA phantom. Shear waves were imaged by coherent plane wave compounding (-2, 0, and 2 degrees) at a frame rate of 5000 Hz. Spatiotemporal maps of shear waves in the transverse view were warped prior to the wave analysis.

Results: The SWI-estimated shear moduli were found to be 18.2±0.5kPa and 17.1±0.9kPa in Model I and the PVA phantom, respectively, in the longitudinal view (Fig. 1a). In the transverse plane, in contrast, underestimation of shear moduli (Model I: 10.0kPa; PVA: 9.2±0.7kPa) at rin and overestimation (Model I: 40.2kPa; PVA: 54.1±20.1kPa) at rout were observed (Fig. 1b). Similar variations of shear moduli across the wall were found in Models II-IV (Fig. 1c, d).

Conclusions: Our results showed that SWI-estimated shear moduli derived from vg and vph in the transverse view of the hollow cylinders agreed with ground truth only at limited radial wall positions, suggesting their cautious use for wall characterization. Our ongoing therefore work includes 1) comprehensive phase velocity analysis in thin-walled phantoms and the porcine aorta and 2) formulation of the wave model in the cross-sectional area of the hollow cylinder.

Acknowledgements: This study is supported by NSFC/RGC (N_HKU713_15), University Development Fund, and in part by Hong Kong Research Grants Council (ECS 739413E).

References: [1] Couade, Mathieu, et al. “Quantitative assessment of arterial wall biomechanical properties using shear wave imaging.” Ultrasound in medicine & biology 36.10 (2010): 1662-1676.

[2] Maksuti, Elira, et al. "Arterial Stiffness Estimation by Shear Wave Elastography: Validation in Phantoms with Mechanical Testing." Ultrasound in medicine & biology 42.1 (2016): 308-321.

[3] Hansen, Hendrik HG, et al. “Shear wave elastography for lipid content detection in transverse arterial cross-sections.” Ultrasonics Symposium (IUS), 2015 IEEE International. IEEE, 2015.

[4] O’Rourke, Michael F., and Wilmer W. Nichols. "Aortic diameter, aortic stiffness, and wave reflection increase with age and isolated systolic hypertension." Hypertension 45.4 (2005): 652-658.

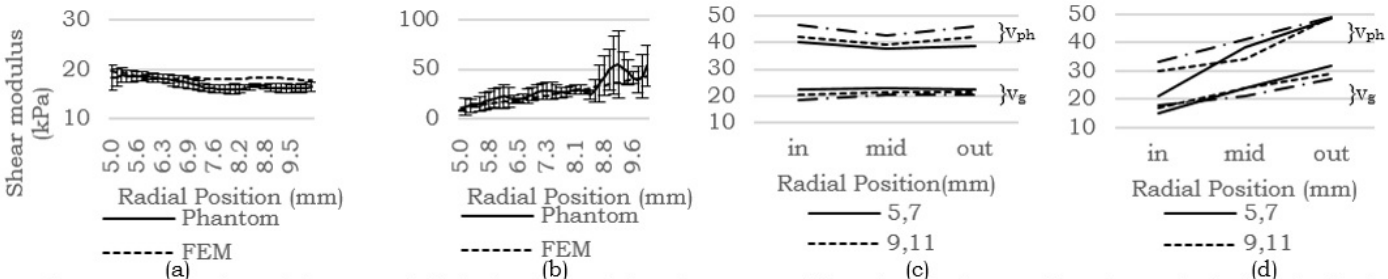

Figure 1 Comparison of shear moduli obtained from finite-element model I and PVA phantom based on v_g in the longitudinal view (a), in the transverse view (b), from finite-element models II-IV based on v_g and v_{ph} in the longitudinal view (c), in the transverse view (d).

043 **THREE-DIMENSIONAL *IN-VIVO* ELASTICITY IMAGING OF THE BREAST.**

M Tyagi[1], Y Wang[2], T.J Hall[2], P.E.Barbone[3], A.A. Oberai[1].*
[1]Rensselaer Polytechnic Institute, Troy, NY, USA; [2]University of Wisconsin-Madison, WI, 5, USA; [3]Boston University, Boston, MA, 02215, USA.

Background: In quasi-static elastography, strain maps within the tissue are often displayed as a reciprocal measure of stiffness. A potentially more accurate approach involves using the displacement measurement obtained from elastography to determine the spatial distribution of elastic moduli like the shear or the Young's modulus. This approach requires the solution of a challenging inverse problem. The computational costs of this problem can be kept under control through the use of an adjoint problem [1]. In this talk, we apply this method to map the three-dimensional distribution of shear modulus for a region of breast tissue for two subjects. The displacement data is acquired in three dimensions using a one-dimensional array that is swept in the elevational direction. The acquisition time is such that the subjects take multiple breaths during a scan. This breathing motion adds yet another source of "noise" to the measurements. When reconstructing the modulus we account for this, and other types of noise, by using the principal component analysis (PCA) [2] to remove the noisy component of displacement data.

Aims: The aim of this study is to perform three-dimensional modulus reconstruction of breast tissue using ultrasound based quasi-static elastography.

Methods: Quasi-static displacement data on two female subjects was acquired using a swept transducer array while the breast was compressed to about 15 % strain in stages. The acquisition times were long enough to introduce noise due to the subject's breathing. PCA was used to de-noise this data, and the resulting displacement data was used in an inverse problem to determine the spatial distribution of the shear modulus, which was determined up to an unknown multiplicative parameter.

Results: In the Figure below, we present data from one of the subjects. Fig. (a), shows a strain image at the mid-elevational plane. Figs. (b)-(d), show the three dominant principal components which comprise of compression and rocking/breathing motions. Fig. (e), shows the strain image obtained from the de-noised displacement data. We note that this image is less noisy than Fig. (a). Finally Fig. (f), shows the three-dimensional shear modulus image reconstructed from the de-noised data. In this image we can clearly see the volumetric extent of the lesion.

Conclusions: We have generated three-dimensional elasticity images from clinical data, and demonstrated the effectiveness of PCA in improving elasticity imaging.

Acknowledgements: Support from the NIH (NCI-R01CA100373 & NCI-R01CA140271) and the NSF (Grant Nos. 1148124, and 1148111) is acknowledged.

References: 1. Richards, Michael S., Paul E. Barbone, and Assad A. Oberai. "Quantitative three-dimensional elasticity imaging from quasi-static deformation: a phantom study." Physics in medicine and biology 54.3 (2009): 757.
2. Shlens, Jonathon. "A tutorial on principal component analysis." arXiv preprint arXiv:1404.1100 (2014).

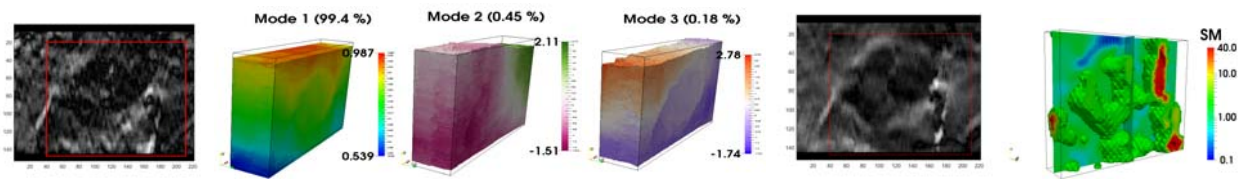

(a) (b) (c) (d) (e) (f)

Figure 1. (a) Strain image on mid-elevational plane, (b)-(d) Three dominant principal components, (e) Strain image on mid-elevational plane obtained from the de-noised displacement data, (f) Three-dimensional shear modulus image.

032 **NON-LINEAR CHARACTERIZATION OF THE LIVER BY COMBINING SHEAR AND LONGITUDINAL WAVE SPEED WITH STRAIN OBSERVATIONS.**

S J Sanabria[1], M. Rominger[2], C. F Otesteanu[1], E.Mazza[3], O.Göksel[1].*
[1]Computer-assisted Applications in Medicine (CAiM), ETH Zurich, SWITZERLAND; [2]Diagnostic and Interventional Radiology, University Hospital of Zurich (USZ DIR), SWITZERLAND;[3]Dept. of Mechanical and Process Engineering, ETH Zurich, SWITZERLAND.

Background: With the advance of ultrasound elastography (USE), tissue biomechanical parameters can be imaged, providing valuable information for both diffuse (e.g. cirrhosis) and focal liver diseases (tumors). However, non-linear tissue characteristics limit the repeatability of USE, likely yielding different measurements under different probe compressions/manipulations by the operator. Non-linear stress-strain plots $\sigma(\varepsilon)$ have been shown to significantly improve the differentiation of tumors with respect to linear elastic moduli. It is therefore of strong interest to augment USE with non-linearity information. Previous works (e.g. [1]) focus on the non-linearity of the shear wave velocity (c_S), which relates to the dynamic Elastic modulus (E). c_S variations with strain ε are typically fitted to pre-defined non-linear functions, from which non-linear parameters are extracted. In a clinical setting, these functions may not be defined or change in time, and a direct estimation of the non-linear stress states $\sigma(\varepsilon)$ is desirable.

Aims: USE imaging of both shear c_S and longitudinal wave c_L velocities over multiple compressive cycles. Correlation of non-linear stress $\sigma(\varepsilon)$ estimated from USE (*dynamic*) with force sensor values (*quasi-static*).

Methods: *Ex-vivo* bovine liver was subjected to successive quasi-static compression cycles and the strain ε (gauging) and stress σ state (force sensor) were recorded. Combined Shear Wave Elastography (SWE, GE Logic E9), and Hand-Held Speed-of-Sound Imaging (HH-SoSi, [2]) simultaneously image the shear c_S and longitudinal c_L wave speeds at each compression state ε. In particular, c_L is calculated from the time-of-flight between transducer elements and a planar reflector (Fig. 1a). Given c_S and c_L, $E=2(1+\nu)\rho c_S^2$ and $K=\rho(c_L^2-4/3c_S^2)$ are measured in the dynamic regime, with v=0.5 and $\rho=10^3\ kg/m^3$ (Fig.1b-c). Assuming quasi-uniaxial stress, the slope of σ(ε) is hypothesized to correlate with the dynamic E values: $\sigma'(\varepsilon) \propto E(\varepsilon)$. Given $E(\varepsilon)$, USE non-linear stress values $\sigma(\varepsilon)|_{USE}$ are then reconstructed as a piece-wise linear function, with $\sigma'(\varepsilon)|_{USE}=E(\varepsilon)$. Finally, $\sigma(\varepsilon)|_{USE}$ are compared to quasi-static force sensor readings $\sigma(\varepsilon)|_{FORCE}$ (Fig.1d-e)

Results: K was found to be insensitive to the compression state (0.5% error) (Fig.1b). E measurements at the same compression level ε are reproducible (9% error). However, uncontrolled compression (ε=0-22%) acts as a measurement confounder, leading to 64% error in E (Fig. 1c). These variations are successfully projected into convex non-linear stress-strain trends (Fig. 1d). Upon multiple compression cycles, the *ex-vivo* liver sample became stiffer, potentially due to the permanent loss of fluid, and the trend $\sigma(\varepsilon)$ changes. Remarkably, despite different loading regimes, $\sigma(\varepsilon)|_{USE}$ quantitatively follows $\sigma(\varepsilon)|_{FORCE}$, and allows for monitoring the stiffening process (Fig. 1d). Linear regression shows an almost equivalent relation (slope=1.01) with correlation R^2=0.7 between USE stress estimates and force sensor readings (Fig. 1e).

Conclusions: The Bulk modulus K, as measured from c_L, is shown to be to non-linearity. Combining USE dynamic values of E with observed strain levels ε allows direct reconstruction of non-linear stress states $\sigma(\varepsilon)$. $\sigma(\varepsilon)$ and K provide robust mechanical biomarkers, with potential for staging of liver disease.

Acknowledgements: This project is supported by the Swiss NSF and a Hoschulmedizin Zurich (HMZ) Seed Grant.
References: [1] Jiang Y *et al.* Med Imag Anal 20 (2015) 97-111. [2] Sanabria SJ, Goksel O. Hand-held Sound-Speed Imaging Based on Ultrasound Reflector Delineation. In Proc: MICCAI, Athens, 2016.

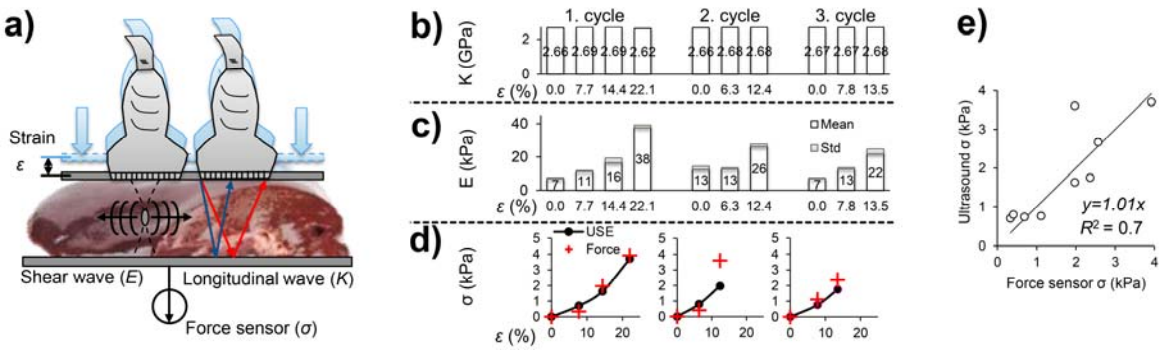

Figure 1: (a) Setup; (b) K and (c) E measurements in successive compression cycles; (d) reconstructed non-linear plots σ(ε), (e) correlation of σ obtained from US data and force sensor. Tissue temperature variations were negligible.

063 **APPARATUS FOR IMAGING AND MODEL FITTING OF EX-VIVO PORCINE KIDNEY.**

C Schneider[1], M. Honarvar[1], R Rohling[1], S E Salcudean[1], C Nguan[2]*

[1] The University of British Columbia, Vancouver, British Columbia, CANADA. [2]Department of Urology, Vancouver General Hospital, British Columbia, CANADA.

Background: Elastic imaging of native and transplant kidneys has been studied in depth recently using several different methods. The development of fibrosis within the kidney is one of the leading causes of kidney failure and difficult to monitor and diagnose without biopsy. Missing in the literature is an in depth study of the elastic and viscous properties of the kidney in a controlled environment.

Aims: To develop an apparatus for repeatable imaging of ex-vivo kidneys. The apparatus is used for steady state shear wave imaging for elastic measurement of tissue. With repeated imaging of the kidney at multiple frequencies, we are able to fit the frequency response of the tissue to 3 different mechanical models of the tissue and solve for both the elastic and the viscous parameters of the tissue.

Methods: The constructed apparatus is able to hold the excitation device, the 3D ultrasound transducer and the kidney. The shaker is attached to the stainless steel frame and a plunger is pressed against a silicon gel pad, approximately 2cm thick. The gel pad helps hold the kidney against the shaker and distribute the waves from the shaker into the kidney tissue. On the other side of the silicon pad, the ex-vivo kidney is held in place with a thin silicon sheet. The width of the space for the kidney is adjustable to allow for variations in the shape and size of the kidneys. The thin silicone mat allows the side of the kidney facing the ultrasound probe to vibrate more freely than if were pressed directly again the face of the ultrasound probe. This allows for better wave propagation throughout the kidney without any restrictions on the motion. The entire apparatus is submerged in a water bath; approximately 1-2cm of water separates the thin mat, and kidney, from the ultrasound probe.

The kidneys were excited at frequencies between 50 and 200 Hz, every 25 Hz. 3D volumes of the kidney were taken at each frequency of excitation. Ultrasound volumes were collected with an Ultrasonix Touch machine and a 4DL14 mechanical 3D ultrasound transducer (Analogic Ultrasound, BC, Canada). The resulting phasor volumes were then analyzed with the Local Frequency Estimation (LFE) technique [1]. The calculated results of the elasticity were then fit to three different rheological models, a) Voigt Model, b) Maxwell Model and c) Zener Model.

Results: The apparatus allows for repeated high quality 3D volume acquisition of elasticity data in an *ex-vivo* environment. We have examined the resulting wave propagation and found that the waves within the kidney are consistent and are tracked with high correlation.

The rheological models were fitted to the results of the elasticity measurements for 11 experiments, and the modeling error was calculated as the square root of the sum of the squared difference between the observed measurement and the model over the excitation frequencies. The rheological models had average errors of a) 0.30 m/s, b) 0.35 m/s and c) 0.30 m/s, respectively. Although the error measurements are similar, the Voigt model was less sensitive to initial conditions. Further testing and model development is needed.

Conclusions: We have shown that this apparatus can be used for the controlled study of *ex-vivo* kidneys and could be used for further investigation of other organs. We anticipate its use for measurements of other variables such as changes with input pressure or temperature, or storage conditions. From the model fitting, we have learned that the kidney, in particular, has a strong viscous component that should be taken into account when measuring elasticity at different frequencies or with different elasticity methods.

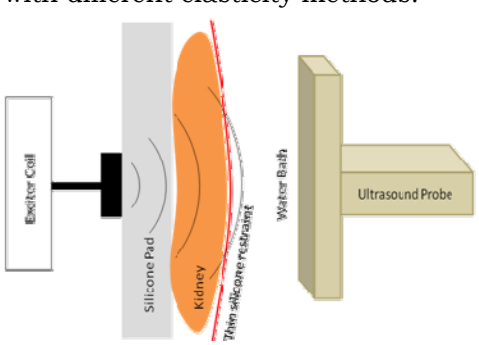

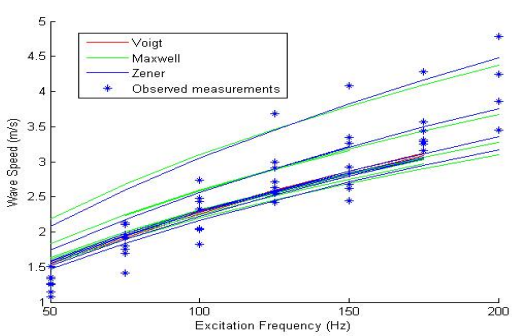

References:

[1] Manduca et al. *Magnetic resonance elastography. Med Image Analysis Vol. 5 (4), 2001.*

007 **APPLICATION OF CARDIAC MRI TAGGING SEQUENCES FOR LIVER FIBROSIS STAGING.**

L Petitclerc[1], G Gilbert[2], G Cloutier[1,3], A Tang[1].*

[1]University of Montreal Hospital Research Center, Montreal, Quebec, CANADA; [2]Philips Healthcare Canada, Montreal, QC, CANADA; [3] Laboratory of Biorheology and Medical Ultrasonics, Montreal, Quebec, CANADA.

Background: Liver fibrosis is becoming an important health concern worldwide, because of the growing incidence of chronic liver disease. Until recently, liver biopsy was the reference standard for diagnosis and staging of liver fibrosis. However, it is invasive and vulnerable to sampling errors. Several imaging techniques have been developed for staging of liver fibrosis. Magnetic resonance elastography (MRE) has shown high diagnostic performance for liver fibrosis staging but requires additional hardware and software. Alternatively, MRI cine-tagging originally developed for assessing intrinsic cardiac motion requires no additional hardware and can be done on any clinical MR system. Prior studies assessing cardiac motion-induced liver strain have shown lower values in cirrhotic than in normal patients [1,2]. However, the diagnostic performance of MRI cine-tagging has not been assessed for staging liver fibrosis.

Aims: (1) To assess the diagnostic performance of MRI cine-tagging for the staging of liver fibrosis. (2) To compare post-processing methods for the measurement of liver strain.

Methods: Patients were examined on a 3.0 T clinical MRI system (Achieva TX, Philips Healthcare, Best, The Netherlands) using a 2D multi-slice gradient-recalled echo sequence with peripheral pulse-wave triggering. The SPAMM preparation sequence was used for tagging, with the following parameters: tag spacing, 8 mm; tag orientation, 0 and 90°; and number of phases per cardiac cycle, 12-15. Four slices were acquired in breath-hold at end expiration. The HARP [3] image analysis method was used to calculate strain maps for each patient. Four different methods were investigated to extract a single strain measurement from these maps. The first consisted in averaging the strain in a 100-pixel region of interest (ROI) adjacent to the heart, the second used the same ROI but averaged the strain over two coronal slices, the third measured the average of the 100 pixels with the highest strain in the entire liver, and the fourth used this maximal strain and normalized it by the displacement of the myocardium. Spearman's ρ was used to assess the correlation between strain and fibrosis stages. The Mann-Whitney test allowed to compare strain values between dichotomized fibrosis stages. Receiver operating characteristic (ROC) curve analysis was performed to estimate the diagnostic performance of MRI cine-tagging for the differentiation of dichotomized fibrosis stages.

Results: Twenty-two patients underwent MRI cine-tagging (Fig. 1) and had available biopsy results. Liver strain was lower in higher fibrosis stages. Spearman's ρ for the single ROI, dual ROI, maximum, and normalized maximum strain methods were -0.566, -0.611, -0.257, and -0.292, respectively. The post-processing method that included two ROIs provided the following *p*-values for differentiation of fibrosis stages ≤1 vs. ≥2 ($p = 0.47$), ≤2 vs. ≥3 ($p = 0.02$), and ≤3 vs. 4 ($p < 0.01$). The area under the ROC curve for differentiation of fibrosis stages ≤1 vs. ≥2 was 0.632, ≤2 vs. ≥3 was 0.813, and ≤3 vs. 4 was 0.931 (Fig. 2).

Conclusions: Liver strain decreased with higher fibrosis stages. The moderate to high accuracy of MRI cine-tagging for separation of liver fibrosis stage 3 or higher suggest that this technique may be complementary to MRE, especially for assessment of the left liver lobe.

Acknowledgements: Dr. An Tang was supported by a clinical research scholarship of the FRQS and FARQ (#26993).

References: [1] Manelli L et al. JMRI 2012;36:1490-1495. [2] Harouni AA et al. Magn Reson Med. 2014. PMID: 25081734. [3] Osman NF, Faranesh AZ, Magnetic Resonance in Medicine 1999;42:1048-1060.

Fig1: Coronal gradient-recalled echo sequence with tagging in a patient with biopsy-proven fibrosis stage 2.

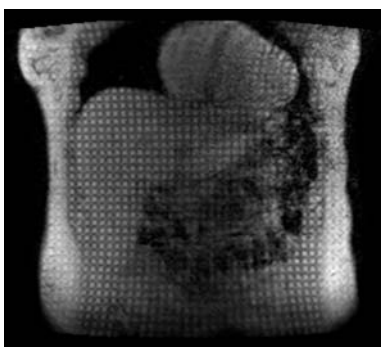

Figure 2: Receiver operating characteristic curve analysis of MRI cine-tagging for classification of dichotomized fibrosis stages determined by liver biopsy: ≤1 vs. ≥ 2, ≤2 vs. ≥3, ≤3 vs. 4.

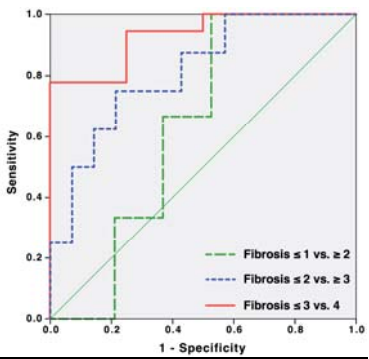

020 **PANCREATIC CANCER DETECTION IN HUMAN RESECTED SPECIMEN USING HARMONIC MOTION IMAGING (HMI).**

T Payen[1], K P Olive[2], E E Konofagou[1,3] .*

[1]Biomedical Engineering, Columbia University, New York, NY, USA; [2]Departments of Medicine and Pathology & Cell Biology, Herbert Irving Comprehensive Cancer Center, Columbia University Medical Center, New York, NY, USA; [3]Department of Radiology, Columbia University Medical Center, New York, NY, USA.

Background: Pancreatic ductal adenocarcinoma (PDA) is one of the deadliest cancers with the lowest prognosis due to late diagnosis and non-specific symptoms. PDA is characterized by an unusually dense stroma limiting chemotherapy perfusion [1]. Harmonic Motion Imaging (HMI) assesses tissue mechanical properties by inducing localized oscillation resulting from a periodic acoustic radiation force [2, 3]. The stiffer the tissue is, the smaller the displacement amplitude.

Aims: The objective of this study was to evaluate the capability of HMI to detect PDA in human resected pancreatic cancer specimen and differentiate the tumor for surrounding fibrotic tissue and normal tissue based on their mechanical properties.

Methods: A 4.5-MHz focused ultrasound transducer (FUS) generated an amplitude-modulated beam resulting in harmonic tissue oscillations at its focus. Axial tissue displacement was estimated using 1D cross-correlation of RF signals acquired with a 2.5MHz diagnostic transducer (P4-2, ATL) confocally aligned with the FUS. Four resected specimens (approximate dimensions = 24 x 12 x 80 mm3) were obtained from distal pancreatectomy surgeries of PDA. The HMI planes were chosen perpendicular to the pancreatic duct to correlate with standard histology analysis.

Results: Histology showed that the HMI scan did not damage the tissue in any aspect, and did not impact the subsequent analysis. HMI was able to scan the whole specimens with measurements as deep as 3 cm in the tissue and covering the whole range of stiffness from tumor to normal pancreas. The figure shows the B-mode image of the maximal cross section of the tumor, and the HMI map overlaid on the B-mode image. The mean displacement inside the tumor is 1.41 ± 1.00 µm versus 11.25 ± 3.69 µm in the surrounding tissue. Measurements in normal pancreatic tissue demonstrated a mean HMI displacement of 17.05 ± 3.98 µm. A sharp delineation is visible on the HMI maps between the tumor and the surrounding tissue which correlates very well with the B-mode image.

Conclusions: This initial feasibility study showed that HMI is capable of scanning whole resected pancreatic cancer specimens without any damage to the tissue. The technique can assess deep parts of the tissue with greatly different stiffness. HMI significantly detected PDA within the specimen with mean displacement lower by a ratio of 9.8 compared to the surrounding tissue and 12.1 compared to normal pancreas away from the mass. This may indicate possible presence of fibrotic tissue close to the tumor. HMI could be a very important tool for screening patients at risk of developing pancreatic cancer and showing the non-specific symptoms.

Acknowledgements: This work was supported by the funding source NIH R01EB014496.

References: [1] World Cancer Report 2014. World Health Organization; [2] Maleke C et al (2006), Ultrason. Imaging 28 144–58; [3] Chen H et al (2015), IEEE Trans. Ultrason., Ferroelect. Freq. Control, 62(9), 1662-1673.

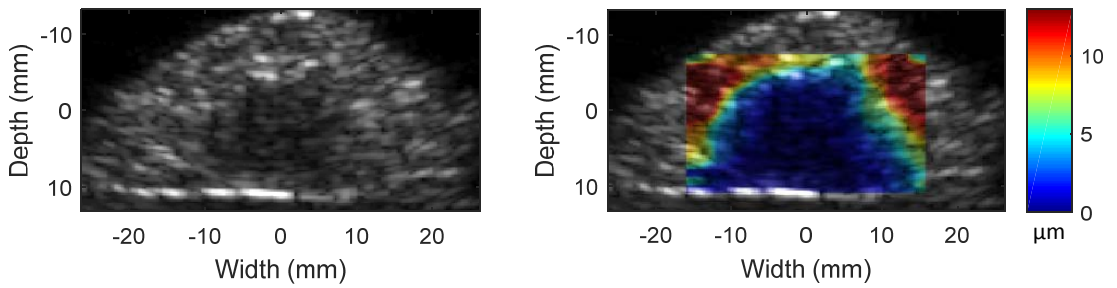

Figure: Pancreatic ductal adenocarcinoma (PDA) in a distal pancreatectomy specimen. The B-mode image (left) is shown as well as the overlaid HMI displacement map (right) showing the sharp contrast between the mass and the surrounding tissue.

018 **GLOBAL TIME DELAY ESTIMATION IN ULTRASOUND ELASTOGRAPHY.**

H S Hashemi[1,2], H Rivaz[1,2].*

[1]Department of Electrical and Computer Engineering, Concordia University, 1455 De Maisonneuve Blvd. W., Montreal, Quebec, H3G1M8, CANADA; [2]PERFORM Center, 7200 Sherbrook St. W., Montreal, Quebec, H4B1R6, CANADA.

Background: Correlation methods are commonly used for Time-Delay Estimation (TDE) of tissue displacement. Large correlation windows utilize more information and reduce the estimation variance, but result in significant signal decorrelation and decrease the spatial resolution. Furthermore, most correlation techniques only estimate axial strain because of the poor resolution of ultrasound data in the lateral direction. An attractive alternative approach to correlation-based methods is minimization of a regularized cost function. These methods exploit the prior information that tissue deformation is smooth, and therefore are robust to signal decorrelation [1]. A disadvantage of these methods is their computational complexity, and as such, they are not suitable for real-time implementation. Previous work [2] proposed a real-time method for optimization of the cost function, but only exploited individual RF-lines at during each optimization, which results in artifacts in the form of vertical streaks (Fig. 1).

Aims: This paper presents a novel technique for time-delay estimation of all RF-lines simultaneously instead of utilizing individual RF-lines, thereby exploiting all the information in the entire image. In other words, we optimize for the displacement of all samples of all RF-lines simultaneously, which requires optimizing a cost function with close to 1 million variables.

Methods: The main idea is to incorporate similarity of RF data intensity, as well as prior information of displacement continuity in a cost function. The cost function optimization entails solving a sparse linear system which is computationally efficient. Let $I_1(i,j)$ and $I_2(i,j)$ be two ultrasound RF frames acquired before and after some tissue deformation, and i and j respectively be samples in the axial and lateral directions. The global cost function with the summation on all image pixels is defined as $C = min \sum\{ [I_1(i,j) - I_2(I + a_{i,j} + \Delta a_{i,j} , j + l_{i,j} + \Delta l_{i,j})]^2 + \alpha_1(a_{i,j} + \Delta a_{i,j} - a_{i-1,j} - \Delta a_{i-1,j})^2 + \beta_1(l_{i,j} + \Delta l_{i,j} - l_{i-1,j} - \Delta l_{i-1,j})^2 + \alpha_2(a_{i,j} + \Delta a_{i,j} - a_{i,j-1} - \Delta a_{i,j-1})^2 + \beta_2(l_{i,j} + \Delta l_{i,j} - l_{i,j-1} - \Delta l_{i,j-1})^2 \}$ where α and β are regularization terms for axial and lateral displacements respectively. I_1 and I_2 are the corresponding intensity of each pixel in first and second RF frame. Assume an initial estimate of the 2D displacement field is available from Dynamic Programming (DP) [3]. By minimizing the cost function using DP initial guess, the sub-sample axial and lateral displacements ($\Delta a_{i,j}$, $\Delta l_{i,j}$) for the total image are calculated. The integer initial displacements ($a_{i,j}$, $l_{i,j}$) provided through the previous step are added to the subsample displacements. This presents us the final lateral and axial displacements i.e. ($a_{i,j} + \Delta a_{i,j}$, $l_{i,j} + \Delta l_{i,j}$). The spatial gradient of the displacement field is used to acquire the strain image.

Results: We show that the proposed method substantially outperforms the two previous methods of DPAM [2] and normalized cross correlation (NCC) [1] methods using simulation data, phantom experiments and *in-vivo* patient data (Figs. 1, 2 and 3).

Acknowledgements: Supported by the Richard and Edith Strauss Canada Foundation. The *in-vivo* data was collected at Johns Hopkins Hospital. The principal investigators were Drs. E. Boctor, M. Choti and G. Hager.

References:

[1] Hall, TJ, et al. "Recent results in nonlinear strain and modulus imaging," Cur Med Imaging Rev pp 313–327, 2011

[2] Rivaz, H., et al., "Real-time regularized ultrasound elastography," IEEE Trans Medical Imaging, vol. 30, no. 4, pp. 928–945, 2011.

[3] Rivaz, H., et al., "Ultrasound elastography: a dynamic programming approach," IEEE Trans Medical Imaging, vol. 27, no. 10, pp. 1373–1377, 2008.

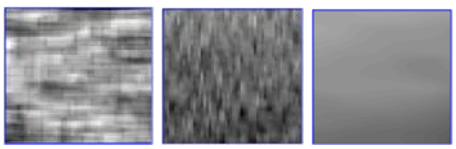

Fig. 1 Left to right: NCC strain, DPAM strain, GTDE strain.

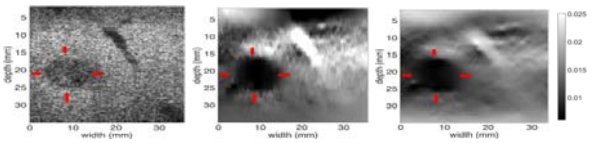

Fig. 2 In-vivo data: BMODE image, DPAM strain, GTDE strain.

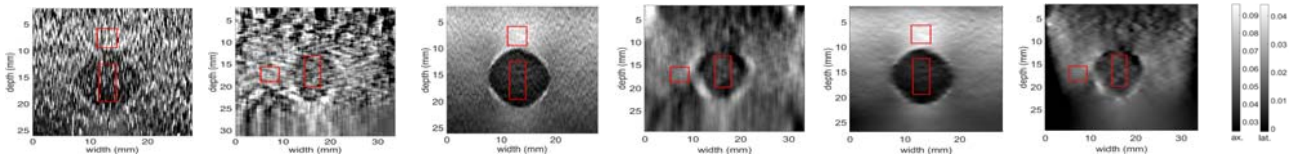

Fig. 3 Axial & Lateral strains of phantom data. Left to right: CC (Ax.), CC (Lat.), DPAM (Ax.), DPAM (Lat.), GTDE (Ax.), GTDE (Lat.)

067 **ULTRASOUND ACTIVITY IN THE RSNA-QUANTITATIVE IMAGING BIOMARKER ALLIANCE.**

T J Hall[1], B.S Garra[2], P L Carson[3], A Milkowski[4], R.G.Barr[5,7], J B Fowlkes[3], O Kripfgans[3], M Averkiou[6].*

[1]University of Wisconsin, Madison, WI, USA; [2]VA Medical Center, Washington DC, USA; [3]University of Michigan, Ann Arbor, MI, USA. [4]Siemens Ultrasound, Issaquah, WA, USA; [5]Southwoods Imaging, Boardman, OH, USA; [6]University of Washington, Seattle, Washington, USA.

Background: The Radiological Society of North America (RSNA) created the Quantitative Imaging Biomarker Alliance (QIBA) to convert "imaging systems" with subjective image interpretation to "measurement systems" with objective measurands having actionable numerical values.

Aims: The goal is to create QIBA protocols and profiles that specify methods for data acquisition, analysis, and interpretation. QIBA profiles also provide specific claims of what can be accomplished by following the QIBA protocol. The intent is to validate the profile across imaging systems in a collaboration between industry, government (NIH, FDA, NIST), Pharma, clinicians, and academics.

Methods: The RSNA/QIBA effort includes over 850 volunteers worldwide with Biomarker Committees for all major imaging modalities. The effort is expanding with collaborations in Japan (the Japan Radiological Society's QIBA-Japan) and in Europe (European Institute for Biomedical Imaging Research and the European Imaging Biomarker Alliance; EIBIR – EIBALL). The QIBA ultrasound group began with a committee to investigate and minimize sources of bias and variance in shear wave speed estimates for liver fibrosis assessment. The group has grown to about 200 members and includes committees to advance biomarkers based on measurement of volume blood flow and parameters derived from contrast-enhanced ultrasound. The status and implications of these efforts will be presented.

Conclusions: The QIBA effort has already led to changes in ultrasound system modifications to reduce bias and variance in liver shear wave speed estimates. A QIBA profile document that describes how to make low-variance estimates of liver shear wave speed is nearly ready for public comment and advancement through the QIBA process for clinical adoption. Other biomarkers are under active development. This approach to transition from early developers to clinical adoption is very well suited to the efforts of the ultrasound research community.

Acknowledgements: RSNA/QIBA – NIBIB/HHSN 268201300071C, HHSF 223201400703P. The authors of this presentation are only the leadership of the QIBA ultrasound effort and represent many active participants in QIBA ultrasound.

069 **THE RSNA-QIBA SHEAR WAVE SPEED PROFILE: CURRENT STATUS, METHODS IN GENERATING THE PROFILE AND A DISCUSSION OF CURRENTLY OPEN AND CLOSED ISSUES.**

M Dhyani[1], A E. Samir[1], ML Palmeri[2], A Milkowski[3], R G Barr[4], D Cosgrove[5], T J Hall[6], P L Carson[7], B S Garra[8].*

[1]Massachusetts General Hospital, Boston, MA; [2]Duke University, Durham, NC; [3]Siemens Ultrasound, Issaquah, WA, USA; [4]Southwoods Imaging, Boardman, OH, USA; [5]Imperial College School of Medicine, London, UK; [6]University of Wisconsin, Madison, WI, USA; [7]University of Michigan, Ann Arbor, MI, USA; [8]VA Medical Center, Washington DC.

Background: Each biomarker committee within the Radiological Society of North America's – Quantitative Imaging Biomarker Alliance is entrusted with generating a Profile document. The ultrasound (US) Shear-Wave Speed (SWS) biomarker committee is entrusted with generating the profile for use of shear wave speed measurements as an indicator of severity of liver fibrosis. The aims of the QIBA profile is to inform users what quantitative results can be achieved by following the claims and procedures defined in the profile. The Profile details serve two purposes; (1) Advise vendors what must be achieved with their product (not how to achieve it), (2) Communicate the necessary procedures to users.[1]

Aims: To review the structure of the QIBA profile document and the purpose of each section. To stress the importance of the claims sections and to present the proposed claims for SWS as laid out in the draft profile. To summarize the steps in creation, validation and implementation of the SWS profile and to discuss some of the problems encountered as well as potential problems that lie ahead. The purpose of this talk would be to bring the elasticity community abreast with the remaining open issues within the US – SWS profile document. This would stimulate discussions of the open issues and lead to research efforts in the field of SWS imaging that need priority attention.

Methods: Discussions were held with the various working groups and committees involved with profile creation, profile templating and profile validation including other biomarker committees much further along in the process. Discussions with the metrology working group chair regarding the claims section and associated statistical parameters.

Results: A QIBA Profile is a document that organizes and records the work of several volunteer collaborators within the US-SWS Biomarker Committee, that includes partners from industry, government, pharma, and clinicians. A QIBA Profile is largely composed of the following parts; (1) Clinical Context - Biomarker Committee and Task Forces, comprised of clinicians, engineers and medical physicists, define the clinical context of assessing liver fibrosis using US shear wave speeds; (2) Profile Claims – The biomarker committees define the Profile claims by characterizing methods to minimize bias, repeatability and reproducibility in SWS estimates. Results are recorded in the Profile, outlining the various claims in terms of science and supporting issues, such as interoperability or system support issues; (3) Groundwork - Groundwork activities may include, Quality control metrics, rationale for covariates (such as patient preparation), software version tracking; (4) Profile Details - Profile Details bring together the results of clinical context, profile claims, and groundwork to specify what is necessary to achieve the claim.[1]

Conclusions: The Ultrasound Shear Wave Speed Biomarker committee has made significant progress in the development of the profile. The current version is nearing completion and availability for public comment.

Acknowledgements: RSNA/QIBA – NIBIB/HHSN 268201300071C, HHSF 223201400703P. The authors of this presentation are only the leadership of the QIBA ultrasound effort and represent many active participants in QIBA ultrasound.)

References:

1. https://www.rsna.org/QIBA-Profiles-and-Protocols/

068 **THE QIBA SHEAR WAVE SPEED PROFILE: IMPLICATIONS FOR QUALITY ASSURANCE, QUALITY MONITORING, REGULATORY EVALUATION AND CLINICAL ACCEPTANCE OF QUANTITATIVE ELASTOGRAPHY.**

B S Garra[8], M Dhyani[1], A E Samir[1], R G Barr[4], T J Hall[6], A Milkowski[3], P L Carson[7], D Cosgrove[5].*
[1]Massachusetts General Hospital, Boston, MA; [3]Siemens Ultrasound, Issaquah, WA, USA; Duke University, Durham, NC; [5]Southwoods Imaging, Boardman, OH, USA; [3]University of Michigan, Ann Arbor, MI, USA; [2]University of Wisconsin, Madison, WI, USA; [8]VA Medical Center, Washington DC.

Background: The Shear Wave Speed (SWS) biomarker committee of the Quantitative Imaging Biomarker Alliance (QIBA) is drafting a "profile" that outlines procedures and equipment required to achieve high quality shear wave speed/liver stiffness estimates for liver fibrosis evaluation. The profile will soon be in the public comment phase to be followed by clinical testing. This profile could have a profound effect on the acceptance of SWS imaging/quantification by the medical community as well on regulation of devices intended for SWS estimation.

Aims: To discuss the effects of the QIBA profile on clinical estimates of SWS speed compared to the current status; to discuss the potential advantages of various QIBA profile components in clinical practice; and to outline the possible effects of the profile regulatory review of SWS devices. Discussion of possible changes in clinical usage/acceptance of SWS imaging systems is also an important goal.

Methods: Examination of the existing QIBA SWS profile plus planned additions and revisions followed a review of the state of clinical SWS usage for liver fibrosis. We also reviewed the current status of the FDA biomarker qualification program and public records relating to reviews of recently cleared SWS devices.

Results: The acquisition protocols described in the profile will have a significant impact on clinical practice. This is partly because the protocols are more manufacturer specific (and therefore easier to implement) than protocols currently published yet they are still in overall conformance to a standard acquisition approach and also to one another. Also, the protocols will result in SWS values that meet well-specified, improved standards for bias and variance enabling SWS values obtained from one ultrasound system to be directly compared to results obtained from other systems. The equipment needed is also clearly specified along with quality tests and protocol conformance checklists that will improve the quality of both SWS imaging and numerical estimates. Once validated, the quality tests and phantoms may significantly influence the tests that are recommended or required during regulatory review. Having such standard tests may speed up both development of new SWS systems and FDA review of those systems. As the profile is adapted to other forms of elastography such as quantitative strain elastography, greater clinical acceptance of those methods is likely.

Conclusion: The QIBA SWS profile holds great potential for improving clinical use of SWS systems and for quantitative elastography in general. This should improve the care of patients with diffuse liver disease and, in the future, of patients with other diseases where tissue stiffness estimates are needed.

Acknowledgements: The authors gratefully acknowledge funding support for the QIBA effort from: RSNA/QIBA – NIBIB/HHSN 268201300071C and HHSF 223201400703P. The authors also acknowledge the efforts of the numerous members of the SWS Biomarker Committee and its working groups without which the profile would not be possible.

References:

1. https://www.rsna.org/QIBA-Profiles-and-Protocols/

070 **RSNA-QIBA SHEAR WAVE SPEED PROFILE – WHAT THE CLINICAL WORKFLOW WOULD LOOK LIKE AND A REVIEW OF BIOLOGICAL CONFOUNDERS.**

A E. Samir[1], M Dhyani[1], ML Palmeri[2], A Milkowski[3], R G Barr[4], D Cosgrove[5], T J Hall[6], P L Carson[7], B S Garra[8].*

[1]Massachusetts General Hospital, Boston, MA; [2]Duke University, Durham, NC; [3]Siemens Ultrasound, Issaquah, WA, USA; [4]Southwoods Imaging, Boardman, OH, USA; [5]Imperial College School of Medicine, London, UK; [6]University of Wisconsin, Madison, WI, USA; [7]University of Michigan, Ann Arbor, MI, USA; [8]VA Medical Center, Washington DC.

Background: There has been wide scale acceptance of a clinical workflow in the use of Shear Wave Speed as a biomarker for liver fibrosis. However, several clinical challenges remain.

Aims: To review the clinical status of liver fibrosis estimation using US SWS. A review of widely acceptable clinical workflow, in particular at the Massachusetts General Hospital and a brief overview of clinical challenges that remain is replacing liver biopsy.

Methods: A detailed review of the literature and identification of questions that remain unanswered. An analysis of the claims on the QIBA profile and outline of potential clinical studies that could help in addressing some of the open issues from a clinical standpoint.

Results: Several underlying clinical confounders such as steatosis, inflammation, cholestasis etc. could cause variation in SWS estimation of liver fibrosis. However, there is enough evidence in the literature to identify specific biological confounders. In addition, there are effects of body mass index, subcutaneous tissue thickness, and intercostal rib space that can cause significant variation of SWS in a given subject. However, on the aggregate, there are methods as specified in the QIBA profile as well as the clinical workflow at the Massachusetts General Hospital that aim to mitigate variations in SWS estimation and also account for biological confounder variability.
Results of several clinical trials at the Massachusetts General Hospital in light of following a detailed protocol will also be discussed.

Conclusions: By following a robust protocol, significant repeatability can be achieved in estimating liver fibrosis via SWS measurements on different US platforms.

Acknowledgements: RSNA/QIBA – NIBIB/HHSN 268201300071C, HHSF 223201400703P. The authors of this presentation are only the leadership of the QIBA ultrasound effort and represent many active participants in QIBA ultrasound.)

References:

1. https://www.rsna.org/QIBA-Profiles-and-Protocols/

037 **RSNA-QIBA COMPARISON OF SHEAR WAVE SPEED ESTIMATION IN VISCOELASTIC PHANTOMS.**

M L Palmeri[1], T J Hall[2], B S Garra[3], A Milkowski[4], T Lynch[5], S Chen[6], N C Rouze[1], R G Barr[7], V Shamdasani[8], M Macdonald[9], G Guenette[10], M Dhyani[11], Z Hah[12], A Gee[13], M Couade[14], R Managuli[15], J Chen[7], N A Obuchowski[16], P L Carson[17].*

[1]Duke University, Durham, NC, USA; [2]University of Wisconsin, Madison, WI, USA; [3]VA Medical Center, Washington DC, USA; [4]Siemens Ultrasound, Issaquah, WA, USA; [5]Computerized Imaging Reference Systems, Inc., Norfolk, VA, USA; [6]Mayo Clinic, Rochester, MN, USA; [7]Southwoods Imaging, Boardman, OH, USA; [8]Philips Ultrasound, Bothell, WA, USA; [9]General Electric, Milwaukee, WI, USA; [10]Toshiba Medical Research Institute, Redmond, WA, USA; [11]Massachusetts General Hospital, Boston, MA, USA; [12]Samsung Medison, Seoul, SOUTH KOREA; [13]Zonare Medical Systems, Mountain View, CA, USA; [14]Supersonic Imagine, Aix-en-Provence, FRANCE; [15]Hitachi Aloka Medical America, Inc., Wallingford, CT, USA; [16]The Cleveland Clinic, Cleveland, OH, USA; [17]University of Michigan, Ann Arbor, MI, USA.

Background: Ultrasonic shear wave speed (SWS) is useful to noninvasively evaluate liver fibrosis, but reported inter-system variability in liver SWS measurements can challenge meaningful comparison of measurements performed with different systems and complicate developing SWS thresholds for classifying fibrosis severity. The Radiological Society of North America (RSNA) Quantitative Imaging Biomarker Alliance (QIBA) ultrasound SWS committee has been developing methods to compare system performance in elastic and viscoelastic (VE) phantoms to reduce bias and variance in SWS estimates.

Aims: This study compares SWS measurements between commercially-available systems using phantoms that have viscoelastic properties similar to those observed in normal and fibrotic liver.

Methods: CIRS, Inc. (Norfolk, VA) fabricated three phantoms based on Zerdine® hydrogel that were matched in viscoelastic behavior to healthy and fibrotic human liver data [1]. Phantoms were measured at academic, clinical, government and vendor sites using different systems with curvilinear arrays at multiple focal depths (3.0, 4.5 & 7.0 cm). The phantoms were also measured using Magnetic Resonance Elastography (MRE) at discrete frequencies ranging from 60—200 Hz for comparison with the ultrasound system estimates. Temperature dependencies in the phantoms were also measured from 18—30 °C.

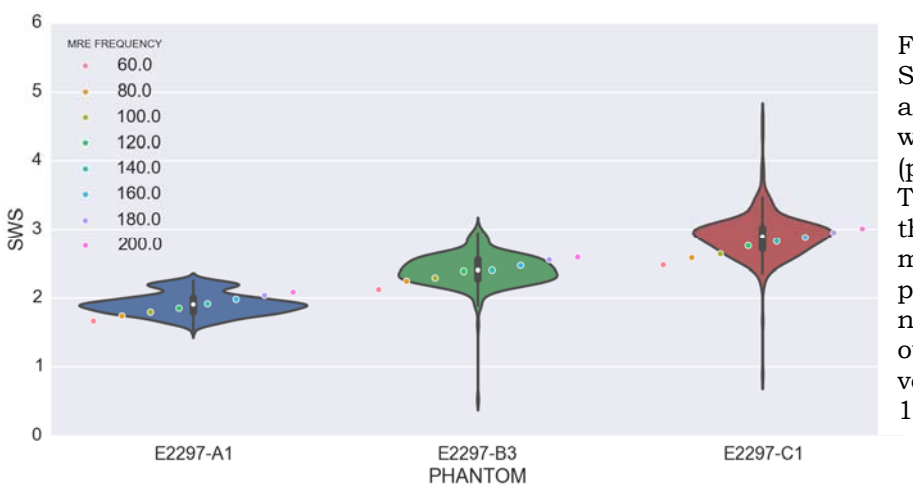

Figure 1. A violin plot of the SWS measurement results among all ultrasound systems with MRE measurements (points) at various frequencies. The violin plots demonstrate that most of the ultrasound measurements for each phantom are described by a narrow distribution with outliers. Those results agree very well with MRE at about 140 Hz.

Conclusions: SWS estimates from various manufacturers are in good agreement, but there is a small bias and some systems demonstrated large variance. Methods to address both errors are under development.

Acknowledgements: RSNA/QIBA – NIBIB/HHSN 268201300071C, HHSF 223201400703P, R01DK092255, R01EB002132, and R01HD072077.

References: [1] M. L. Palmeri, M. H.Wang, N. C. Rouze, M. F. Abdelmalek, C. D. Guy, B. Moser, A. M. Diehl, and K. R. Nightingale. Noninvasive evaluation of hepatic brosis using acoustic radiation force-based shear stiffness in patients with nonalcoholic fatty liver disease. J. Hepatol., 55(3):666-672, Sept. 2011.

080 **A CROSS-MACHINE COMPARISON OF SHEAR WAVE SPEED ESTIMATIONS IN A PHANTOM AND THE NORMAL FEMALE BREAST.**

S Sharma[1], R Sinnatamby [2], E O' Flynn[1], A Kirby[1], JC Bamber[1], EJ Harris [1].*

[1]The Institute of Cancer Research and Royal Marsden NHS Foundation Trust, London, United Kingdom; [2] Cambridge University Hospitals NHS Foundation Trust, Cambridge, United Kingdom.

Introduction: Shear wave speed (SWS) may be a useful quantitative measure of radiation-induced breast hardness, which is a dose-limiting complication of radiotherapy [1, 2]. Any quantitative measure of treatment outcome must be reproducible between centres and preferably measurement systems. This study tests for differences in absolute values of SWS measured from two different ultrasound scanners at different UK centres on healthy volunteers and a phantom.

Aims: (1) to compare SWS measurements between centres on a phantom and normal female breasts, (2) to investigate if the breast tissue type (skin, subcutaneous fat and gland) affects the agreement between centres, and (3) to compare the dependence (if any) of SWS on transducer orientation across centres.

Methods: Aixplorer® (Supersonic Imagine) and S2000® (Siemens) ultrasound shear wave elastography-enabled machines at Royal Marsden Hospital, London and Addenbrookes Hospital, Cambridge respectively were used. Cross-centre, cross-operator and cross-machine measurements were performed by two independent users on an ultrasound elasticity phantom (Model 049A, CIRS) containing 8 inclusions of varying stiffness. Four healthy volunteers were recruited for this study. Measurements were acquired at both the centres on the same day. Eight images were acquired from each breast, with the transducer in radial and anti-radial orientations (see Fig.1a). SWS values were recorded using the onscreen measurement toolbox of each scanner. Paired t-tests were used to test for difference between the centres in mean SWS for measurements from skin, subcutaneous fat and fibroglandular tissues, and from different transducer orientations.

Results: Mean SWS measurements from the elastography phantom were not significantly different between the centres (i.e. machines). The mean SWS estimates of whole breast from the Aixplorer and S2000 were 2.49 m/s and 1.42 m/s respectively ($p<<0.01$) (Fig.1b). The SWS values from skin, subcutaneous fat and fibroglandular tissues measured with Aixplorer and S2000 were: 2.71 & 1.66 m/s, 2.83 & 1.29 m/s and 1.89 & 1.33 m/s respectively (p-values $<<0.01$) (Fig.1c). Comparison of machines for radial and anti-radial probe orientations also showed significant differences ($p << 0.01$).

Conclusions: The SWSs measured in a phantom using the two different systems showed agreement that was broadly consistent with previous findings [3]. However in normal breasts, SWS was significantly greater for the Aixplorer in London compared to the S2000 in Cambridge, in the whole breast, different breast tissues, positions and orientations of the transducer. Further work should determine the source of the bias in the clinical results.

References: 1. Fehlauer F, et al. Int J Radiat Oncol Biol Phys; 55(3):651-8 (2003). 2. Barnett GC, et al. J Eur Soc Therap Radiol & Onc; 105(3):289-95 (2012). 3. Hall T, et al. 10.1109/ULTSYM.2013.0103; 303-400, IEEE (2013).

Acknowledgements: NHS funding to the NIHR Biomedical Research Centre at The Royal Marsden and the ICR, Cancer Research UK funding to the Cancer Imaging Centre at the ICR.

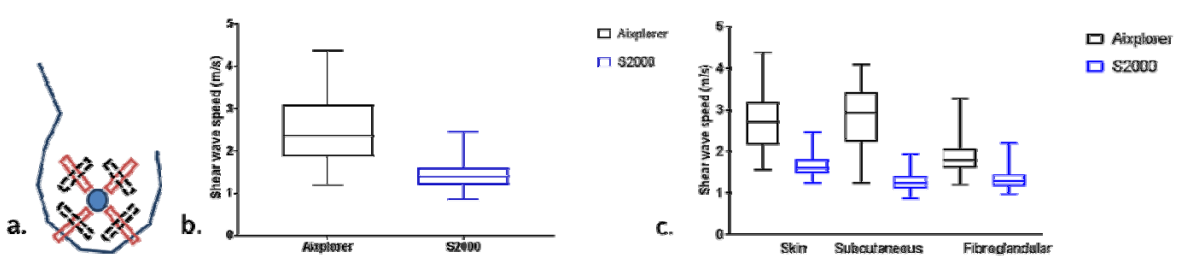

Figure 1. a. Schematic of the breast showing radial and anti-radial positions for US imaging. b. Mean SWS measured for all images using the S2000 and the Aixplorer. c. Mean SWS measured for all images in different tissues of the breast using S2000 and Aixplorer.

039 **PRESSURE BOUNDARY CONDITION ESTIMATION FROM DISPLACEMENT DATA FOR POROELASTIC IMAGE RECONSTRUCTION.**

L Tan[1], M.D.J McGarry[3], E.W Van Houten[4], L.Solamen[1], J.B.Weaver[2], K.D Paulsen[1,2].*
[1]Thayer School of Engineering, Dartmouth College, Hanover, NH, USA; [2]Geisel School of Medicine, Dartmouth College, Hanover, NH USA; [3]Columbia University, New York, NY, USA; [4]University de Sherbrooke, Sherbrooke Quebec, CANADA.

Background: Poroelastic mechanical models provide access to hydrodyamical properties (in addition to traditional stiffness parameters) that may have particular importance and/or relevance to disease states in specific tissues which exhibit porous structural and physiological behavior, such as the brain, which has been mathematically described as a porous medium since the 70s [1]. Recent studies have shown that hydraulic conductivity can be estimated in tofu phantoms from poroelastic models (along with shear moduli), but the inversions require additional stabilization that can be obtained by applying spatial priors derived from structural image (MR) information [2]. One of the weaknesses in the current approach is the assumed boundary conditions on the pressure field for which no observational data is available. The problem is exacerbated when partial volumes are acquired, for example, in the brain, for which even assumptions on pressure information within the brain at the slice-direction "ends' of the acquisition are tenuous. Thus, methods for estimating pressure boundary conditions are of significant interest.

Aims: A numerical framework for estimating pressure boundary conditions (PBCs) from displacement data in biphasic materials is developed and integrated within 3D nonlinear finite element poroelastic inversion. The unknown PBCs are estimated using the full-volume displacement data from MRE. A subzone-based, parallelized nonlinear inversion (NLI) technique is then used to update mechanical and hydrodynamical properties, given the appropriate subzone PBCs obtained by solving a pressure forward problem (PFP) with the estimated pressure boundary data.

Methods: The PBC on the global boundary for the forward problem is defined as a Neumann type (i.e. type II) and estimated from the full volume displacement data available from MRE making it mathematically consistent with the governing equations of motion. When solving the individual subzone inversion problems, type I PBCs are prescribed on the subzone surface by transferring the resulting global pressure field from the PFP to the subzone level. The additional step requires only one-fourth of the computational time needed for the full poroelastic forward problem. The algorithm was evaluated on a single-inclusion phantom, in which the elastic property and hydraulic conductivity images were properly recovered. Two and three parameter reconstruction experiments were performed with noise-free and noisy displacement. Synthetic displacement and pressure fields were obtained from the full global problem with specified material property distributions to use in the validation studies.

Results: Material property images were recovered accurately in the presence of added noise up to 15% in the displacement data in two parameter (mechanical properties only) and 5% in three parameter (mechanical plus fluid properties) cases, respectively, when using the PBC estimates. Spatially-resolved hydraulic conductivity images are recovered without introducing spatial priors. Improvement in image quality was observed when the synthetic measurement data was spatially filtered. Three parameter reconstructions (involving estimation of the spatial distribution of hydraulic conductivity without invoking spatial priors) were more sensitive to errors in the PBC estimates.

Conclusions: An algorithm that estimates global pressure boundary conditions from measured displacement data has been implemented and integrated into nonlinear material property inversion (mechanical and fluid properties). The overall scheme generates sufficiently accurate boundary condition values to enable subsequent estimation of mechanical and fluid-related material property parameters spatially, and without the need for invoking spatial priors (on hydraulic conductivity) as in the past.

Acknowledgements: This work was supported in part by NIH grant R01 EB018230 awarded by NIBIB.

References:

1. Hakim S, Venegas J, The physics of the cranial cavity, hydrocephalus and normal pressure hydrocephalus; mechanical interpretation and mathematical model, Surgical Neurology 5(3); 187-210, 1976.
2. Pattison A, McGarry M, Spatially-resolved hydraulic conductivity estimation via poroelastic magnetic resonance elastography, IEEE Trans Med Imaging, 33(6); 1373-1380, 2014.

049 **CONTRAST DETAIL ANALYSIS AND EVALUATION OF MR ELASTOGRAPHY INVERSION ALGORITHMS.**

L Solamen[1], M.D.J McGarry[2], E.E.W Van Houten[3], J.B Weaver[4], K.D Paulsen[1,4]*

[1]Thayer School of Engineering, Dartmouth College, Hanover, NH, USA; [2]Columbia University, New York, NY, USA; [3]University de Sherbrooke, Sherbrooke Quebec, CANADA; [4]Geisel School of Medicine, Dartmouth College, Hanover, NH USA.

Background: Repeatable detection of low contrast focal lesions is important for characterization of medical imaging technologies. We performed a contrast detail analysis of viscoelastic mechanical property estimation using MR Elastography.

Aims: MRE imaging was performed on a silicone phantom containing 20 cylindrical inclusions of varying size and stiffness contrast. We expect precision and accurate detection of small inclusions with low stiffness contrast using inversion algorithms.

Methods: Stiffness of gelatin phantoms are difficult to control due to factors such as cooling time, but silicone phantoms are easy to fabricate and have a longer lifespan. Phantoms for algorithm evaluation were made from A341 silicone soft gel. Stiffness was controlled by dilution with PMX-200 silicone fluid. A layered phantom was created with 20 cylindrical inclusions of diameter ranging from 8mm to 29mm and stiffness ranging from 55% to 70% A341.[1] Background of the silicone phantom was held at 50% A341. The contrast detail phantom was externally actuated at 60Hz and reconstructed using viscoelastic mechanical property assumptions with a non-linear inversion. [2,3] The phantom was scanned in 3 different orientations to gauge the repeatability for the same material with different motion patterns.

Results: MRE scans of different orientations showed an increase in stiffness (storage modulus) as concentration of silicone A341 increased with a standard deviation less than 0.4kPa. MRE non-linear inversion reconstructions identified changes in stiffness for inclusions as small as 8mm, even at very low stiffness contrast.

Conclusions: This contrast detail analysis provides a measure of the quantitative and spatial accuracy of a viscoelastic nonlinear inversion MRE algorithm, and establishes a baseline for comparison of different MRE imaging and reconstruction methods.

Acknowledgements: This work was supported in part by NIH grant R01 EB018230 awarded by NIBIB

References: [1]Doyley M. et al. “Thresholds for detecting and characterizing focal lesions using steady-state MR elastography” Medical Physics 30 (2003). [2] Mcgarry M., et al. "Suitability of poroelastic and viscoelastic mechanical models for high and low frequency MR elastography." Medical Physics. 42 (2015). [3] Van Houten E.E.W., et al. “An overlapping Subzone Technique for MR-Based Elastic Property Reconstruction.” Magnetic Resonance in Medicine. 42(1999)

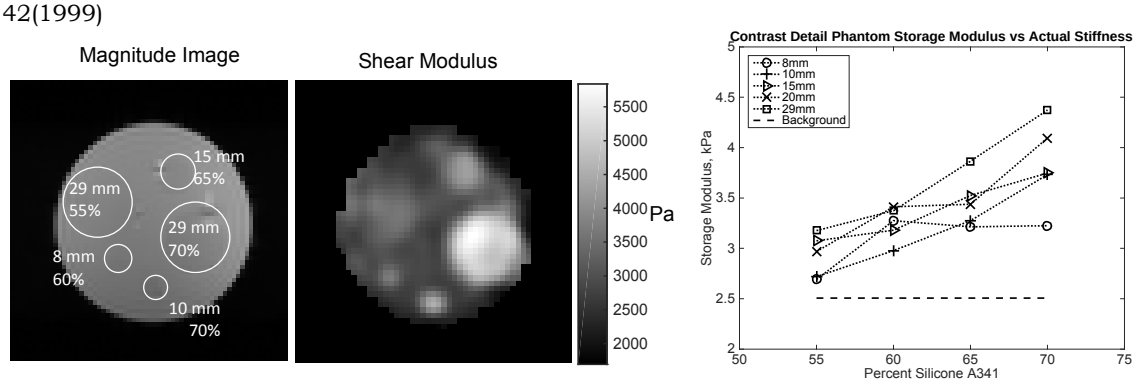

Figure 1: Cross sectional slices of the contrast detail phantom with inclusions of varying diameter and stiffness. Magnitude image (left) and the real shear modulus map (right). Figure 2: Average storage modulus at varying silicone A341. Average value of background silicone (50%) is plotted for comparison.

056 **CALIBRATED AND DIRECT ELASTIC MODULUS RECONSTRUCTION FROM ULTRASOUND COMPRESSION ELASTOGRAPHY.**

O A. Babaniyi[1], A A. Oberai[2], P E. Barbone[3].*

[1]Duke University, Durham, NC, USA; [2]Rensselaer Polytechnic Institute, Troy, NY, USA; [3]Boston University, Boston, MA, USA.

Background: Computing the elastic modulus distribution from ultrasound strain measurements with a direct (i.e. non iterative) method is a challenging problem, characterized by three technical hurdles. First, direct methods need precise measurement of the full displacement vector, but typically only one component of the displacement field is measured precisely with ultrasound. Second, once the displacement vector field is known, a stable and efficient computational method to compute the modulus distribution is needed. Third, a means to calibrate the elastic modulus distribution is required for quantitative reconstructions.

Aims: The goal is to create a direct (i.e. non-iterative) method to reconstruct quantitative estimates of the absolute elastic modulus distribution from ultrasound measurements of quasistatic compression.

Methods: To achieve this goal, we developed the Sparse Relaxation of Momentum Equation (SPREME) displacement processing method [1] to reconstruct precise estimates of the full displacement vector field from partial ultrasound measurements. We then used the displacements produced by SPREME in the Adjoint Weighted Equation (AWE) formulation [2] to reconstruct the shear modulus distribution directly. We calibrated the elastic modulus reconstructions using values in a known region in the image, akin to the "stress meter" concept [3].

Results: We show simulation results in which we accurately reconstruct the shear modulus distribution from displacement data corrupted by noise. We also perform direct reconstructions on ultrasound displacements measured from a tissue mimicking phantom. The phantom had a calibration layer with a known modulus distribution, and this allowed us to reconstruct the absolute modulus with the AWE algorithm. Finally, we successfully reconstruct the shear modulus field using displacement data measured from patients with breast masses.

Conclusions: We have been able to reconstruct the shear modulus distribution from ultrasound displacement measurements using a direct method. This takes us a step closer to getting real time modulus reconstructions.

Acknowledgements: The authors will like to acknowledge T.J. Hall and J.J. Jiang for providing the clinical displacement data. Support from NIH Grant No. NCI-R01CA140271, and NSF Grant No. 1148124, and 1148111 is also gratefully acknowledged

References:

[1]. Olalekan A. Babaniyi, Assad A. Oberai, Paul E. Barbone. "Recovering vector displacement estimates in quasistatic elastography using sparse relaxation of the momentum equation." *Inverse Problems in Science and Engineering* (2016): 1-37.

[2]. Albocher, Uri, et al. "Adjoint-weighted equation for inverse problems of incompressible plane-stress elasticity." *Computer Methods in Applied Mechanics and Engineering* 198.30 (2009): 2412-2420.

[3]. Ophir, J., et al. "Elastography: a quantitative method for imaging the elasticity of biological tissues." *Ultrasonic imaging* 13.2 (1991): 111-134.

014 **MECHANICAL PROPERTY RECONSTRUCTION OF A BREAST PHANTOM USING 3D DIGITAL IMAGE CORRELATION ABD THE DIET METHOD.**

A Brazy [1], E.E.W Van Houtten[1].*
[1]Université de Sherbrooke, Sherbrooke, Québec, CANADA.

Background : Young's modulus offers a greater contrast between healthy and cancerous tissues than traditional X-ray mammography. Furthermore, the vibration amplitude of a tissue is a function of the mechanical parameters of the propagating medium, making it possible to reconstruct the mechanical properties of the medium knowing the motion amplitudes by solving the elasto-dynamic inverse problem. Elastography methods for breast cancer screening must exploit this relationship using low cost, repeatable methods that permit an efficient workflow for imaging personnel.

Aim : The aim of this study is to provide a novel method of estimating the mechanical property of the breast by solving an inverse problem based on surface data obtained by 3D Digital Image Correlation (3D-DIC) methods. 3D-DIC equipment is comparatively low cost and can be arranged for relatively comfortable, non-contact imaging, providing multi-frequency 3D data on the tissue surface. The challenge is to solve the surface based inverse problem in a robust manner.

Methods : A silicon phantom mimicking a generic breast geometry was actuated at a fixed frequency (15 Hz). A commercial 3D-DIC system (Vic 3D, Correlated Solutions, NC, USA) was used to acquire the 3D movement of the surface of the phantom. These data were then used in conjunction with boundary conditions to drive a 3D Finite Element Method (FEM) based property reconstruction process. Different FEM simulations were computed with a Young's modulus varying from 2 to 15 kPa. The reconstruction was made by minimizing an error function between simulated data and the measurement. The material was assumed to be homogenous and incompressible with a density of 1000kg/m^3.

Results : The mechanical properties were successfully reconstructed. The heterogeneous case is discussed.

Conclusions : Results show that it is possible to reconstruct the mechanical property map of a volume using 3D-DIC surface motion data.

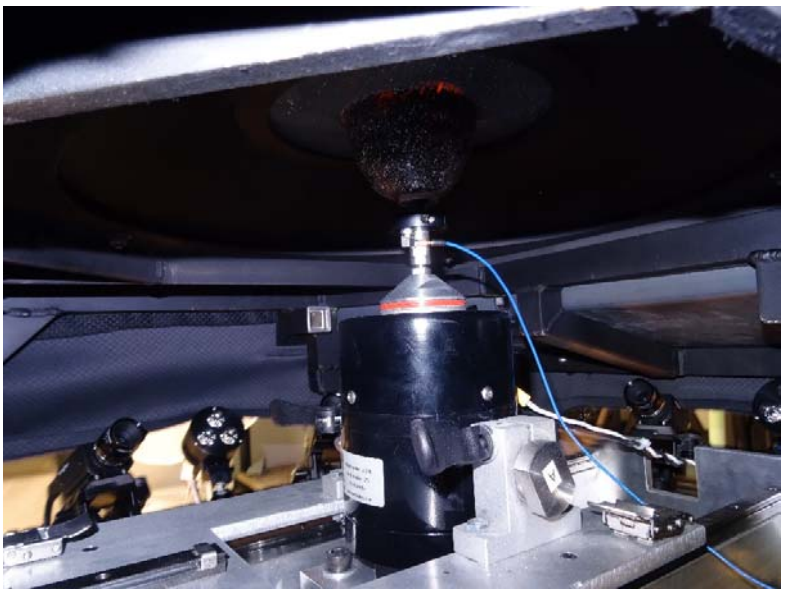

Figure 1 : DIET acquisition set up

057 **COMPARISON OF DIRECT AND NON-LINEAR INVERSION FOR MEASUREMENT OF MECHANICAL PROPERTIES OF THE HIPPOCAMPUS USING MAGNETIC RESONANCE ELASTOGRAPHY (MRE).**

LV Hiscox[1], CL Johnson[2], S Hirsch[3], E Barnhill[3], I Sack[3] MDJ McGarry[4], J Huston[5] E van Beek[1], JM Starr[1], N Roberts[1].*

[1]University of Edinburgh, Edinburgh, UK; [2]University of Delaware, Newark, DE, USA; [3]Charité Universitätsmedizin Berlin, GERMANY; [4]Columbia University, New York, NY, USA; [5]Mayo Clinic, Rochester, MN, USA.

Background: Tissue mechanical properties vary over several orders of magnitude in the disease state and elude current clinical neuroimaging modalities. Magnetic Resonance Elastography (MRE) combines conventional MRI with acoustic wave propagation [1] to generate high-resolution viscoelastic or 'stiffness' maps, and may provide an early indication of disease.

Aims: The purpose of this study was use two high-resolution MRE techniques in order to investigate the hippocampus, a brain structure specifically implicated in Alzheimer's disease (AD). Imaging biomarkers for AD include degree of hippocampal atrophy, however, volume loss is usually only apparent in the later stages of the disease. The current focus of AD research has shifted towards early diagnosis and possible prevention. In this work, we tested the repeatability of measurements of the shear stiffness (kPa) and damping ratio φ of the hippocampus obtained using two alternative MRE techniques in healthy volunteers, namely Direct or Non-Linear Inversion. We also sought to investigate the effects of ageing on mechanical measurements in a group of healthy older volunteers who have undergone cognitive testing to rule out subtle memory problems such as Mild Cognitive Impairment (MCI).

Methods: 12 young subjects (aged 18-30 years) and 12 cognitively healthy older subjects (aged 65 and over) were recruited via the *Join Dementia Research* database. All data were acquired on a 3T Verio MRI system (Siemens Medical Systems), with vibrations generated by the Resoundant actuator and head pillow (http://resoundant.com/). The Direct Inversion (DI) protocol was used to analyze multi-frequency data (20-60Hz) acquired using a modified Cartesian Echo Planar Imaging (EPI) sequence by means of the Elastography Software Pipeline (ESP) [2], which combines Multi-frequency Elasto-Visco inversion (MDEV) [3] with super-resolution methodology. The Non-Linear Inversion (NLI) protocol was used to analyze a high-resolution spiral EPI dataset [4] acquired at 50Hz by means of a Finite-Element-Model (FEM) based approach [5]. For each subject, Freesurfer software (http://surfer.nmr.mgh.harvard.edu/) was used to automatically segment the hippocampus from a T1-weighted image, with elastograms subsequently co-registered to the structural image. Six subjects from each of the younger and older cohort returned for an identical second scan to assess MRE repeatability.

Results: Participant's tolerated the head vibrations and scan time well. Figure 1 shows an example axial slice of the medial temporal lobe obtained using DI. The mean shear stiffness of the hippocampus is 1.89 (SD ± 0.52) kPa, and damping ratio 0.50 (SD ± 0.12) RAD. Figure 2 shows corresponding data obtained using NLI for a different subject. Hippocampal shear stiffness is 2.19 (SD ± 0.63) kPa and damping ratio 0.20 (SD ± 0.09) RAD. Data are presently being analysed to determine mean stiffness and damping ratio for the hippocampus based on subject age and sex, Further analysis will determine reproducibility.

Conclusions: MRE has developed into a high-resolution technique capable of studying specific brain structures such as the hippocampus. Establishing a robust, reliable quantitative protocol is essential prior to large-scale clinical investigations. Our follow on objective is to utilize the preferred DI or NLI MRE protocol in patients at high risk of developing Alzheimer's disease.

Acknowledgements: LV Hiscox is funded through a grant to the University of Edinburgh from Alzheimer Scotland. N Roberts and EJR van Beek are supported by the Scottish Imaging Network, a Platform of Scientific Excellence (SINAPSE, www.sinapse.ac.uk)

References: [1] Muthupillai *et al.* 1995 *Science* **269** 1854–1857. [2] Barnhill E *et al.* 2017 *Med. Im. Anal.* **25** 133-145. [3] Papazoglou S *et al.* 2012 *Phys. Med. Biol.* **57** 2329–2346. [4] Johnson CL et al. 2014 *Magn. Reson.Med.* **71** 477–485. [5] McGarry MDJ 2012 *Med. Phys.* **39** 6388-6396. [6] McGarry et 2013, *IEEE Trans Med Imaging, 10, 1901-1909.*

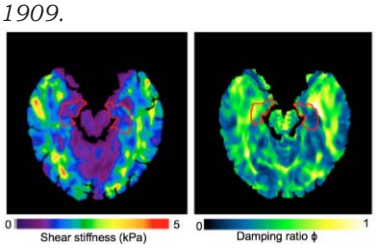

Figure 1. *DI*

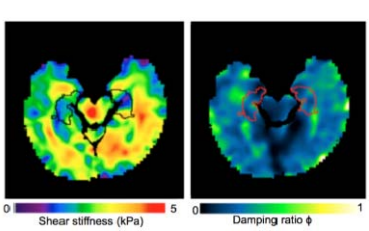

Figure 2. *NLI - *note: the NLI approach used does not include SPR [6].*

Please Fill Out Both Sides

Conference Evaluation and Questionnaire

OVERALL CONFERENCE

	Poor		Mid		Excellent
Overall Conference Evaluation	1	2	3	4	5
General comments:					

SCIENTIFIC PROGRAM

	Poor		Mid		Excellent
Quality of the Presentations	1	2	3	4	5
Relevance of Presentations to the Conference's Theme	1	2	3	4	5
Time Allotted for Presentations	1	2	3	4	5
Time Allotted for Discussion	1	2	3	4	5
Poster Session	1	2	3	4	5
Tutorials	1	2	3	4	5
Short presentation category	1	2	3	4	5
Student Participation	1	2	3	4	5
Equipment Exhibit	1	2	3	4	5
Additional comments/suggestions:					

CONFERENCE MATERIALS

	Poor		Mid		Excellent
Printed Proceedings Book	1	2	3	4	5
Other Registration Materials	1	2	3	4	5
Circle One: Yes, it is acceptable having a CD only.	No, I would like a printed book with the CD.				
Additional comments/suggestions (e.g proceedings on memory stick or password link to online proceedings):					

CONFERENCE FACILITIES & SOCIAL PROGRAMME

	Poor		Mid		Excellent
Lecture Hall	1	2	3	4	5
Registration Desk	1	2	3	4	5
Meals: Dining facilities	1	2	3	4	5
Conference Breakfasts and Lunches	1	2	3	4	5
Conference Dinner and Entertainment	1	2	3	4	5
Coffee Breaks	1	2	3	4	5
Opening Dinner Reception	1	2	3	4	5
Closing Cocktail Party	1	2	3	4	5
Audio–Visual: Screen Visibility	1	2	3	4	5
Sound Level	1	2	3	4	5
Presentation Transition	1	2	3	4	5
Internet Connectivity:	1	2	3	4	5
Additional comments:					

Please Fill Out Both Sides

Conference Evaluation and Questionnaire

VENUE AND HOTEL

	Poor		Mid		Excellent
Venue: Lake Morey Resort & Environs	1	2	3	4	5
Would you return to this area?	Yes		Perhaps		No
Area Attractions	1	2	3	4	5
Hotel: Overall	1	2	3	4	5
Reservations	1	2	3	4	5
Transportation and Accessibility	1	2	3	4	5
Reception and Check–In	1	2	3	4	5
Accommodations	1	2	3	4	5
Facilities	1	2	3	4	5
Parking	1	2	3	4	5
Would you return to this hotel?	Yes		Perhaps		No
Would you like to Co-Host ITEC in the future	Yes		Perhaps		No
If yes, please state your organization name and city:					
Where would you like to see ITEC hosted?					
Additional comments:					

CONFERENCE ADMINISTRATION

	Poor		Mid		Excellent
Website	1	2	3	4	5
Registration off–site	1	2	3	4	5
Registration on–site	1	2	3	4	5
Administrative staff	1	2	3	4	5
Correspondence	1	2	3	4	5
Additional comments:					

GENERAL INFORMATION

I am a Returning Delegate	Yes		No
I plan to attend the next conference in 2017	Yes	Perhaps	No
and present a paper(s) / poster(s)	Yes	Perhaps	No
Other(s) from my lab would attend the next conference	Yes	Perhaps	No
and he/she / they would present a paper(s) / poster(s)	Yes	Perhaps	No
How did you learn of this conference? (Check all that apply)	☐ Email Announcement		
☐ Internet	☐ Website		
☐ Other	☐ Colleague		
Tutorial Topic Suggestions for next year:			
Additional Comments:			

If you would be willing to assist with hosting the Conference in your vicinity, please give your name to the Conference Staff.

Questions or comments are welcome at any time at secretariat@elasticityconference.org Thank you.